

# Dopant-Free Hole Transporting Materials for Perovskite Solar Cells

Ehsan Rezaee, Xiaoyuan Liu, Qikun Hu, Lei Dong, Qian Chen, Jia-Hong Pan,\* and Zong-Xiang Xu\*

This article reviews various dopant-free hole transporting materials (HTMs) used in perovskite solar cells (PSCs) in three main categories including inorganic, polymeric, and small molecule HTMs. PSCs have undergone rapid progress, achieving power conversion efficiencies (PCEs) above 22%. With their low production cost and high efficiencies, PSCs are considered promising next-generation solar cell technology. In all developed architectures for PSCs, including planar and mesoscopic with conventional and inverted structures, HTMs play a significant role in determining the photovoltaic performance of PSCs. Using p-type dopants, however, is considered a common strategy to increase the hole conductivity of HTM, which is usually compensated by a more complicated fabrication procedure, higher production costs, and lower stability of PSC. Although several reviews on HTMs have been published, progress on dopant free HTMs needs to be reviewed and analyzed. Here, a review covering most of the published reports on dopant-free HTMs is presented, and the device structure and fabrication method, HTM layer deposition techniques, and the efficiency and the stability of PSCs are addressed during discussions in each main category. Finally, an outlook on stability and PCE growth in PSCs based on dopant-free HTMs is presented.

satisfying the increasing global energy demand. The past decades have witnessed the continuous increase in the solar cell efficiency, and several novel photovoltaic devices have been reported. Typical, crystalline silicon-based photovoltaics have been developed as a key electric power supplier.<sup>[1]</sup> However, due to high manufacturing cost and limited use of silicon solar cells in large scale, as well as their environmental concerns,<sup>[2]</sup> several alternatives such as cadmium telluride (CdTe) and copper indium gallium selenide/sulfide (CIGS),<sup>[3]</sup> as well as organic/polymer solar cells,<sup>[4]</sup> tandem solar cells,<sup>[5]</sup> dye sensitized solar cells (DSSCs),<sup>[6]</sup> and perovskite solar cells (PSCs),<sup>[7]</sup> often referred to as the second- and third-generation photovoltaics (PVs), respectively, have also been recently developed.

Up to 26.6%, crystalline silicon solar cells have the highest power conversion efficiency (PCE) until now.<sup>[8]</sup> Nevertheless, by the emergence of perovskite solar cells using organic-metal halide perovskites, as a new light absorber, the dominance of photovoltaic market by the first two generation solar cells is now being challenged.

The initial introduction of perovskite materials (Methylammonium lead halides, MAPbX<sub>3</sub>, X = Cl, Br, I) as light-absorber was conducted by Miyasaka and co-workers in 2009. The constructed solar cells succeeding from DSSCs merely showed a PCE of 3.9% with I<sup>3-</sup>/I<sup>-</sup> redox electrolyte.<sup>[9]</sup> Subsequently, in 2011, Park and coworkers increased the PCE to 6.54%; however, the stability of the constructed solar cells was low.<sup>[10]</sup> Significant improvement in PCE and stability has been made due to the replacement of liquid electrolytes with solid hole transporting material (HTM). In 2012, Park, Snaith, Grätzel, and co-workers has used 2,2',7,7'-tetrakis(N,N-di-methoxyphenyl-amine) 9,9-spirobifluorene (spiro-OMeTAD) as HTM and a PCE of 9.1% has been achieved.<sup>[11]</sup> The fast growth of the PCE of PSCs within 6 years, which is multiplied about six times have amazed the research groups in the photovoltaic field and now, a remarkable efficiency as high as 22.7% can be achieved by perovskite solar cells.<sup>[12]</sup>

In very recent years, significant research activities were devoted to the development of PSCs, focusing on different areas, including device structures,<sup>[13]</sup> film deposition techniques,<sup>[14]</sup>

## 1. Introduction

Overconsumption of unsustainable fossil fuels, such as petroleum, coal and natural gas has outpaced the sustainable capacity of ecosystem. Continuous exploration of renewable energies, such as wind, biomass, tidal, hydroelectric, wave, geothermal, and solar energies are vital to meet today's worldwide energy consumption growth. Among them, solar energy is most powerful and reachable source, and its utilization has been considered as the most promising solutions for

Dr. E. Rezaee, Dr. X. Liu, Q. Hu, L. Dong, Q. Chen, Prof. Z.-X. Xu  
Department of Chemistry  
South University of Science and Technology of China  
Shenzhen, Guangdong 518000, P. R. China xu.zx@sustc.edu.cn

Prof. J.-H. Pan  
School of Renewable Energy  
North China Electric Power University  
Beijing 102206, China  
E-mail: pan@ncepu.edu.cn

DOI: 10.1002/solr.201800200

perovskite chemical composition,<sup>[15]</sup> electron transfer layers,<sup>[16]</sup> and engineering of HTMs. However, the theoretical value for power conversion efficiency of perovskite solar cells is 30% and it shows the great future of these category of solar cells.<sup>[17]</sup> In this work, we have reviewed the recent progress of perovskite solar cells using different dopant-free HTMs. Their structural and opto-electronic properties, synthetic developments and challenges, and applications in devices are addressed. The aim is to provide the reader with the most remarkable achievements to date.

## 1.1. Perovskite Solar Cells

### 1.1.1. Perovskite Solar Cells and Their Architecture

Reported by Miyasaka et al., between 2006 and 2008,  $\text{CH}_3\text{NH}_3\text{PbI}_3$  and  $\text{CH}_3\text{NH}_3\text{PbBr}_3$  are the two first organometal halide perovskites used as light absorbers in solar cells.<sup>[18]</sup> Their wide absorption spectrum with high absorption coefficient,<sup>[9]</sup> along with high charge carrier mobility, low exciton binding energy,<sup>[19]</sup> and long electron- and hole-diffusion length<sup>[20]</sup> make them an excellent choice for light absorbers in solar cells. However, the first attempt of using organohalide perovskite in solar cell was based on the structure of dye-sensitized solar cell (DSSC), in which the organic or organometallic dyes in DSSC have been replaced by the perovskite material. Therefore, the organo-lead halide perovskite functioned as a dye sensitizer in first perovskite solar cells. But later, by discovering the ability of perovskites for both charge generation and charge transportation,<sup>[21]</sup> many new configuration and materials were developed for PSCs (**Figure 1**).<sup>[22]</sup>

In a typical PSC device, a perovskite layer is employed between an electron transporting layer (ETL) and a hole transporting layer (HTL). The bottom conducting substrate of a PSC is usually a transparent conducting oxide (TCO). The

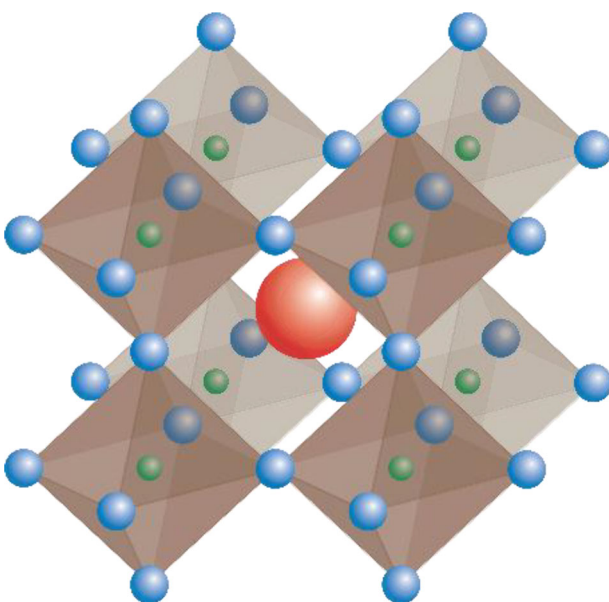


**Figure 1.** The crystal structure of perovskite.



**Ehsan Rezaee** obtained his Ph.D. degree in inorganic chemistry from the University of Mazandaran, Iran in 2013. He attended the University of Messina, Italy, as a visiting researcher to learn about single crystal x-ray crystallography. Now, he is a postdoctoral researcher at South University of Science and Technology of China. Currently, his research is focused on the design and synthesis of semiconducting inorganic materials and coordination compounds and developing new hole transporting materials for perovskite solar cells.



**Xiaoyuan Liu** received his B.S. degree from Henan University of Science and Technology in 2013. Now he is a Ph.D. student of Nanjing Tech University and a visiting student of South University of Science and Technology of China. His research interests focus on the design and synthesis of organic semiconductors as well as their application in perovskite solar cells and organic solar cells.



**Zong-Xiang Xu** is an Associate Professor in the Chemistry Department of South University of Science and Technology of China since 2012. In 2008, Dr. Xu received a Ph.D. degree in chemistry from the University of Hong Kong and then joined the City University of Hong Kong, where he completed postdoctoral research between 2010 and 2012. Currently, his research is focused on molecular materials design and its applications in new energy harvesting, such as perovskite solar cells.

PSCs can be classified into the conventional (n-i-p) and the inverted (p-i-n) devices based on whether the ETL or HTL is located adjacent to this bottom conducting substrate, respectively. There are also two dominant architectures for PSCs: mesoscopic nanostructure and planar heterojunction structure (**Figure 2**).<sup>[23]</sup> In mesoscopic PSCs, perovskite infiltrate a mesoporous scaffold of a semiconducting metal oxide (like  $\text{TiO}_2$ ) or an insulating metal oxide (such as  $\text{Al}_2\text{O}_3$  or  $\text{ZrO}_2$ ) to either aid film formation or charge extraction.<sup>[24]</sup>

However, the capability of ambipolar transport of electrons and holes by perovskites led to not using mesoporous scaffold in PSCs and the emergence of the planar heterojunction configuration. In their study, Etgar and coworkers have shown

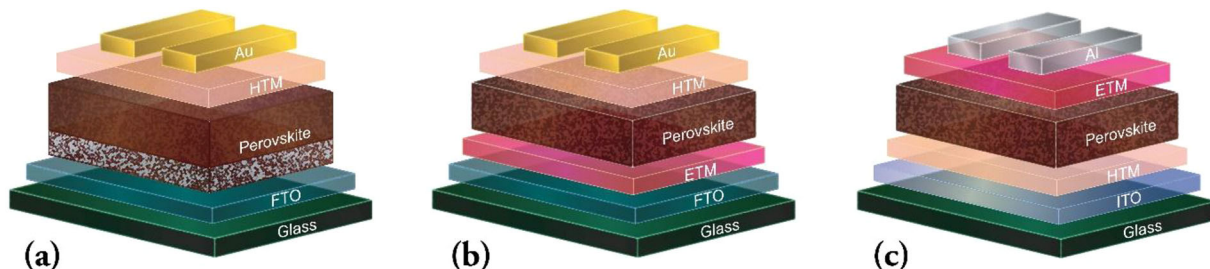


**Figure 2.** Perovskite device architectures: a) mesoscopic, b) conventional and c) inverted planar

that a solar cell with only two components including  $\text{TiO}_2-\text{CH}_3\text{NH}_3\text{PbI}_3$  also demonstrates the power conversion efficiency of 5% under simulated full sunlight, employing a Au cathode.<sup>[22]</sup> Hence, a conventional planar architecture contains conducting glass substrate (e.g., the fluorine doped tin oxide (FTO) substrate), ETL, perovskite layer, HTL, and metal electrode (e.g., Au or Ag), respectively. While, in an inverted planar configuration for PSCs, the perovskite layer is deposited on the hole-transport material (HTM) or directly on a contact electrode for holes extraction and then covered by an ETL (Figure 2).

#### 1.1.2. Fabrication of Perovskite Solar Cells

Solution based methods and physical vapor deposition are mainly used to fabricate perovskite layer in PSCs. Perovskite layer deposition can be carried out in one or two steps. A pre-mixed solution of  $\text{CH}_3\text{NH}_3\text{I}$  and  $\text{PbI}_2$  with high concentration

(e.g., 40 wt%) in a polar aprotic solvent, such as N,N-dimethylformamide (DMF), dimethyl sulfoxide (DMSO), or g-butyrolactone (GBL), is used to perform a one-step solution based fabrication of perovskite layer.<sup>[25]</sup> The perovskite is formed after an annealing process at 100 °C. In two-step solution deposition method, the  $\text{PbI}_2$  film was first formed by spin coating method and perovskite layer formed by subsequent immersing of  $\text{PbI}_2$  film in  $\text{CH}_3\text{NH}_3\text{I}$  solution followed by an annealing step.<sup>[26]</sup> Uniform films with high coverage also can be obtained by vapor deposition techniques, including co-evaporation of  $\text{CH}_3\text{NH}_3\text{I}$  and  $\text{PbI}_2$  and annealing at 100 °C.<sup>[27]</sup> The solar cell device performance depends on the properties of the fabricated perovskite film, such as the surface coverage, film uniformity and perovskite domain size, which is in turn highly dependent on the processing conditions.

Fabrication of PSCs starts with cleaning of FTO coated glass. Then a compact  $\text{TiO}_2$  layer is deposited as a hole blocking layer. In mesoscopic architecture, with careful controlling the

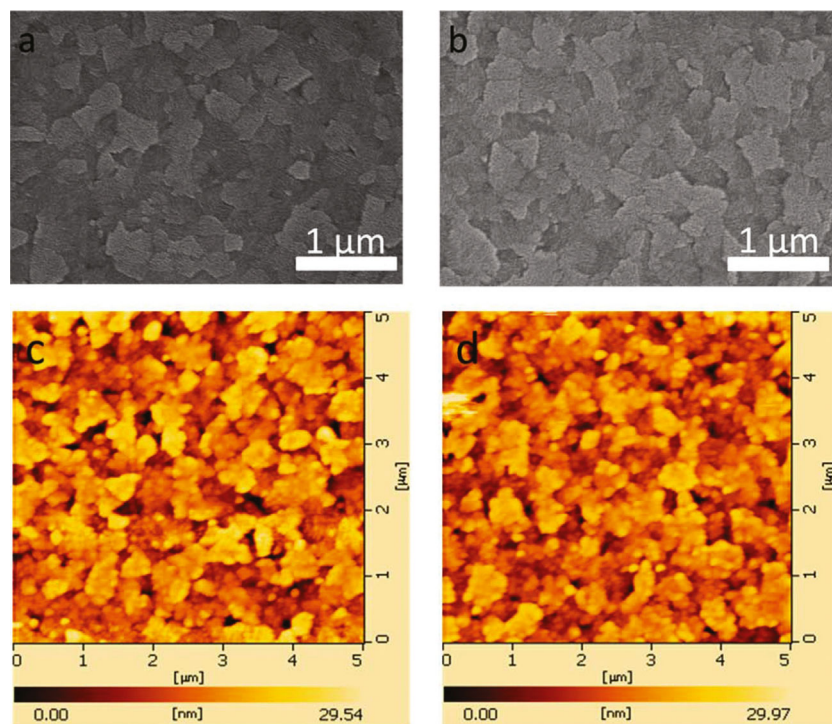


**Figure 3.** SEM images of bare ITO a) and  $\text{CuO}_x$  film b). AFM images of bare ITO c) and  $\text{CuO}_x$  film d). Reproduced with permission.<sup>[80]</sup> Copyright 2016, the Royal Society of Chemistry.

parameters like the thickness, pore size and porosity, a mesoporous  $\text{TiO}_2$  is added by spin coating and sintered at the temperature up to 500 °C. The perovskite layer is then deposited on  $\text{TiO}_2$  compact layer or infiltrated in the mesoporous scaffold. Deposition of HTM on perovskite layer, followed by thermally evaporated of a metallic cathode of gold (Au) or silver (Ag) onto the HTM layer, makes the PSC fabrication process complete.

PSCs can be fabricated on rigid glass and flexible plastic substrates. Large area perovskite solar modules have also been fabricated and their photovoltaic performances have been investigated by many research teams.<sup>[28]</sup> Flexible PSCs and large area modules build the future of solar energy conversion technology by realization of maximum solar light harvesting. However, in both cases, the device efficiencies still lagged their rigid and small area counterparts, due to the difficulties in their fabrication process, such as distortions, low temperature processing only, etc.<sup>[29]</sup> To date, different fabrication techniques have been employed for various active layers deposition for large area modules including spin coating, casting, blade coating, spray coating, and slot-die coating. It can be said that the first step towards commercialization of PSCs is to realize high efficiency of large area perovskite solar modules.<sup>[30]</sup>

### 1.1.3. Charge Transfer Process in PSC and the Role of HTM

Charge transfer process in PSCs starts with the photo-excitation of perovskite layer and generation of electron-hole pair. Then, the charge separation happens, and the photo-generated electrons and holes are transferred to the conduction band of ETM and the HOMO orbital of HTM, respectively. Eventually, photocurrent is generated due to the collection of electrons and holes by front and back electrodes.<sup>[31]</sup> Back electrons transfer from ETM to perovskite and back holes transfer from HTM to perovskite, as well as recombination of photo-generated charges can be mentioned as undesirable charge transfer processes in PSC devices.

Based on a study carried out by Cahen et al.,<sup>[32]</sup> perovskite layer has a better hole transporting ability than electrons. This result brought up the idea of HTM free PSCs.<sup>[22a,33]</sup> In this structure, the metal back contact is deposited directly on the perovskite layer. However, due to some researches comparing the performance of devices with and without HTM, there are some considerable differences in both charge recombination resistance ( $R_{\text{REC}}$ ) and series resistance ( $R_s$ ) in these devices.<sup>[34]</sup> This is mainly because of the high charge recombination rate at the perovskite/electrode interface, which definitely resulted in the relatively low PCE.<sup>[34b,35]</sup> Blocking electron transfer to anode by serving as a barrier between anode and perovskite, improving the efficiency of hole transporting process, influencing the open voltage circuit ( $V_{\text{oc}}$ ) and avoiding the degradation at the metal (Au)/perovskite interface are the most important roles that HTM can play in a PSC. Efficient device operation can be achieved using HTMs with high hole mobility, compatible ionization potential, high thermal stability and resistance to external degradation factors such as oxygen and moisture, as well as low electron affinity. For commercializing, HTMs should also be low cost.

It should be noted that, many HTMs are still expensive<sup>[36]</sup> or suffering from low hole mobility and low conductivity in their pristine forms.<sup>[36c]</sup> Ionic additives or *p*-type dopants, such as

lithium bis(trifluoromethylsulfonyl) imide (Li-TFSI)<sup>[37]</sup> and 4-*tert*-butylpyridine (tBP)<sup>[37]</sup> can be introduced to improve the free charges generation and the conductivity of HTMs. However, as their first and main disadvantage, due to the deliquescent properties of some *p*-type dopants, cell degradation might be accelerated. This can significantly jeopardize the future commercialization of PSCs. As their second problem, using dopants can increase the difficulty of the cell production and consequently the overall cost and also requires some special optimization of the doping conditions, such as the species of the dopants and the solvent used, as well as the concentrations of the dopants.<sup>[38]</sup> The third disadvantage of using *p*-type dopants with HTMs can be their strong tendency to diffuse, as they are not covalently bonded to the HTM host molecules.<sup>[39]</sup> It should also be noted that in most cases, the high PCEs have been achieved by PSCs with doped spiro-OMeTAD, so far. Therefore, developing dopant-free HTMs with facile synthesis routes, operation stability, well-matched HOMO energy levels, and good hole mobility are paramount. However, using dopants in inorganic HTMs follows a quite different concept compared to organic ones and brings up some advantages, including perovskite crystallization, improving the electrical conductivity, and energy level matching. The fact is the dopants are used in organic small molecular and polymeric HTMs because of their poor electrical properties and in most cases, this leads to the additional hole conduction of HTM molecules due to oxidation of HTM molecules and the presence of additional hole concentration. In case of inorganic HTMs, the incorporation of ions into semiconducting films and substitution of different ions contributes to both increased carrier concentration and carrier mobility. Together with increased work function of the films, the charge transfer and extraction of HTM films are improved.<sup>[40]</sup> Up to now various dopant-free solid-state HTMs have been developed, and can be classified to three main categories, including inorganic, small molecules, and polymeric HTMs, which are reviewed in this study.

## 2. Dopant-Free Hole Transporting Materials For PSCs

### 2.1. Inorganic HTMs

Solution processed inorganic *p*-type semiconductors appear to be an appealing alternative for hole transporting layer in PSCs, owing to their high hole mobility, high thermal and chemical stability and cost-effective fabrication process. However, the solvents using for inorganic HTMs film fabrication can dissolve the perovskite layer, which may cause the perovskite layer degradation and decrease the stability of PSC.

#### 2.1.1. CuI

CuI has large band gap (3.1 eV), high hole mobility (0.2–2  $\text{cm}^2 \text{V}^{-1} \text{s}^{-1}$ ), good chemical stability and low production cost.<sup>[41]</sup> These unique properties make CuI as an excellent choice as a hole conductor. Pioneering works done by Kamat et al. achieved a PCE as high as 6% using CuI as HTM for highly

stable PSCs. Higher fill factor (FF) observed for CuI-based devices was explained by its higher electrical conductivity.<sup>[42]</sup> Although, the efficiency obtained with dopant-free CuI was still lower than with spiro-OMeTAD, however it was considered as an encouraging value for low cost hole conductor for PSCs. In 2016, Moshaii et al., obtained a CuI thin film as HTM. A gas-solid reaction was employed to avoid the excessive wetting and dissolution.<sup>[43]</sup> The best PCE was 7.4% with a low hysteresis in the normal PSC architecture of fluorine-doped tin oxide (FTO)/ $\text{TiO}_2/\text{CH}_3\text{NH}_3\text{PbI}_3/\text{CuI}/\text{Au}$ .

CuI was also widely used in inverted planar heterojunction PSCs. A PSC with PCE of as high as 13.58% was achieved by employing low-cost solution processed CuI as the HTM in a study carried out by Chen et al.<sup>[44]</sup> This result is slightly exceeding the PEDOT:PSS based device with a PCE of 13.28% under the same experimental conditions. Due to the deeper valence band (VB) position and the higher efficiency in charge transport, CuI-based devices showed higher  $V_{OC}$  and short-circuit photocurrent density ( $J_{SC}$ ). In 2016, Sun et al. reported an impressive PCE of 16.8% for an inverted planar perovskite device employing low-temperature solution-processed pristine CuI as HTM.<sup>[45]</sup> The high efficiency obtained was ascribed to be mainly due to the effectiveness of CuI hole selective layer in reducing energy loss at the interface between the HTM and perovskite layer, leading to improved charge extraction and inhibited charge recombination in the HTM/perovskite interface. Higher efficiencies of CuI-based PSCs with inverted structure, compared to ones with conventional structure, can be attributed to easy fabrication of compact and uniform solution-processed CuI films on FTO or ITO substrate rather than perovskite layer. Dissolving perovskite layer by solvents using for CuI film fabrication is one of the main obstacles for achieving homogeneous HTM film with full coverage on perovskite layer.

### 2.1.2. CuSCN

Solution precipitated CuSCN is formed in two crystal phases,  $\alpha$ -phase with orthorhombic and  $\beta$ -phase with hexagonal or rhombohedral crystal lattice. While the latter is mostly exhibited in thin films. The *p*-type conductivity of CuSCN originates from copper vacancies in the crystal lattice, which creates a stoichiometric deficiency of copper atoms in the solid and leads to the hole transporting character of CuSCN.<sup>[46]</sup> This copper deficiency also broadens its optical bandgap and improve the optical transparency of CuSCN. Since, decomposition of CuSCN into copper sulfide is only observed at temperatures above 300 °C, this high thermal stability of CuSCN also helps for applications in thin film transistors,<sup>[47]</sup> quantum dot sensitized solar cells,<sup>[48]</sup> organic photovoltaics,<sup>[49]</sup> DSSCs,<sup>[50]</sup> and PSCs.<sup>[51]</sup>

In a study by Ito et al., a conventional PSC with  $J_{SC}$  of 15.2 mA cm<sup>-2</sup>,  $V_{OC}$  of 0.64 V, FF of 0.5 and power conversion efficiency as high as 4.85% has been fabricated by applying hot-air drying during spin coating of the  $\text{CH}_3\text{NH}_3\text{PbI}_3$  layer and using CuSCN as a dopant-free HTM.<sup>[52]</sup> This was the first report on using CuSCN as HTM for conventional PSC. Chavhan et al. has demonstrate the viability of using CuSCN as

a hole selective layer in planar heterojunction-based perovskite solar cell with a power conversion efficiency of 6.4%.<sup>[53]</sup> Using doctor blading deposition method, an improved PCE as high as 12.4% under full sun illumination has been obtained for conventional mesoscopic PSC employing CuSCN HTM.<sup>[54]</sup> In a study, Madhavan et al. also reported a high efficiency PSC employing CuSCN as inorganic dopant-free HTM.<sup>[55]</sup> Doctor blading and spin coating deposition methods have been used to prepare films with different thicknesses. The devices based on doctor blading deposited CuSCN HTM with the thickness of 500 nm displayed a PCE of as high as 16.6%, and the comparable efficiency of 15.43% has been achieved for PSCs with spin coated uniform CuSCN layer with 30 nm thickness. Under similar conditions, the device without CuSCN showed a PCE of 9.5%, with a significant decrease in the  $J_{SC}$  and  $V_{OC}$  that was mainly due to the effective charge transfer between perovskite and CuSCN, followed by the fast hole transport through CuSCN to the Au. In a recent report, Arora and coworkers have demonstrated conventional PSCs achieving stabilized efficiencies exceeding 20% with CuSCN as hole extraction layer, without using any *p*-type dopants.<sup>[56]</sup> Employing a fast solvent removal method, highly conformal CuSCN compact layer has been obtained that facilitate fast carrier extraction and collection. Based on time-correlated single photon counting (TCSPC) spectroscopy studies, they also disclosed the faster hole transfer across the perovskite-CuSCN junction as compared to the perovskite/spiro-OMeTAD interface, which was attributed to stronger interfacial interactions between the Pb ions of the perovskite and sulfide of CuSCN than with the organic layer. Additionally, the homogeneous coverage of the perovskite over the CuSCN layer has been revealed by the help of scanning electron microscopy (SEM). Studies have also been carried out to employ CuSCN as HTM in inverted PSCs. Zhao et al. have reported an inverted planar PSC, in which a highly facile, solution processed CuSCN film has been implemented as dopant-free HTM.<sup>[57]</sup> HTM film has been fabricated by spin coating the solution of CuSCN in dipropylsulfide (DPS). Compared to a reference cell based on the PEDOT:PSS HTM, a substantial increase in PCE (10.8% compared to 9.7% for the reference cell) has been observed that was suggested to be mainly attributed to a considerable increase in  $V_{OC}$  by 0.23 V. Using aqueous ammonia as a novel alternative to conventional *n*-alkyl sulfide solvents, in a study by Wijeyasinghe et al., ultrathin (3–5 nm) spin coating deposited CuSCN layer have been obtained in an inverted PSC, which provided higher hole mobilities due to better and uniform coverage films and led to a remarkably improved PCE of 17.5%.<sup>[58]</sup> However, highest efficiencies have been achieved for normal PSCs employing spin coated CuSCN HTM. Spin coating deposition method can be a proper choice due to the solubility of CuSCN in some solvents like DPS, DES (diethylsulfide), and aqueous ammonia, and the ability of this method to deposit thin, compact, and uniform films. CuSCN is an extremely cheap and abundant *p*-type semiconductor that has a large band gap of 3.8 eV and exhibits high hole mobility (0.01–0.1 cm<sup>2</sup> V<sup>-1</sup> s<sup>-1</sup>) and good thermal and chemical stability.<sup>[46,59]</sup> With these merits of CuSCN, the realization of the large-scale deployment of PSCs with efficiencies over 20% can be an achievable goal.

### 2.1.3. $\text{NiO}_x$

$\text{NiO}_x$ , as a typical *p*-type semiconductor with hole collection characteristics has been previously used as a photocathode material of dye-sensitized solar cell (DSSC).<sup>[60]</sup> In 2008, Irwin and coworkers have reported an enhancement in performance of polymer bulk heterojunction solar cells by inserting a thin *p*-type semiconducting  $\text{NiO}$  layer between the active organic layer and the ITO.<sup>[61]</sup> Since then,  $\text{NiO}$  became one of the HTM choice in DSSC and in organic photovoltaic (OPV) devices.<sup>[62]</sup> However, the first attempt to use  $\text{NiO}$  as HTM of PSCs reported by Docampo et al. merely resulted in an extreme low PCE of 0.1%.<sup>[63]</sup> An efficiency up to 0.71% have been achieved on the basis of the  $\text{CH}_3\text{NH}_3\text{PbI}_3/\text{NiO}$  solar cell at  $100 \text{ mW cm}^{-2}$  light intensity in a study by Wang et al. in 2014.<sup>[64]</sup> Further studies have led to higher efficiencies for PSCs. Zhu et al. have employed a simple sol-gel-processed  $\text{NiO}$  nanocrystal (NC) layer, with the optimum thickness of 40 nm, as the hole-transport layer in an inverted perovskite solar cell, and improved the PCE of 9.11%.<sup>[65]</sup> The layer of  $\text{NiO}$  nanocrystals with the size of 10–20 nm showed a higher transparency than that of conventional  $\text{NiO}$  thin films. Its corrugated surface also could support an approximately 300 nm thick film of perovskite with good coverage and interconnectivity. A remarkable efficiency of 9.51% of power conversion have been achieved by Wang et al. based on a methylammonium lead iodide ( $\text{CH}_3\text{NH}_3\text{PbI}_3$ ) perovskite/ $\text{NiO}$  heterojunction solar cell, in which a mesoscopic  $\text{NiO}$  acted as an efficient hole collecting contact.<sup>[66]</sup> In the device structure, a very compact layer of  $\text{NiO}_x$  without pinholes or crevices has been fabricated on FTO glass followed by a mesoscopic  $\text{NiO}$  nanocrystalline layer with sizes around few tenths of nanometers. In 2016, Yin et al. fabricated  $\text{NiO}_x$  film using spin coating of a pre-synthesized high quality  $\text{NiO}_x$  nanoparticle solution. The solution-based  $\text{NiO}_x$  showed excellent hole extraction and electron blocking property and fabricated inverted PSCs based on  $\text{NiO}_x$  HTM demonstrated a PCE of 16.47% on an ITO-glass substrate, with  $V_{\text{OC}}$  of 1.07 V,  $J_{\text{SC}}$  of  $20.6 \text{ mA cm}^{-2}$ , and FF of 74.8%.<sup>[67]</sup> In comparison, the PEDOT:PSS-based device only outputs a PCE of 11.39%, due to the lower  $V_{\text{OC}}$  and  $J_{\text{SC}}$ . Efficient  $\text{NiO}_x$  film deposition methods mostly need high temperature post annealing treatment, which are incompatible with flexible substrates. Using the solution-based deposition of hole contact layer at a temperature as low as  $130^{\circ}\text{C}$  without any post-treatments, Yin et al. have also developed a flexible perovskite solar cell using ITO-PEN (polyethylene naphthalene) substrate and achieved preliminary efficiency of 13.43%. PCE of as high as 15.2% has been reported for a highly stable PSC in a study by Islam et al.<sup>[68]</sup> The sputter-deposited polycrystalline  $\text{NiO}_x$  HTL has been used to develop an efficient and hysteresis-free inverted planar lead halide perovskite ( $\text{MAPbI}_{3-x}\text{Cl}_x$ ) solar cell. The PSCs fabricated in this method have showed no degradation under dark conditions at  $85^{\circ}\text{C}$ . They maintained over 85% of their initial efficiency for more than 670 h at the maximum power point tracking (MPPT) under 1 sun illumination at  $30^{\circ}\text{C}$ , and over 73% of the initial efficiency for more than 1000 h, at the accelerating aging test ( $85^{\circ}\text{C}$ ) under the same MPPT condition. Due to these results, it has been suggested that  $\text{NiO}_x$  as HTM can be a good candidate to solve the stability problems in inverted planar PSCs. Employing undoped

solution-processed  $\text{NiO}_x$  film with the optimum thickness of 334.2 nm as HTM in PSC, Yin et al. have achieved a PCE of 15.71% with a  $J_{\text{SC}}$  of  $20.51 \text{ mA cm}^{-2}$ , a  $V_{\text{OC}}$  of 988 mV, and a FF of 77.51% with almost no hysteresis.<sup>[69]</sup> Recently,  $\text{NiO}_x/\text{CuSCN}$  hybrid inorganic dopant-free HTL has been used in an air stable, conventional planar PSC to achieve the PCE of as high as 17.2%.<sup>[70]</sup> A uniform film with a dense morphology has been obtained by enabling direct deposition of  $\text{NiO}_x$  nanoparticle film on perovskite layer. It has been found that introducing an interfacial layer of CuSCN between  $\text{NiO}_x$  film and the top metal electrode can effectively improve the PCE of PSC from 10.4 to 17.2%. The two beneficial effects of the interfacial layer on device performance are ascribed to shutting off the charge recombination paths and increasing charge percolation paths. However, it should be noted that power conversion efficiencies between 15 and >17% also achieved by employing heavily doped  $\text{NiO}$  layer with oxygen<sup>[71]</sup> or metal ions like  $\text{Li}^+$ ,  $\text{Mg}^{2+}$ ,<sup>[72]</sup> or  $\text{Cu}$ .<sup>[73]</sup> Using solution-processed Cu-doped  $\text{NiO}_x$  as HTM, Kim et al. have reported PCEs up to 15.40% and good stability for Perovskite devices.<sup>[73]</sup> The device based on pristine  $\text{NiO}$  showed a considerably lower PCE ( $\approx 8.9\%$ ). It has been demonstrated that Cu-doping with a very simple and effective method can improve the electrical conductivity of  $\text{NiO}_x$  and lead to a favorable perovskite crystallization. Moreover, energy level matching between the VB of Cu-doped  $\text{NiO}_x$  HTM and a deep lying VB perovskite like  $\text{MAPb(I}_x\text{Br}_{1-x})_3$  has been suggested to be a key to maximize the performance of perovskites with higher  $E_g$ .  $\text{Cu:NiO}_x$  has also been used as HTM in an inverted PSC by Zhang and coworkers and an evolution of photovoltaic performance has been observed over time, which was demonstrated to be associated with the variety of crystallized quality and conductivity of as-prepared films.<sup>[74]</sup> The normalized PCE of the device with  $\text{Cu:NiO}_x$  layer increases up to above 120% from the initial PCE value. Chen et al. have fabricated large area perovskite modules with inverted planar device architecture, employing  $\text{Mg}^{2+}$  doped  $\text{NiO}$ -based HTM layer, deposited by mean of spray pyrolysis.<sup>[72]</sup> The large-scale devices with active areas  $>1 \text{ cm}^2$  showed excellent performances with  $J_{\text{SC}}$ ,  $V_{\text{OC}}$ , and FF values of  $20.21 \text{ mA cm}^{-2}$ , 1.072 V, and 0.748, respectively. The efficiencies of such cells have reached to the value of 16.02%.

### 2.1.4. $\text{Cu}_2\text{O}$ , $\text{CuO}$ , and $\text{CuO}_x$

Wang et al. have performed a device modeling study on planar PSCs with  $\text{Cu}_2\text{O}$  as HTM.<sup>[75]</sup> They have suggested efficiencies above 13% could be achieved with an optimized HTL. With its high hole mobility, wide band gap and high optical transmittance,  $\text{Cu}_2\text{O}$  is considered as a promising inorganic HTM with great potential of application in PSCs. Based on a computational study, Hossain et al. also suggested  $\text{Cu}_2\text{O}$  as a good candidate for low cost high efficiency HTMs in PSCs.<sup>[76]</sup> Their results based on the assumption of defect free perovskite and HTM layers, showed that solar cells containing  $\text{Cu}_2\text{O}$  as HTM, with the PCE over 24%, outperform all other devices with organic or inorganic HTM previously tested. In 2015, Zuo and coworkers developed method to prepare  $\text{Cu}_2\text{O}$  and  $\text{CuO}$  films for employing as dopant-free HTM in PSCs.<sup>[77]</sup>  $\text{Cu}_2\text{O}$  film was prepared via in situ conversion of  $\text{CuI}$  film in an aqueous NaOH solution and  $\text{CuO}$

film was made by heating Cu<sub>2</sub>O film at 250 °C in air. PCEs of 13.35 and 12.16% were achieved for PSCs with Cu<sub>2</sub>O and CuO as HTMs, respectively. Based on XRD studies, the crystallinity of perovskite film was improved on Cu<sub>2</sub>O compared to that on CuO layer. In 2016, Chatterjee et al. reported a PCE of 8.23% for a direct p-i-n planar PSC (Cu<sub>2</sub>O/MAPbI<sub>3</sub>/PCBM).<sup>[78]</sup> However, achieving a uniform and full coverage film of Cu<sub>2</sub>O by using solution deposition method faced still difficulties. Nejand et al. have used rotational angular deposition method to obtain a compact and crack-free Cu<sub>2</sub>O layer with high surface coverage of the perovskite layer, which resulted in high rate of charge extraction. A PCE of as high as 8.93% has been achieved for Cu<sub>2</sub>O based PSC.<sup>[79]</sup> In a study by Sun et al., a CuO<sub>x</sub> film has been fabricated through deposition of a cupric acetylacetone (Cu(acac)<sub>2</sub>) precursor onto ITO by a spin-coating method, followed by annealing at 80 °C in air and ultraviolet-ozone (UV-O<sub>3</sub>) treatment.<sup>[80]</sup> **Figure 3** shows the surface microstructure of CuO<sub>x</sub> film deposited on ITO substrate characterized by scanning electron microscopy (SEM) and atomic force microscopy (AFM). Modification of ITO surface with CuO<sub>x</sub> film provided a smoother surface with root mean square (RMS) of 4.2 nm compared to 4.7 nm for bare ITO. This can be beneficial in decreasing the possibility of current leakage. Smooth surface of CuO<sub>x</sub> film also led to improved light transmittance of ITO substrate. The ratio of Cu<sup>+</sup>/Cu<sup>2+</sup> in the CuO<sub>x</sub> film was also investigated by the help of X-ray photoelectron spectroscopy (XPS). Calculated from the deconvolution of the Cu 2p<sub>3/2</sub> peak, this ratio was 2.0:1. The highest PCE of 17.1% was obtained in an inverted planar PSC with the CuO<sub>x</sub> film as HTM. Electrochemical impedance spectra (EIS) of PSCs based on CuO<sub>x</sub> HTM suggested the low contact resistance at the CuO<sub>x</sub>/perovskite interface, which is a major factor for the high FF obtained in these devices. The time-resolved photoluminescence (PL) spectra of the CuO<sub>x</sub>/perovskite interface has been studied. The fast decay lifetime of CuO<sub>x</sub>/perovskite interface of 0.9 ns with weight fraction of 79.9% indicated that the hole carriers are efficiently transferred from the perovskite layer to the CuO<sub>x</sub> layer rather. Therefore, fast hole carrier transfer from the perovskite to the CuO<sub>x</sub> layer was also considered as one of the effective factors controlling the high performance of CuO<sub>x</sub> based devices. The same group also reported a remarkable efficiency of 19.0% for PSCs with Cl-doped perovskite layer and same CuO<sub>x</sub> HTM layer.<sup>[81]</sup> A novel Cl doping process based on a modified one-step fast deposition-crystallization method has been used to fabricate a hybrid CH<sub>3</sub>NH<sub>3</sub>PbI<sub>3-x</sub>Cl<sub>x</sub> to enhance the hole mobility of perovskite film and improve its morphology.

In 2017, Yu et al. reported a best PCE of 17.43% with a V<sub>OC</sub> of 1.03 V, a J<sub>SC</sub> of 22.42 mA cm<sup>-2</sup>, and a fill factor of 0.76, for an inverted PSC with the structure of ITO/CuO<sub>x</sub>/MAPbI<sub>3</sub>/PC<sub>61</sub>BM/ZnO/Al.<sup>[82]</sup> Under the same experimental condition, a PSC with PEDOT:PSS as HTM showed a PCE of 11.98%. These studies showed that high-quality CH<sub>3</sub>NH<sub>3</sub>PbI<sub>3</sub> films grown on the CuO<sub>x</sub> and the efficient hole extraction through the CuO<sub>x</sub> layer are declared as the two important factors in enhancing the performance of PSCs. Therefore, the preparation method of CuO<sub>x</sub> layer can be considered as a crucial factor on controlling the quality of perovskite layer on it and the photovoltaic performance of PSCs.

### 2.1.5. Inorganic Nanomaterials as HTM

Wu et al. have applied Kesterite-structured quaternary semiconductor Cu<sub>2</sub>ZnSnS<sub>4</sub> (CZTS) nanoparticles as an inorganic HTM for PSCs for the first time, and a PCE of 12.75% has been achieved under the optimized conditions (size of CZTS nanoparticles is 20 ± 2 nm, the thickness of CZTS HTM layer is ca. 200 nm).<sup>[83]</sup> Koo et al. employed octadecylamine-capped pyrite nanoparticles (ODA-FeS<sub>2</sub> NPs) as a bi-functional layer (charge extraction layer and moisture-proof layer) for PSCs and the best-performing device shows a power conversion efficiency of 12.6% and maintains stable photovoltaic performance in 50% relative humidity for 1000 h.<sup>[84]</sup> CuS nanoparticles were also introduced as a hole-selective contact material in an inverted planar heterojunction (PHJ) perovskite solar cell in a study by Rao et al.<sup>[85]</sup> In this report, the CuS nanoparticles were spin coated on the surface of ITO substrate to reduce the surface energy level of ITO substrate from -4.9 to -5.1 eV and serve as HTM. With high transmittance of ITO:CuS substrate in the visible range of 400 to 800 nm, enough absorption of light by perovskite layer to generate large photoelectron can also be ensured (**Figure 4**). A maximum PCE over 16%, with low hysteresis, excellent stability, and reproducibility has been achieved for the PSCs based on CuS nanoparticles.

A dopant-free HTM of MoO<sub>2</sub> nanoparticles has been employed in a planar type CH<sub>3</sub>NH<sub>3</sub>PbI<sub>3</sub> perovskite solar cell and a stable efficiency of 15.5% has been exhibited.<sup>[86]</sup> A scalable new process of combining the ultrasonic spray pyrolysis and solvothermal cracking process has been used to synthesize ≈10 nm sized MoO<sub>2</sub> nanoparticles with high BET surface area of 170.14 m<sup>2</sup> g<sup>-1</sup>. In 2017, a new hole transporting material was presented in a study carried out by Jin et al.<sup>[87]</sup> They employed Cu<sub>2-x</sub>GeS<sub>3</sub> (CGS) nanoparticles film as a new kind of cost-effective HTM for perovskite solar cell. The best performed cell with CGS HTL delivered a PCE of 14.48%. Compared with the conventional spiro-OMeTAD, the Cu<sub>2-x</sub>GeS<sub>3</sub> nanoparticle film generated 5% improvement in PCE. Due to high hydrophobicity of CGS nanoparticle film, an enhancement was also observed in the moisture stability of the PSC devices. It was indicated that at a relative humidity (RH) of 50% in air, the device maintained 95% of its initial PCE after storing for 30 days. Zhang et al. have reported the use of solution-processed inorganic nanoplates CuGaO<sub>2</sub> as dopant-free HTM in the n-i-p configuration PSCs.<sup>[88]</sup> They have achieved an impressive PCE of 18.51% and significant improvement in the long-term stability of PSCs. It was demonstrated that based on its good optical transparency (due to its large band-gap, 3.58 eV), proper low-lying valence band maximum (≈-5.3 eV), and high hole mobility (10<sup>-2</sup>-10<sup>1</sup> cm<sup>2</sup> V<sup>-1</sup> s<sup>-1</sup>),<sup>[89]</sup> CuGaO<sub>2</sub> can be a promising HTL candidate for improving photovoltaic performance, device stability, and fabrication cost of PSCs.

### 2.1.6. Quantum Dots (QDs)

Quantum dots have many distinctive features that make them suitable for application in photovoltaic devices. They have tunable bandgap,<sup>[90]</sup> inherently high absorption coefficient,<sup>[91]</sup> hot electron transfer,<sup>[92]</sup> and multiple exciton generation.<sup>[93]</sup> Metal chalcogenide QDs have been demonstrated with the new record efficiency in

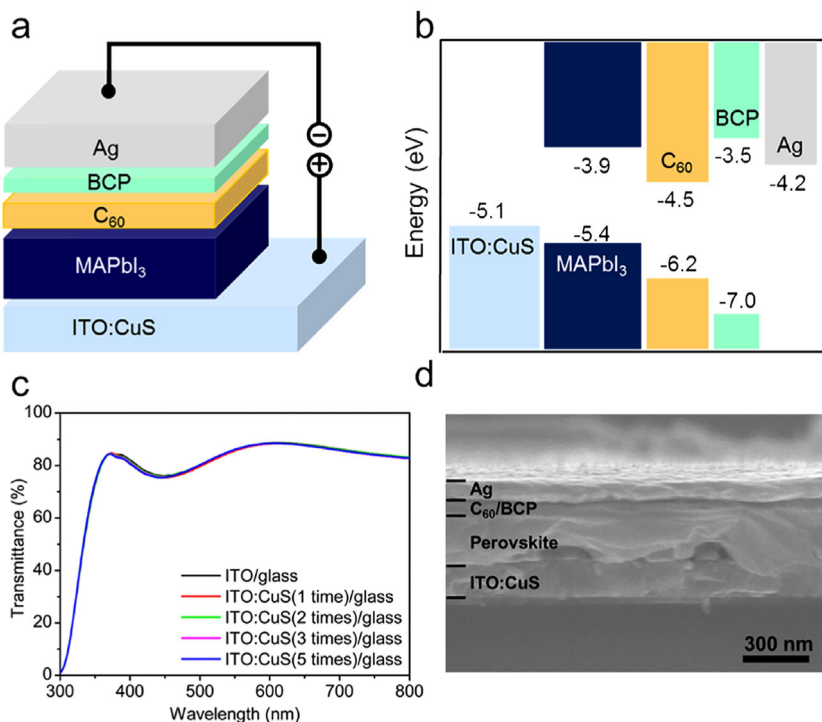


**Figure 4.** a) Schematic of the device structure (ITO:CuS/CH<sub>3</sub>NH<sub>3</sub>PbI<sub>3</sub>/C<sub>60</sub>/BCP/Ag). b) Energy-level diagram of the device components (relative to the vacuum level). c) Optical transmission spectra of the ITO:CuS/glass with ITO/glass as a reference. d) Cross-sectional image of the CuS NPs-based device. Reproduced with permission.<sup>[85]</sup> Copyright 2016, American Chemical Society.

liquid quantum dot dye sensitized solar cells (QDSSCs).<sup>[94]</sup> Long et al. have used doped PbS colloidal quantum dots (CQD) as an effective HTM for planar PSCs and a PCE of 7.5% has been achieved.<sup>[95]</sup> Since PbS CQDs have a large excitonic Bohr radius of 18 nm and a low bulk energy bandgap of 0.41 eV, the bandgap of PbS CQDs can be engineered through size-tuning in PbS CQDs synthesis. Employing CuInS<sub>2</sub> QDs as dopant-free HTMs in PSC, Zhu et al. have reported a PCE of as high as 8.38%.<sup>[96]</sup> In 2016, Yuan et al. have addressed recombination and band-edge shift as the two important factors that play important roles in open-circuit voltage ( $V_{OC}$ ) improvement of metal chalcogenide HTM based PSCs.<sup>[97]</sup> The quaternary Cu<sub>2</sub>ZnSnS<sub>4</sub> (CZTS) and Cu<sub>2</sub>ZnSnSe<sub>4</sub> (CZTSe) QDs were employed as HTM into PSCs. By replacing sulfur with selenium atom, the band gap of HTM was tuned from 1.64 to 1.14 eV. A PCE of 10.72 and 9.72% are achieved for PSCs with CZTS and CZTSe QDs as dopant-free HTMs, respectively. The  $V_{OC}$  of CZTSe device was remarkably lower than that of CZTS device, which was mainly attributed to its lower valence band rather than the larger recombination process. They have proposed that the  $V_{OC}$  enhancement of CZTS device was mainly ascribed to the more downward valence band-edge shift of HTM (Figure 5).

#### 2.1.7. Graphene Oxide (GO)

Wu et al. has employed graphene oxide (GO) as HTM in PSC for the first time in 2014.<sup>[98]</sup> In a device with CH<sub>3</sub>NH<sub>3</sub>PbI<sub>3-x</sub>Cl<sub>x</sub> as light absorber, a PCE of up to 12.4% has been achieved. It has been

found that the perovskite films grown on GO possess highly textured perovskite crystal domains and preferential in-plane orientation of the (110) plane. Li et al. have used graphene oxide (GO) with amphiphilic function as a buffer layer between the perovskite and the HTL to improve the interface wettability of the HTL solution on a perovskite surface.<sup>[99]</sup> In a PSC with spiro-OMeTAD as HTM and GO as insulating buffer layer, an enhance in the average efficiency from 10 to 15.1% has been observed. Using spin-coated GO as buffer layer between the perovskite and spiro-OMeTAD in PSCs, Agresti et al. observed the maximum PCE of 14.11%.<sup>[100]</sup> However, doping the mesoporous TiO<sub>2</sub> layer with graphene flake increased the PCE up to the remarkable value of 18.19%. In 2017, a high PCE of 16.5% with no hysteresis was also observed for PSCs using GO thin film with optimized thickness and high work function as a HTM.<sup>[101]</sup> The PSCs showed excellent light-soaking photocurrent stability in comparison with a commonly used organic-based HTM. It was demonstrated that the improvement in photovoltaic performance of PSCs was attributed to the larger grain size of perovskite growing on a GO film, enhanced charge collection efficiency with better alignment of interfacial energy, and higher optical absorption of the active layer.

#### 2.1.8. Carbon Nanomaterials

Due to their excellent stability and low cost, carbon materials have been used in perovskite solar cells to replace the expensive

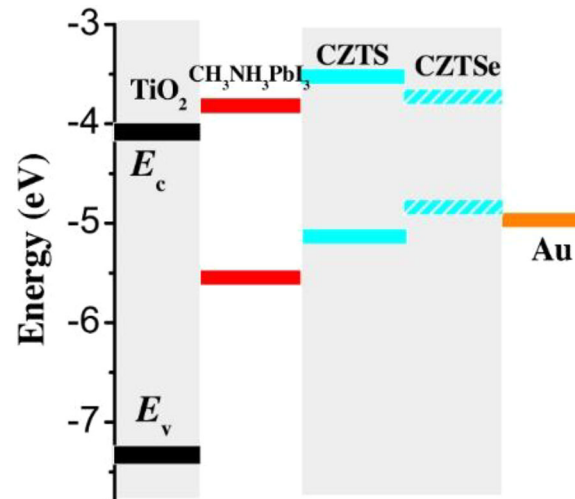


**Figure 5.** Energy level alignment of perovskite solar cells with CZTS and CZTSe QDs as HTM layers. Reproduced with permission.<sup>[97]</sup> Copyright 2016, Elsevier Ltd.

HTM and noble metal electrode.<sup>[102]</sup> Li et al. have reported a PCE up to 5.28% with high open circuit voltage ( $V_{OC}$ ) close to 1.4 V under AM 1.5, 100 mW cm<sup>-2</sup> conditions for perovskite devices using carbon nanotube (CNT) as hole conductor.<sup>[103]</sup> A thin layer of poly(methyl methacrylate) (PMMA) has been deposited on the carbon nanotube layer to improve the contact between CNTs and perovskite. Using a double layer structure of polymer-wrapped single-walled carbon nanotubes and undoped spiro-OMeTAD as HTM, Habisreutinger et al. reported a steady-state efficiency of up to 18.8% for PSCs with both mixed organic A-site cations and mixed halides (FA<sub>0.83</sub>MA<sub>0.17</sub>Pb(I<sub>0.83</sub>Br<sub>0.17</sub>)<sub>3</sub>).<sup>[104]</sup> The scanned efficiency of 18.7% and stabilized efficiency of 17.6% have been recorded for the control device with fully doped spiro-OMeTAD.

### 2.1.9. Other Inorganic HTMs

Other various categories of inorganic semiconducting materials have also been investigated as dopant free HTMs in PSCs in last 2 years to achieve higher PCEs for more stable PSCs. Chen et al. have used MoSe<sub>2</sub> as HTM in a PSC with an FTO/MoSe<sub>2</sub>/perovskite/C<sub>60</sub>/bathocuproine (BCP)/silver structure.<sup>[105]</sup> Optimization of the crystallinities of the perovskite layers through an annealing process of the CH<sub>3</sub>NH<sub>3</sub>PbI<sub>3</sub> (MAPbI<sub>3</sub>) perovskite films, deposited on the MoSe<sub>2</sub> HTM films led to the maximum power-conversion efficiency was 8.23%. Sanehira et al. have significantly improved the stability of PSCs with introducing various hole collecting anode configurations.<sup>[106]</sup> They have found that PSCs with MoO<sub>x</sub>/Al electrodes are more stable than devices with more conventional, and costlier, Au and Ag electrodes. It has been demonstrated that thinner MoO<sub>x</sub> interlayers yield more durable devices. A thin MoO<sub>x</sub> layer can prevent photobleaching of the MAPbI<sub>3</sub> film and mitigates decomposition. Two water-soluble two dimensional transition metal dichalcogenide, MoS<sub>2</sub> and WS<sub>2</sub> are used as HTM in PSCs in a study by Huang et al.<sup>[107]</sup> The highest PCEs of 14.35 and 15.00% were obtained for the PSCs with MoS<sub>2</sub> and WS<sub>2</sub>, respectively. In a very recent study, Qin et al. have achieved high PCE of 17.19% on glass and 15.53% on flexible PET substrates, introducing and employing a novel copper-chromium binary metal oxide as HTM for PSCs.<sup>[108]</sup> The copper-chromium binary metal oxide films have wide band gaps of around 3.1 eV, as well as suitable energy levels for both electron-blocking and hole-transporting. It has been shown that the energy level and phase composition of Cu<sub>y</sub>Cr<sub>z</sub>O<sub>2</sub> films can be modulated with different copper acetylacetone (y)/chromium acetylacetone (z) volume ratios in the reacting solution precursors. It has also been demonstrated that both mono Cu<sub>y</sub>O(z=0) or Cr<sub>z</sub>O(y=0) and binary CuCrO<sub>2</sub> and CuCr<sub>2</sub>O<sub>4</sub> phases can be formed in the film (Figure 6). In 2018, Zhang et al. reported an inverted PSCs based on low temperature solution-processed CuCrO<sub>2</sub> nanocrystals as HTM. A ≈45 nm thick compact CuCrO<sub>2</sub> layer was incorporated into an inverted planar configuration of indium tin oxides (ITO)/c-CuCrO<sub>2</sub>/perovskite/[6,6]-phenyl-C61-butric acid methyl ester (PCBM)/bathocuproine (BCP)/Ag and resulted in a high steady-state PCE of 19.0% versus 17.1% for the typical low temperature solution-processed NiO<sub>x</sub>-based devices. The CuCrO<sub>2</sub> HTM was also enabled to inhibit the UV-induced decomposition of perovskite, allowing a significant improvement of device

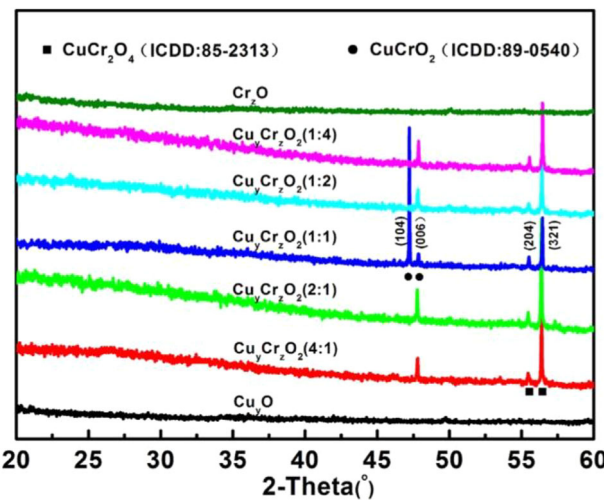


**Figure 6.** X-ray diffraction spectra of Cu<sub>y</sub>Cr<sub>z</sub>O<sub>2</sub> films on FTO substrate with copper acetylacetone and chromium acetylacetone as precursors, which were mixed at different volume ratios (that is y:z) of: 1:0, 4:1, 2:1, 1:1, 1:2, 1:4, and 0:1, respectively. Reproduced with permission.<sup>[108]</sup> Copyright 2017, Wiley-VCH.

photostability. Improved crystallinity of the perovskite film grown on the CuCrO<sub>2</sub>-based substrate led to more efficient charge carrier generation and transport through the perovskite film.<sup>[109]</sup>

A simple fabrication method for fabrication of VO<sub>x</sub> thin film as HTL in PSCs has been used by Yao et al. and average PCE of 10.47 ± 0.93% has been achieved.<sup>[110]</sup> By employing an aminopropanoic acid (APPA) interfacial layer to modify VO<sub>x</sub> thin film for reducing the charge carrier recombination rate, the average PCE,  $V_{OC}$ , FF, and  $J_{SC}$  have been improved to the values 13.45 ± 0.39%, 0.96 ± 0.02 V, 71.95 ± 1.61%, and 19.57 ± 0.63 mA cm<sup>-2</sup>, respectively.

Compared to organic HTMs, inorganic p-type semiconductors have simpler fabrication procedures with cheap starting materials. With their large band gaps, inorganic HTMs are mostly transparent across the whole visible-light region. They show high hole mobility in pristine form, which makes them suitable dopant-free HTMs for PSC. As a result, the optimization process is simpler, and the fabricated devices exhibit higher stability. In conventional n-i-p PSCs, inorganic HTMs are needed to be deposited on perovskite, without degradation of this layer. Due to the dearth of solvents that dissolve inorganic HTMs but not the perovskite, the number of choices of fabrication methods are limited in conventional rather than inverted configuration. However, PCEs around 20% have been achieved in both structures. The photovoltaic properties of some selected perovskite devices using inorganic HTMs are summarized in Table 1.

## 2.2. Polymer HTMs

### 2.2.1. Triarylamine Polymer Derivatives

Triarylamine polymer derivatives as conjugated homopolymers were used in PSCs for the first time by Heo et al.<sup>[111]</sup> In their

**Table 1.** Photovoltaic properties of some selected perovskite devices with inorganic HTMs.

$V_{OC}$ [V]	$J_{SC}$ [mA cm $^{-2}$ ]	FF	PCE [%]	ETL	Perovskite	HTM	Band edges (HOMO)	Hole mobility [cm $^2$ V $^{-1}$ s $^{-1}$ ]	Device architecture	References
1.1	21.8	69.2	16.6	TiO $_2$	(CH $_2$ (NH $_3$ ) $_2$ PbI $_3$ ) $_{0.85}$ (CH $_3$ NH $_3$ PbBr $_3$ ) $_{0.15}$	CuSCN	-5.3	0.01–0.1	n-i-p	[55]
1.24	22.7	71.5	16.0	C $_{60}$	CH $_3$ NH $_3$ PbI $_3$	CuS NPs	-5.1		p-i-n	[85]
1	22.2	75.7	17.1	C $_{60}$	CH $_3$ NH $_3$ PbI $_3$	CuO $_x$	-5.2		p-i-n	[80]
1.07	20.58	74.8	16.47	PCBM	CH $_3$ NH $_3$ PbI $_3$	NiO $_x$			p-i-n	[67]
1.01	19.8	77.5	15.5	TiO $_2$	CH $_3$ NH $_3$ PbI $_3$	MoO $_2$			n-i-p	[86]
1.08	20.33	69	15.2	PC $_{61}$ BM	CH $_3$ NH $_3$ PbI $_{3-x}$ Cl $_x$	NiO $_x$	-5.4		p-i-n	[68]
1.08	21.05	71	17.19	PCBM	CH $_3$ NH $_3$ PbI $_3$	Cu $_y$ Cr $_z$ O $_2$ (y: z = 2:1)	-5.18		p-i-n	[108]
1.03	22.42	76	17.43	PC $_{61}$ BM	CH $_3$ NH $_3$ PbI $_3$	CuO $_x$	-5.4		p-i-n	[82]
1.11	21.66	77	18.51	TiO $_2$	CH $_3$ NH $_3$ PbI $_{3-x}$ Cl $_x$	CuGaO $_2$	-5.29	10 $^{-2}$ –10 $^1$	n-i-p	[88]
1.00	21.6	76.2	16.5	C $_{60}$	CH $_3$ NH $_3$ PbI $_3$	GO	-5.2		p-i-n	[101]
1.14	23.35	77.5	20.4	TiO $_2$	CsFAMAPbI $_{3-x}$ Br $_x$	CuSCN		1.2 × 10 $^{-3}$	n-i-p	[56]

study, PTAA (poly[bis(4-phenyl)(2,4,6-trimethylphenyl)amine]) (1); the most studied triarylamine polymer, along with other types of polymers such as P3HT (poly-3-hexylthiophene) (2); PCPDTBT (poly-[2,1,3-benzothiadiazole-4,7-diyl[4,4-bis(2-ethylhexyl)-4H-cyclopenta[2,1-b:3,4-b']dithiophene-2,6-diyl]]) (3); and PCDTBT (poly-[[(9-(1-octylonyl)-9H-carbazole-2,7-diyl]-2,5-thiophenediyl-2,1,3-benzothiadiazole-4,7-diyl-2,5-thiophenediyl]]) (4) were employed as HTM in PSCs with mesoscopic structures. The highest PCE of 12.0% was obtained for the best device with LiTFSI and tBP doped PTAA as HTM. However, an efficiency of 10.9% for PSCs was reported with employing PTAA as HTM, without using LiTFSI and in the presence of tBP, in a study carried out by Bi et al.<sup>[112]</sup> Jeon et al. have reported a PSC with a bilayer architecture comprising mesoscopic and planar structures and MAPb(I $_{1-x}$ Br $_x$ ) $_3$  perovskites formed by a solvent-engineering technology.<sup>[113]</sup> They have achieved a PCE of as high as 16.5% by employing PTAA as HTM with using dopants. A series of poly(tetraphenylbenzidines) (PTPDs) was synthesized via Yamamoto polycondensation, and employed as HTM for PSCs by Neumann et al.<sup>[114]</sup> (Figure 7). A PCE of 3.59% was obtained for the devices with dopant-free HTMs. The average efficiency for PSC devices with HTM, doped by LiTFSI and tBP was 4.39%.

In 2016, Matsui et al. reported triarylamine-based polymers with different functional groups as dopant-free HTMs for stable PSCs.<sup>[115]</sup> They achieved PCE of 12.3% for devices employing poly(triarylamine) with methylphenylethynyl functional groups (5). The device was stable under 1 sun illumination at maximum power point tracking for approximately 40 h at room temperature, and in the dark under elevated temperature (85 °C) for more than 140 h. Using anode and cathode modifying layers in a PSC, Chang et al. have increased the device efficiency up to 18.08%.<sup>[116]</sup> In their study, a hole transporting composite material based on vanadium oxide (VO $_x$ ) and DPITPFB-doped X-DVTPD (a thermally cross-linked triarylamine-based material) (6) and fulleropyrrolidinium iodide as a hole-blocking interfacial layer at the interface with Ag have been employed in an inverted PSC. It was demonstrated that the presence of these

electronically active materials at the interfaces with the perovskite layer and the electrodes improved charge collection and transport characteristics and resulted in a high  $V_{OC}$  of 1.07 V and an improved  $J_{SC}$  of ~23.10 mA cm $^{-2}$ . Using PTAA as HTM, in a study by Stolterfoht and coworkers, stable dopant-free hybrid perovskite devices have been fabricated with a remarkable PCE of above 20% for an active area of 6 mm $^2$  and 18.9% for a device area of 1 cm $^2$ .<sup>[117]</sup> Based on their results, the transit time through the hole transport layer is the key figure of merit for maximizing the fill factor (FF) and efficiency. Therefore, employing ultrathin undoped HTLs in which the active perovskite fills nearly 95% of the cell volume can lead to highly efficient and stable devices.

## 2.2.2. Thiophene-Based Polymer Derivatives

In 2014, Agrawal et al. employed P3HT and PEDOT:PSS (poly(3,4-ethylenedioxythiophene): poly(styrenesulfonate)) (7) conjugated homopolymers as HTMs for PSCs without using dopants and efficiencies of 3 and 4.8% were achieved, respectively.<sup>[118]</sup> Before them, Conings et al. also reported the efficiencies up to 10.8% for PSC devices, in which the perovskite layer was sandwiched between selective contacts of TiO $_2$  and dopant-free P3HT.<sup>[119]</sup> By optimization of thickness and morphology of perovskite layer, with using vapor-phase deposition method of the PbI $_2$  precursor film, Liu et al. have reported efficiencies of up to 11.3% for PSC devices with P3HT as undoped HTM.<sup>[120]</sup> They have suggested that the efficiency of PSC can be declined sharply once the film thickness significantly exceeded the carrier diffusion lengths in CH $_3$ NH $_3$ PbI $_3$ . At the optimum thickness of 330 nm for perovskite layer, fabricated by solution-processed method, comparable efficiency of 11.8% has also been achieved. In another study in 2014, they reported an ETL free device with efficiency of as high as 11.6% (Figure 8).<sup>[121]</sup> With comparable performances obtained for devices with ZnO ETL, it was demonstrated that the ETL is not a prerequisite for obtaining excellent device efficiencies. Based on photoluminescence and impedance spectroscopy measurements, they suggested that this high performance is originated from both

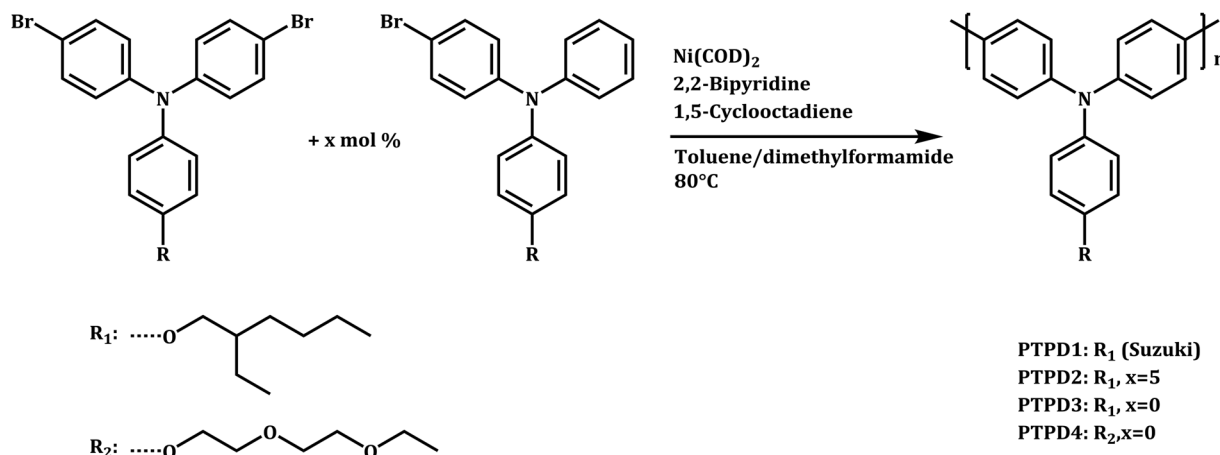


**Figure 7.** Synthesis of poly(tetraphenylbenzidines) (PTPDs). Reproduced with permission.<sup>[114]</sup> Copyright 2014, the Royal Society of Chemistry.

highly efficient hole extraction at the CH<sub>3</sub>NH<sub>3</sub>PbI<sub>3</sub>/HTL interface and reduced surface recombination at the ETL-free interface.

Researches have been carried out employing P3HT as dopant-free HTM for PSCs during the years 2015 and 2016, and PCEs about 6.17,<sup>[122]</sup> 7.5,<sup>[123]</sup> 8.3,<sup>[124]</sup> and 11.8%,<sup>[38b]</sup> have been reported. Significant power conversion efficiency of up to 13.82% has been reported in 2016 by Ye et al. for PSC devices using P3HT modified with F-graphene as HTM.<sup>[125]</sup> In 2017, however, in a research by Colorado, two different conjugated polymers, P3HT and PTB7:Th (8) were employed as dopant-free HTMs in PSCs.<sup>[126]</sup> Performances of around 14 and 12% in reverse voltage scans, or 13 and 10% in forward scans, were obtained for pristine P3HT and PTB7:Th based solar cells, respectively.

### 2.2.3. PEDOT:PSS

In 2016, Xiao et al. introduced a bifacial PSC employing a highly transparent PEDOT as the *p*-type HTM. Due to its well-matched

band positions for the charge separation and transport, PEDOT can play both roles of hole selecting and electron blocking layer at the CH<sub>3</sub>NH<sub>3</sub>PbI<sub>3</sub>/PEDOT interface to reduce the electron recombination rate (**Figure 9**).<sup>[127]</sup> The bifacial PSC has reached to for front and rear efficiencies of 12.33 and 11.78%, respectively. PSCs have been fabricated by Gelmetti et al. using PEDOT:PSS as hole and PCBM-C70 fullerene derivative as electron selective contacts.<sup>[128]</sup> Efficiency up to 10% has been obtained through optimization of the thickness of perovskite and the selective contact layers. Best device had the thickness of 440, 40, and 65 nm for perovskite, PCBM-C70 and PEDOT:PSS layers, respectively. An excellent PCE of 17.0%, for a PSC with conventional mesoscopic architecture has been reported by Jiang et al.<sup>[129]</sup> In their study, a very simple in situ solid-state polymerization method has been used to fabricate PEDOT film as HTM. Confirmed by photoluminescence measurements, the PEDOT film possesses the highest occupied molecular orbital (HOMO) energy level of -5.5 eV, which facilitates an effective hole extraction from the perovskite layer. Low production cost, high efficiency and simple processing of PEDOT, make it a good candidate material for cost-effective and large-area manufacture of PSCs.

### 2.2.4. Polyaniline

Due to its high conductivity and good stability, as well as ease of synthesis, polyaniline (PANI) (9) is the most extensively studied conducting polymer.<sup>[130]</sup> PANI nanomaterials have improved optical, structural, electronic, and electrical properties and can adopt various nanostructures such as nanofibers, nanorods, nanowires, nanotubes, and nanoflakes with a high surface to volume ratio and low diffusional resistance.<sup>[131]</sup> These materials are widely used for the fabrication of efficient electronic devices such as field-effect transistors (FETs), sensors, catalysts, photovoltaics, etc.<sup>[132]</sup> Using PANI nanoparticle (PANI-NP) as dopant-free HTM in 2014, Xiao et al. reported a PCE of 5.13% for a PSC with a good long stability.<sup>[133]</sup> However, adding Li<sup>+</sup> ion and tBP to PANI-NP to increase the charge mobility of HTM led to a higher PCE of 7.34%. Pristine and surfactant-modified PANI:PSS (10) also have been used as HTM in inverted planar perovskite solar

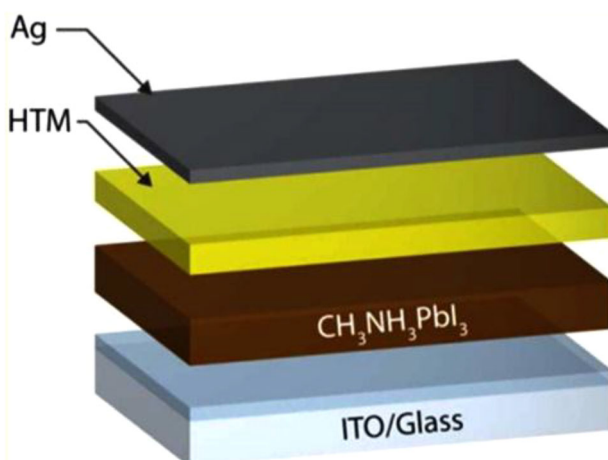


**Figure 8.** Device architecture of the perovskite solar cells without an ETL, the HTL is P3HT. Reproduced with permission.<sup>[121]</sup> Copyright 2014, American Chemical Society.

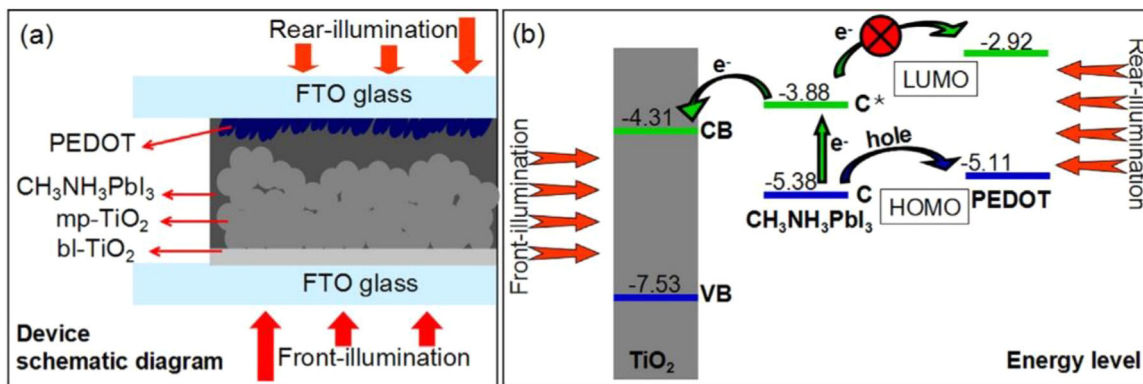


**Figure 9.** Device schematic diagram and energy level diagram of the bifacial PSC. Reproduced with permission.<sup>[127]</sup> Copyright 2016, Elsevier.

cells (PSCs) by Lee et al. and PCEs of 6.59 and 10.90% has been achieved, respectively.<sup>[134]</sup>

#### 2.2.5. Conjugated Donor-Acceptor Copolymers

Lee et al. have used TT-BDT (thieno[3,4-b]thiophene (TT) and benzo[1,2-b:4,5-b']dithiophene (BDT)) alternating copolymers with and without a 3,4-dichlorobenzyl group, as HTMs for perovskite devices without including any additives.<sup>[135]</sup> PCEs of 8.7 and 7.4% were obtained for PTB-DCB21 (the functionalized HTM [a polymer composed of 2'-butyloctyl-4,6-dibromo-3-fluorothieno[3,4-b]thiophene-2-carboxylate (TT-BO), 3',4'-dichlorobenzyl-4,6-dibromo-3-fluorothieno-[3,4-b]thiophene-2-carboxylate (TT-DCB), and 2,6-bis(trimethyltin)-4,8-bis(2-ethylhexyloxy)benzo[1,2-b:4,5-b']dithiophene (BDT-EH)) (11) and PTB-BO (the nonfunctionalized polymer [a polymer composed of TT and BDT] (12), respectively. PTB1 (13) (with hole mobilities of  $4.5 \times 10^{-4} \text{ cm}^2 \text{ V}^{-1} \text{ s}^{-1}$ ) and PTB7 (14) (with hole mobility of  $5.8 \times 10^{-4} \text{ cm}^2 \text{ V}^{-1} \text{ s}^{-1}$ ) have been employed as additive free HTMs in PSCs and PCEs of 6.0 and 7.5% have been achieved, respectively.<sup>[136]</sup> Using no dopants, a PCE of 6.64% has been also achieved for PSCs with a conjugated donor-acceptor copolymer, P (15), having benzodithiophene donor and benzo[1,2,5]thiadiazole acceptor, in a study by Nagarjuna et al.<sup>[137]</sup> Due to its higher hole mobility compared to P3HT, an enhancement has been observed in FF and  $V_{OC}$  of the devices based on P as HTM. New polymeric HTM series based on semiconducting 4,8-dithien-2-yl-benzo[1,2-d;4,5-d']bistriazole-*alt*-benzo[1,2-b:4,5-b']dithiophenes (pBBTa-BDTs) (16 and 17) were reported by Liao et al.<sup>[138]</sup> A stabilized PCE of 12.3% has been achieved by employing intrinsic HTMs in conventional planar PSCs. The high efficiency of PSCs was suggested to be attributed to efficient hole extraction/collection (due to  $\pi$ -face-on orientation of the polymers on the perovskite layer) and balanced electron/hole transport of the reported polymeric HTMs. Moreover, the perovskite devices with undoped polymeric HTMs showed higher stabilities under thermal stresses at 80 °C and 65% RH (Figure 10).

Using another BDT based conjugated copolymer, in 2017, Lee et al. reported a remarkable efficiency of 18.3% for a robust PSC, using a green-solvent-processable HTM, an asymmetric donor-

acceptor polymer (asy-PBTBDT) (18), comprising BT (benzothiadiazole) and BDT.<sup>[139]</sup> The HTM exhibited a high hole mobility of  $1.13 \times 10^{-3} \text{ cm}^2 \text{ V}^{-1} \text{ s}^{-1}$  and was also well-matched with perovskite in term of energy levels. These properties along with the favorable film formability of asy-PBTBDT, because of its high solubility in 2-methylanisole were proposed as the origin of PSC devices' high performances. In a very recent study, a novel BDT-BT-based D- $\pi$ -A type conducting homopolymer (PTEG) (19) has been introduced by Kim et al.<sup>[140]</sup> With the presence of tetra ethylene glycol (TEG) groups, the synthesized HTM showed a high solubility in chlorobenzene. It has been demonstrated that flexible TEG groups can also enhance the hole mobility by preventing backbone twisting and increasing  $\pi$ - $\pi$  stacking. The highest efficiency of 19.8% has been achieved for a conventional n-i-p type planar PSC without using any dopants. It has been considered that deep HOMO energy level of PTEG and its good contact with perovskite resulted in the high efficiency of PSCs. In 2018, Kyeong et al. developed novel conjugate polymers of BDT and 4,4-difluoro-4-bora-3a,4a-diaza-*s*-indacene (BODIPY) as dopant free HTMs for PSCs.<sup>[141]</sup> The HOMO and LUMO levels of the resulting polymers were minutely adjusted by choosing different alkyl chains on BDT and meso substituents on BODIPYs, respectively. Application of pBDT-BODIPY copolymers (20) as dopant free HTMs in PSCs yielded over 16% of PCE with high durability under ambient condition (over 80% of its original PCE, even after 10 days). In another study, Kim et al. have used a random copolymer (RCP) based on BDT (Figure 11), as a dopant-free donor-acceptor polymeric HTM, in PSC devices with the configuration of FTO/SnO<sub>2</sub>/CH<sub>3</sub>NH<sub>3</sub>PbI<sub>3</sub>/RCP/Au and attained a high PCE of 17.3%.<sup>[142]</sup> Without adding hygroscopic dopants to HTM, the long-term stability of PSCs was dramatically improved. RCP based perovskite devices maintained their initial efficiency for over 1400 h at 75% humidity, whereas devices made of HTMs with additives failed after 900 h. Combining P-OR with P-R, with nearly the same structure but different HOMO energy levels, the HOMO level have been increased up to  $-5.43 \text{ eV}$  (Figure 12). RCP showed hole mobility as high as  $10^{-3} \text{ cm}^2 \text{ V}^{-1} \text{ s}^{-1}$ , which further analysis by GIWAXS (grazing-incidence wide-angle X-ray scattering) indicated the face-on orientation of all polymers on the substrate and explained the high mobility of RCP. Recently, dopant-free PSCs have been fabricated employing new

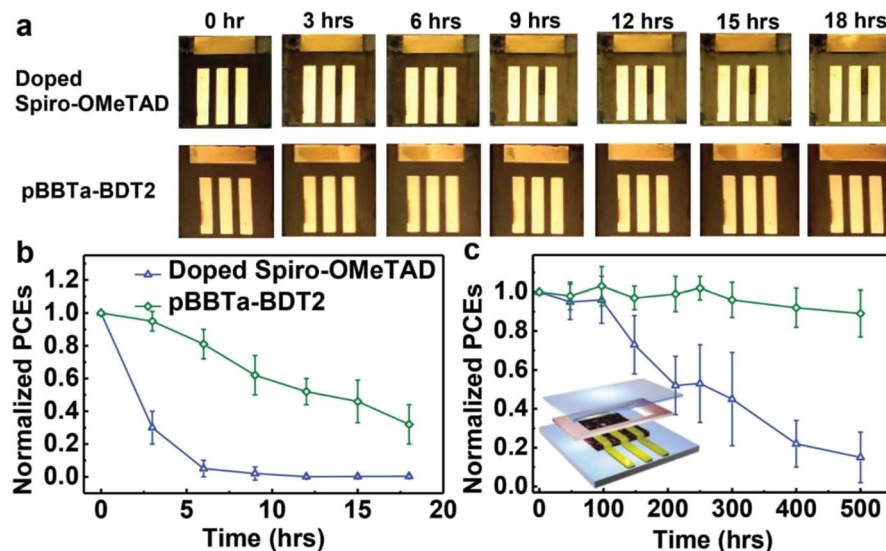


**Figure 10.** Environmental stability of perovskite solar cells over-coated with the indicated HTMs under thermal stress at 85 °C and 65% RH. a) Images of un-encapsulated solar devices over time. b) PCE evolutions of un-encapsulated solar cells. c) PCE evolutions of encapsulated solar cells over time. The inset illustrates the encapsulation process in which the patterned thermoelastic film is sandwiched between the device and a cover glass. Reproduced with permission.<sup>[138]</sup> Copyright 2016, Wiley-VCH.

multirole donor-acceptor type 2D  $\pi$ -conjugated polymers, based on alkoxy naphthalylthienyl-substituted BDT unit (donor) along with fluorine atoms on BT unit (acceptor) by Kranthiraja et al.<sup>[143]</sup> High efficiency of 17.28%, as well as long-term stability of up to 700 h without a significant drop in PCE, has been observed for PSCs based on P3 (poly[4-(5-(4,8-bis(5-((2-hexyldecyl)oxy)naphthalen-2-yl)thiophen-2-yl) benzo[1,2-*b*:4,5-*b'*]dithiophen-2-yl)-4-octylthiophen-2-yl]-5,6-difluoro-7-(4-octylthiophen-2-yl)benzo[c][1,2,5]thiadiazole]) (21) as HTM. In 2018, Cai et al. have fabricated PSC devices with an n-i-p structure incorporating series of carbazole and BT based donor-acceptor copolymers as dopant-free hole transport materials.<sup>[144]</sup> A superior performance of 19.1% was achieved using PCDTBT1 (22) as the HTM, its success is attributed to the more effective suppression of charge recombination at the perovskite/PCDTBT1 interface by coupling the passivation effect

from the thiophene and methoxy units. It has been demonstrated that the ordered  $\pi$ - $\pi$  stacking structure can facilitate charge carrier transport, and the flanked methoxy groups have significant impacts on the reduction of trap-mediated recombination in PSC devices. The storage lifetime of this device is also superior, due to its hydrophobic surface that prevents water penetration, as well as the lower density of trap sites.

Wang et al. have introduced another two donor-acceptor copolymers based on dithienosilole (DTS) and thiazolothiazole (TTz), PDTSSTz (23), and PDTSSTz-4 (24), and used them as additive free HTM in the n-i-p type PSCs, with the device structure of ITO/compact TiO<sub>2</sub>/CH<sub>3</sub>NH<sub>3</sub>PbI<sub>3-x</sub>Cl<sub>x</sub>/HTL/MoO<sub>3</sub>/Ag.<sup>[145]</sup> PCEs of as high as 14.4 and 15.8% were achieved for optimized PSCs based on PDTSTTz and PDTSTTz-4, respectively.

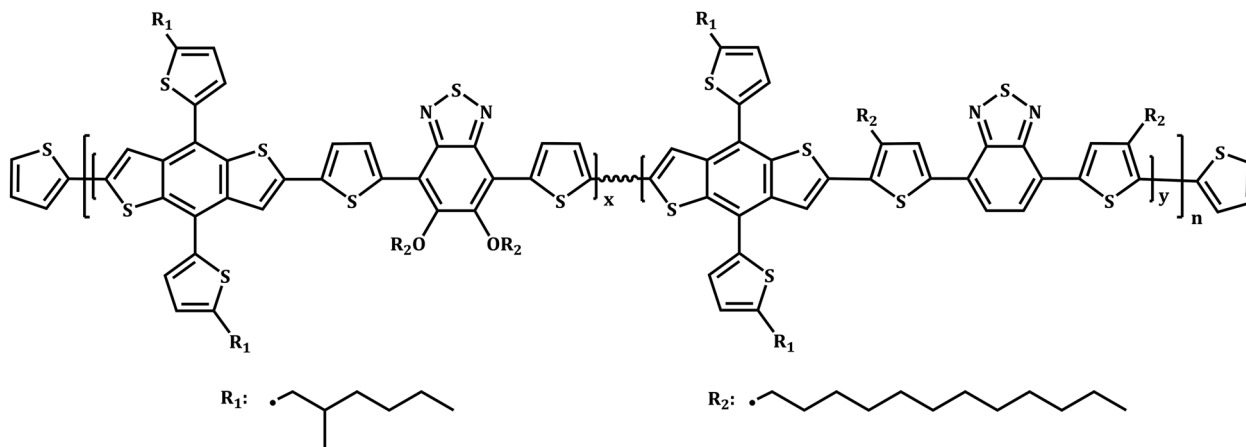


**Figure 11.** The chemical structure of RCP is composed of P-OR and P-R. Reproduced with permission.<sup>[142]</sup> Copyright 2016, the Royal Society of Chemistry.

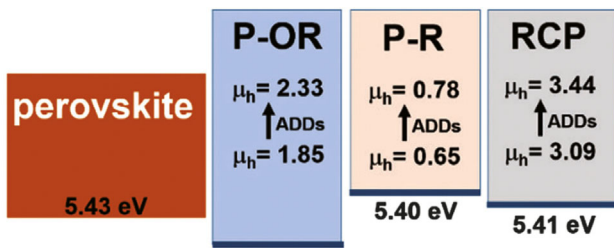


**Figure 12.** Energy diagrams and the changes in mobility due to the presence of additives (ADDs) for the perovskite and polymers. Reproduced with permission.<sup>[143]</sup> Copyright 2008, the Royal Society of Chemistry.

### 2.2.6. Other Polymeric HTMs

Compared to other *p*-type polymers such as P3HT ( $\mu \approx 10^{-3} \text{ cm}^2 \text{ V}^{-1} \text{ s}^{-1}$ ),<sup>[146]</sup> pristine poly(diketopyrrolopyrrole-terthiophene) (PDPP3T) (25) has a high hole mobility ( $\mu \approx 0.04 \text{ cm}^2 \text{ V}^{-1} \text{ s}^{-1}$ ). In the structure of this polymer, terthiophene unit is attached to the conjugated DPP unit, it has high planarity that helps induce packing across the chains and enhance charge carrier mobility. Using PDPP3T in its pristine form as dopant-free HTM, Dubey et al. have fabricated PSCs with photovoltaic performance of 12.32%.<sup>[147]</sup> The efficiency of doped spiro-OMeTAD based cell in same conditions has been reported as 12.34%. Poly[2-methoxy-5-(2-ethylhexyloxy)-1,4-phenylenevinylene] (MEH-PPV) (26) was used as HTM in PSC without adding dopant, by Chen et al.<sup>[148]</sup> They used one-step and two-step methods for preparing the perovskite layer, with or without post-treatment of the mesoporous TiO<sub>2</sub> layer using TiCl<sub>4</sub>. The PCE of as high as 9.65% was achieved for the devices with best performance. The same condition for doped spiro-OMeTAD based devices led to a performance of 13.38%. In a very recent study, using ultraviolet surface modification method to fabricate hole transporting layers with MEH-PPV and Poly-TPD (poly[N, N'-bis(4-butylphenyl)-N,N'-bis(phenyl)benzidine]) has led to PSC with high PCEs of 10% for MEH-PPV based devices and PCEs exceeding 18% for Poly-TPD based PSCs, together with enhanced long-term stability.<sup>[149]</sup> By improving the quality of perovskite layer, an air-processed PSC with remarkable PCE of 18.11% has been reported by Cheng et al.<sup>[150]</sup> In their study, Poly-TPD has been used as dopant free HTM in an inverted PSC. They have found that preheating the substrate and PbI<sub>2</sub> solution could help the deposition of a fully covered and uniform PbI<sub>2</sub> film in air. It has been suggested that this could be due to the increased vapor pressure of the solvent at higher temperatures to reduce the ingress of oxygen and moisture during the PbI<sub>2</sub> deposition. It has been demonstrated that with precise control of UVO time, the surface wettability of HTM film can be tuned. Because of the large water contact angle of MEH-PPV, the perovskite cannot be spin-coated on it. With UVO modification of MEH-PPV for 20 or more seconds, continuous perovskite film with high quality can be easily deposited and inverted planar PSCs with MEH-PPV can be fabricated. A uniform perovskite

film with good morphology can always be a crucial factor in enhancing the efficiency of a PSC.

Carbazole-based polymers have tunable optical and electrochemical properties<sup>[151]</sup> and are widely used in a variety of organic electronics, such as OLEDs, OFETs, and bulk heterojunction solar cells.<sup>[152]</sup> Two carbazole-based polymers, 3,6-Cbz-EDOT (27) and 2,7-Cbz-EDOT (28), were used as dopant-free HTMs for perovskite devices by Li et al.<sup>[153]</sup> In these conjugated polymers, carbazole monomers were copolymerized with the electron-rich 3,4-ethylenedioxythiophene (EDOT) unit to enhance the electron donating properties of the obtained HTMs. Employing 2,7-Cbz-EDOT, PCE of 4.47% has been obtained for PSC devices, which was higher than the efficiency obtained for 3,6-Cbz-EDOT. This was due to the deeper HOMO level and higher hole mobility of 2,7-Cbz-EDOT. In a study by Su et al., hydrophobic and conductive polymer poly-N-vinylcarbazole (PVK) (29) has recently used as dual-functional interlayer between perovskite and HTM of PSCs, to shield perovskite from moisture, suppress charge combination, and promote hole transport simultaneously (Figure 13).<sup>[154]</sup> With triazatruxene-based HTMs and PVK as the interlayer, PSCs with remarkable PCEs exceeding 18% have been achieved.

In 2017, Yang et al. also employed PVK without using any doping or post treatments, as an efficient HTM for inverted planar PSCs.<sup>[155]</sup> Due to good wettability of PVK solution, a smooth and uniform thin films were formed on ITO glass substrate. As a result, the perovskite film (MAPbI<sub>3</sub>) subsequently deposited by spin-coating was also smooth, uniform, compact, and of high quality. The high crystallinity of perovskite photoactive layer with low PbI<sub>2</sub> residue, deposited on PVK HTM led to a high charge recombination resistance of the device. For devices with the structure of ITO/PVK/MAPbI<sub>3</sub>/PCBM/Ag, a 15.8% stabilized power conversion efficiency was achieved for optimum PVK thickness around 6.5 nm. However, devices based on PEDOT:PSS HTM displayed the PCE of 12.1%. Their study indicated that after a storage of 1000 h, the PCE of PVK- and PEDOT:PSS-based devices dropped to 82.5 and 56%, respectively and demonstrated that the PVK-based perovskite devices is more stable compared with the PEDOT:PSS-based devices (Figure 14).

Choi et al. have introduced a solution-processable conjugated polyelectrolyte, poly[2,6-(4,4-bis-potassiumbutylsulfonate-4H-cyclopenta-[2,1-b;3,4-b']dithiophene)-alt-4,7-(2,1,3-benzothiadiazole)] (CPE-K) as HTM for an inverted planar PSC.<sup>[156]</sup> The efficiency of 12.51% with enhanced device stability under ambient conditions has been achieved without using any additives. A cross-linkable hole transporting layer, made of 4,4',4''-tris(N-carbazolyl) triphenylamine (TCTA) functionalized with two vinyl benzyl ether (VB) groups, named as TCTA-BVP, was employed by Li et al.<sup>[157]</sup> (Figure 15). In comparison with the commonly used HTM, spiro-OMeTAD, the cross-linked HTM exhibited higher hole mobility, better morphological stability, and enhanced hydrophobicity. Without using any dopants, an impressive PCE of 18.3% was reported for PSCs with a typical planar n-i-p device configuration of FTO/TiO<sub>2</sub>/C60/MAPbI<sub>3</sub>/HTL/Ag.

Xue et al. have introduced polar functional groups on the polymer side chains to increase the surface energy of the hole selective layer, which led to the formation of better perovskite film with full coverage and high crystallinity.<sup>[158]</sup> HSL1 (30) and HSL2 (31) have employed as HTMs in PSCs without using any

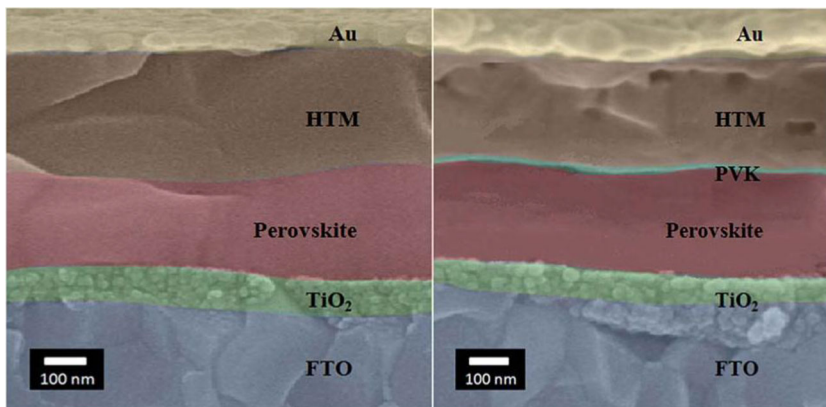


**Figure 13.** Cross-sectional SEM images of the planar PSCs containing spiro-OMeTAD alone (left) and PVK interlayer (right). The individual layers have been colored to improve visibility. Reproduced with permission.<sup>[154]</sup> Copyright 2017, the Royal Society of Chemistry.

dopants. For  $\text{CH}_3\text{NH}_3\text{PbI}_x\text{Cl}_{3-x}$  PSCs, highest PCEs of 15.4 and 16.6% have been achieved for HSL1 and HSL2 based devices, respectively. In a very recent study, Xu et al. have been developed a novel non-conjugated polymer to employ as an efficient dopant-free HTM for PSCs.<sup>[159]</sup> PVCz-OMeDAD (32) has been obtained by integrating non-conjugated polyvinyl main chain with carbazole-based hole transporting side chain. Due to its flexible non-conjugated polyvinyl backbone, the non-dopant PVCz-OMeDAD HTM could form a smooth, defect-free ultra-thin film ( $\approx 30$  nm) on the rough mix-ion perovskite layer in PSCs, resulting in a shorter

hole transportation pathway and thus reducing charge recombination chance.  $\text{FA}_{0.85}\text{MA}_{0.15}\text{Pb}(\text{I}_{0.85}\text{Br}_{0.15})_3$  perovskite-based n-i-p type PSCs employing low cost, ultra-thin film of PVCz-OMeDAD as dopant-free polymer HTM layer have exhibited high PCE up to 16.09%.

As promising HTM alternatives for low cost high efficiency PSCs, polymeric HTMs provide unique advantages such as good thermal stability, tunable energy levels, interfacial adhesion, mechanical flexibility, and thin film uniformity. With their hydrophobicity, polymeric HTMs can provide good protection for perovskite layer and enhanced stability for perovskite devices. The photovoltaic properties of some selected perovskite devices using polymeric HTMs are summarized in Table 2. Molecular structures of all discussed polymeric HTMs are shown in Figure 16.

### 2.3. Small-Molecule HTMs

#### 2.3.1. Triarylamines

Small molecules can be considered as the most popular category of compounds using in PSCs as HTM. Because of the ease of the synthesis and purification of these materials, as well as their ability to form films with good crystallinity and therefore, with high mobility and conductivity, various classes of small

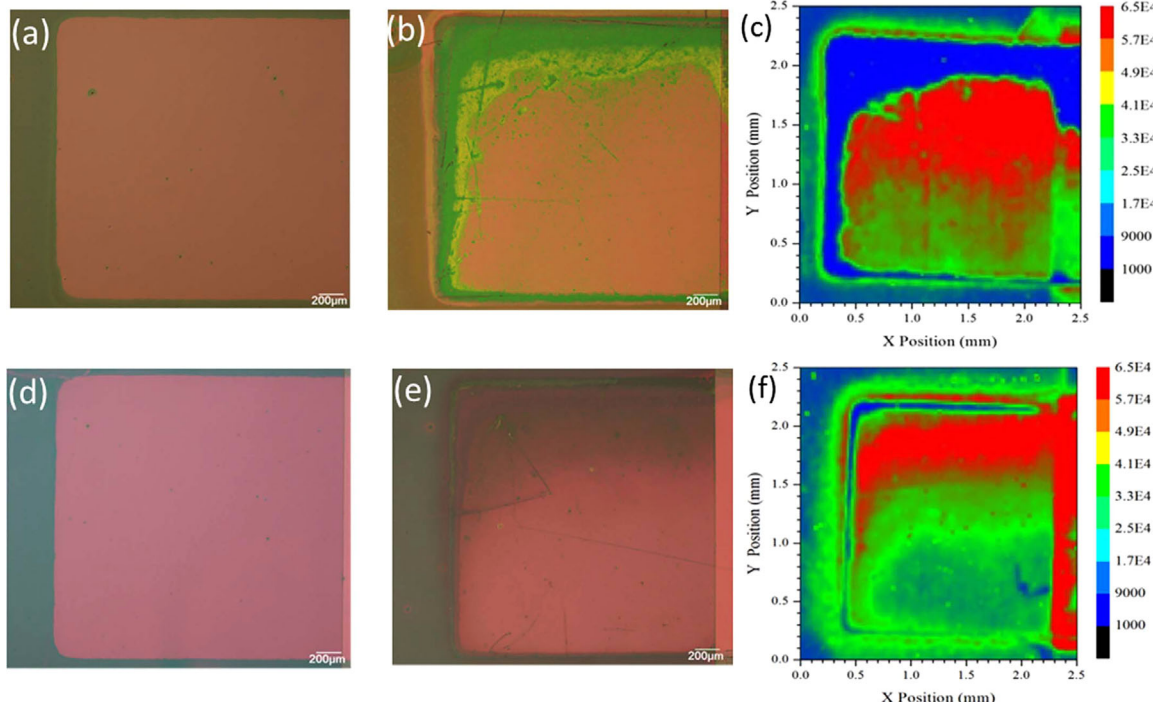


**Figure 14.** Optical images of unsealed perovskite solar cells cast on PEDOT:PSS and stored in ambient condition for a) 0 day, b) 30 days. And perovskite solar cells cast on PVK stored for d) 0 day, e) 30 days. Panels c) and f) are PL mapping images of panel (b) and (e), respectively. Reproduced with permission.<sup>[155]</sup> Copyright 2017, Elsevier.

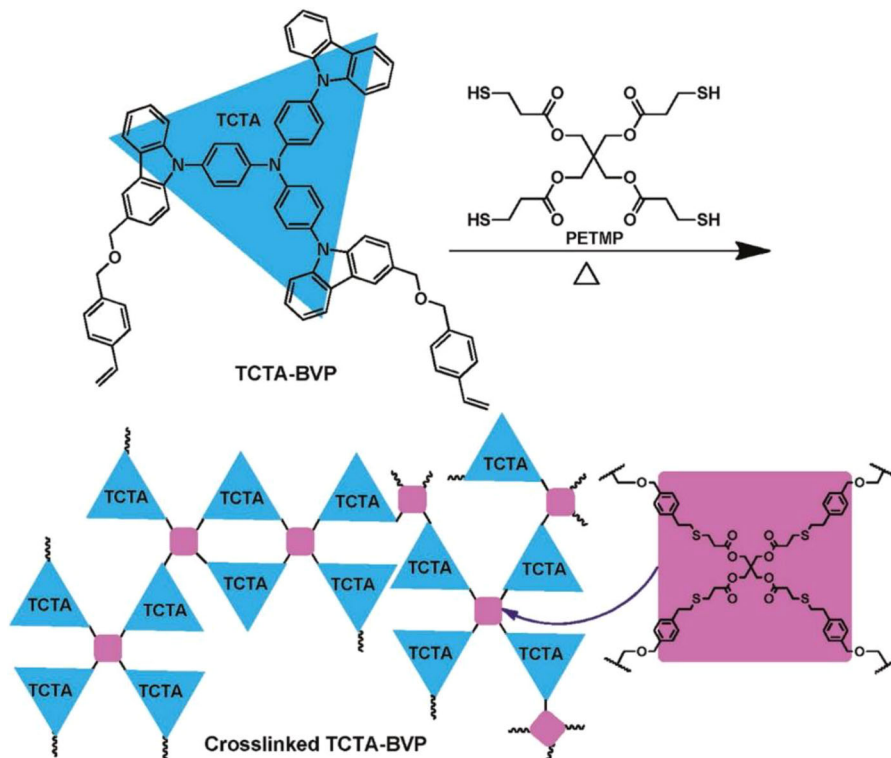


**Figure 15.** The synthetic route of crosslinked TCTA-BVP via the thiol-ene thermal polymerization. Reproduced with permission.<sup>[157]</sup> Copyright 2016, Wiley-VCH.

molecules including organic and organometallic compounds have been employed as the hole selective layer in PSC devices in last years. Their easily tunable frontier orbitals' energy level helps to achieve an appropriate alignment with various perovskite absorbers. Most of studies in this category of HTMs are focused on triphenylamine (TPA)-based compounds such as spiro-OMeTAD, which is the most reported small molecule HTM. Although, using dopants to increase the conductivity of spiro-OMeTAD is common, however, studies have been carried out by research groups to increase the efficiencies of PSCs with using undoped spiro-OMeTAD HTM as well as introducing new HTMs in this class of small molecules.

In 2015, Frankevicius et al. achieved a PCE of 13.4% for a PSC using a new triarylamine-substituted spiro-cyclopentadithiophene based HTM (33) without adding any chemical dopants.<sup>[160]</sup> Another spiro-thiophene derivative with 4,4'-spirobi [cyclopenta[2,1-b;3,4-b']dithiophene] as the spiro core (SCPDT-BiT) (34) has been employed by Ma et al. in a PSC, achieving a PCE of 10.4% with an open circuit voltage of 0.94 V, and a short circuit current density of  $16.54 \text{ mA cm}^{-2}$  under standard testing conditions.<sup>[161]</sup> A cost-effective spiro-type HTM, PST1 (35) has been developed by Ganesan et al. and employed in perovskite devices.<sup>[162]</sup> Using undoped form of the HTM has led to a PCE of as high as 12.74% for PSCs. In 2016, Wang et al. introduced new HTM named SAF-OMe (36), yielded by chemical combination of spiro-OMeTAD and triphenylamine.<sup>[163]</sup> Perovskite devices based on dopant-free SAF-OMe, exhibited efficiencies as high as 12.39%. Habisreutinger et al. reported a steady-state efficiency of as high as 18.8% for a planar n-i-p PSC device.<sup>[164]</sup> In their

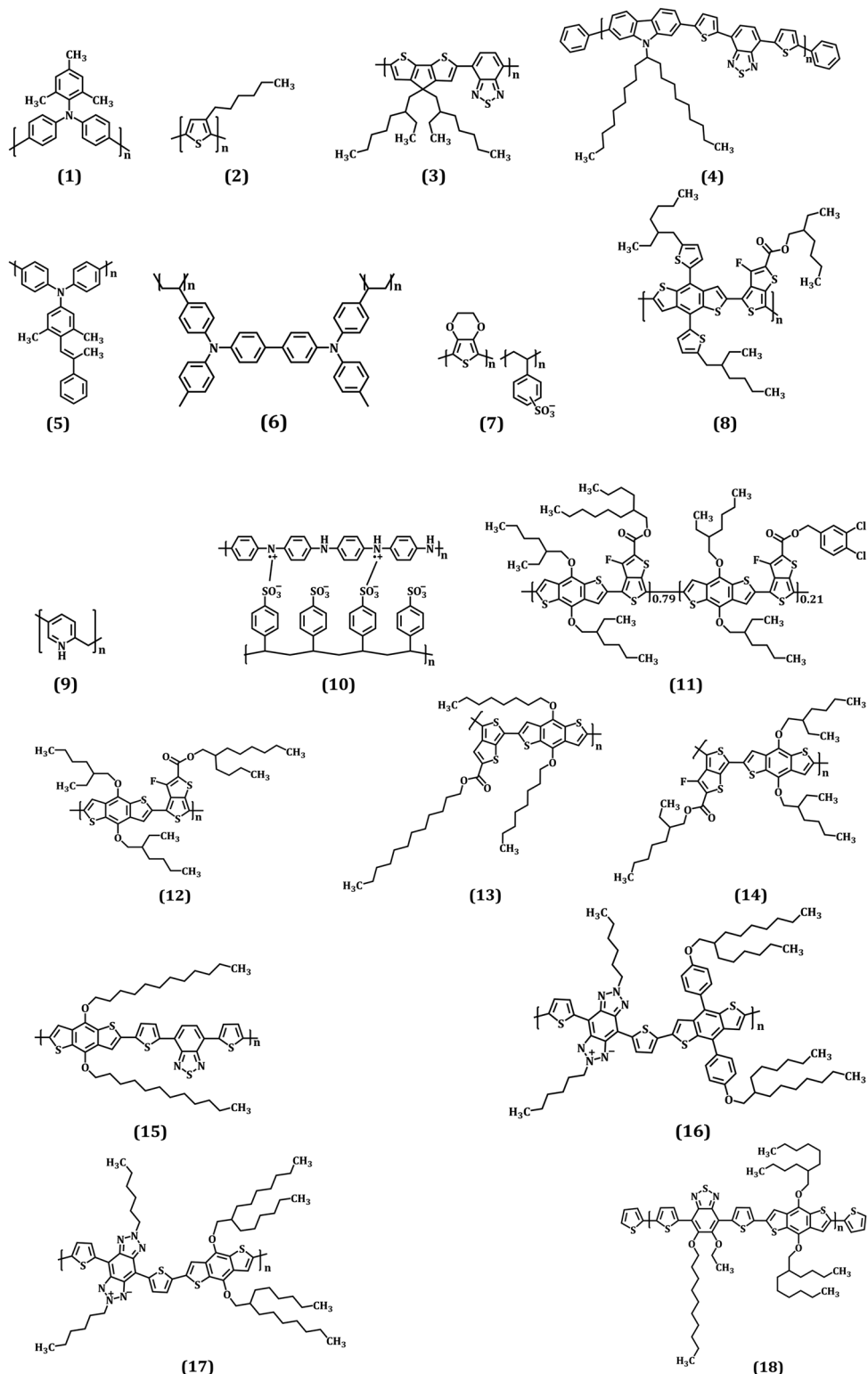
report, undoped spiro-OMeTAD along with a polymer-wrapped single-walled carbon nanotubes (SWNTs) made a HTM with a double layer structure (**Figure 17**).

Designing, synthesizing, and employing novel triarylamine based dopant-free HTMs have also attracted a great attention in many researches in the field of optoelectronic devices. Due to their efficient hole mobilities, triarylamine derivatives have been widely used as HTM in PSCs. In 2014, Choi et al. introduced two new HTMs, OMeTPA-TPA (37) and OMeTPA-FA (38), which contain triphenylamine and incorporated planar amine as core unit, respectively.<sup>[164]</sup> An overall conversion efficiency of 11.7%, with a  $J_{SC}$  of  $19.42 \text{ mA cm}^{-2}$ , a  $V_{OC}$  of 0.905 V, and a FF of 0.63, were obtained by a PSC with mesoscopic structure comprising mp-TiO<sub>2</sub>/MAPbI<sub>3</sub>/OMeTPA-FA/Au without any additives in HTM. In another study in 2014, they also introduced two other symmetrical starshaped triphenylamine based HTMs, TPA-MeOPh (39) and FA-OMePh (40).<sup>[165]</sup> With the same device architecture, PCEs of 7.45 and 9.18% were reported for TPA-MeOPh and FA-MeOPh based PSCs, respectively. Qin et al. have designed a low band gap HTM with triarylamine core, Fused-F (41), for PSC devices and achieved a PCE of 12.8% under the illumination of  $98.8 \text{ mW cm}^{-2}$ .<sup>[166]</sup> Its flattened star-shaped structure helped to enhance the intermolecular  $\pi-\pi$  packing interactions and face-on stacking on the surface resulting efficient hole transport and increasing the lifetime of the charge-separated state. Due to the high hole conductivity of Fused-F, there was no need to add *p*-type additives. A PCE of 11.4% has been also reported by Xiao et al. for perovskite devices employing 4-(4-phenyl-4-a-naphthylbutadienyl)-N,N-bis(4-benzyl)-aniline (PNBA) (42) as an additive free HTM.<sup>[167]</sup> In two

**Table 2.** Photovoltaic properties of some selected perovskite devices with polymeric HTMs.

$V_{OC}$ [V]	$J_{SC}$ [ $\text{mA cm}^{-2}$ ]	FF [%]	PCE [%]	ETL	Polymer	HTM	Band edges (HOMO)	Hole mobility [ $\text{cm}^2 \text{V}^{-1} \text{s}^{-1}$ ]	Device architecture	Reference
1.12	19.65	76	16.5	TiO <sub>2</sub>	$\text{CH}_3\text{NH}_3\text{Pb}(\text{I}-x\text{Br})_3$ ( $x = 0.1-0.15$ )	PTAA	-5.5		n-i-p mesoporous	[113]
1.05	23.5	69	17.0	TiO <sub>2</sub>	$(\text{NH}_2\text{CH} = \text{NH}_2\text{PbI}_3)_{1-x}(\text{CH}_3\text{NH}_3\text{PbBr}_3)_x$ ( $x = 0.15$ )	PEDOT	-5.41	$3.09 \times 10^{-3}$	n-i-p	[129]
1.08	21.9	75	17.3	$\text{SnO}_2$	$\text{CH}_3\text{NH}_3\text{PbI}_3$	RCP	-5.23	$2.01 \times 10^{-3}$	n-i-p	[142]
1.09	20.74	75.78	17.28	TiO <sub>2</sub>	$\text{CH}_3\text{NH}_3\text{PbI}_3$	P3	-5.36	$1.34 \times 10^{-3}$	n-i-p	[143]
1.11	22.4	73.2	18.3	TiO <sub>2</sub>	$\text{CH}_3\text{NH}_3\text{PbI}_3$	asy-PBTBDT	-5.2	$7.7 \times 10^{-4}$	n-i-p	[139]
1.07	21.7	78.7	18.27	C <sub>60</sub>	$\text{CH}_3\text{NH}_3\text{PbI}_3$	TCTA-BVP	-5.2		p-i-n	[157]
1.08	22.5	80.9	18.9	C <sub>60</sub>	$(\text{CsPbI}_{0.05})(\text{CH}(\text{NH}_2)_2\text{PbI}_3)_{0.85}(\text{CH}_3\text{NH}_3\text{PbBr}_3)_{0.17}]_{0.95}$	PTAA	-5.4		n-i-p	[117]
1.04	23.20	75.4	18.19	BCP	$\text{CH}_3\text{NH}_3\text{PbI}_3$	poly-TPD	-5.4		n-i-p	[149]
1.085	21.96	67.5	16.09	TiO <sub>2</sub>	$(\text{CH}(\text{NH}_2)_2)_{0.85} (\text{CH}_3\text{NH}_3)_0.15 \text{Pb}(\text{I}_{0.85}\text{Br}_{0.15})_3$	PVCz-OMeDAD	-5.24		n-i-p	[159]
1.07	20.4	75.9	16.6	PC <sub>61</sub> BM	$\text{CH}_3\text{NH}_3\text{PbI}_3\text{Cl}_{3-x}$	HS12	-5.39	$3.2 \times 10^{-5}$	p-i-n	[158]
0.96	21.93	74.97	15.8	PCBM	$\text{CH}_3\text{NH}_3\text{PbI}_3$	PVK			p-i-n	[155]

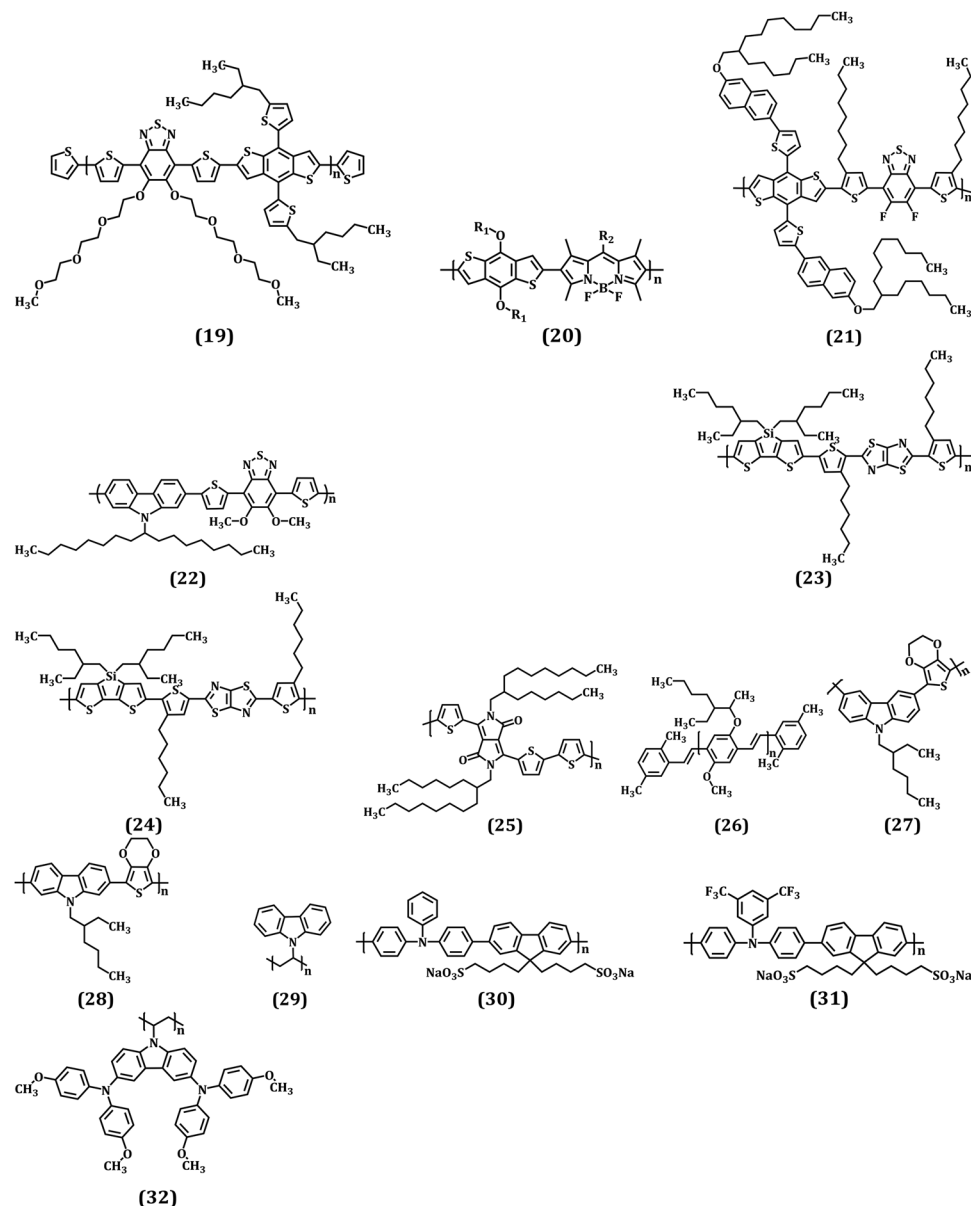
studies in 2014 and 2015, by extending the conjugation of triphenylamine group, Lv et al. have reported four new triphenylamine based linear type HTMs containing butadiene, (43) and (44) and vinyl derivatives, apv-T (45) and apv-EC (46), for PSCs.<sup>[168]</sup> Without using any dopants, PCEs up to 12% have been achieved for perovskite devices with mesoscopic architecture. In a study, Ma et al. have used N,N'-di(3-methylphenyl)-N,N'-diphenyl-4,4'-diaminobiphenyl (TPD) (47) as the HTM of PSC and without using any dopants, a low efficiency of 3.2% has been obtained.<sup>[169]</sup> However, employing 1,4,5,8,9,11-hexaazatriphenylenehexacarbonitrile (HAT-CN), as a buffer layer between HTM and Au electrode, with the optimum thickness of 3 nm, has improved the PCE up to 7.1%. With its deep LUMO level, HAT-CN can increase the conductivity by several orders of magnitude. It can improve  $J_{SC}$  by forming the charge-transfer complex (dipole) between HTM and metal electrode, which is helpful for blocking electrons and extraction holes. The resulting device also showed a long lifetime of 1000 h with only 10% degeneration. In 2016, new type of HTMs based on silver metal-organic complexes were designed and used in perovskite devices.<sup>[170]</sup> In their study, Hua et al. used organic ligands containing triphenylamine part and coordinating pyridine unit to synthesize two new HTMs, HA1 (48) and HA2 (49). In these metal organic HTMs, Ag–Ag interactions can assist the strong face-on-face  $\pi$ – $\pi$  stacking and lead to the high conductivities of  $1.78 \times 10^{-3} \text{ S cm}^{-1}$  and  $1.05 \times 10^{-3} \text{ S cm}^{-1}$  for HA1 and HA2, respectively. The efficiency of 11.98% was reported for PSCs based on HA1. Star-shaped HTM, ST1 (50), was synthesized by a low cost, facile one-step synthetic method by Zhao et al. in 2016 and employed in PSCs without using any dopants and additives.<sup>[171]</sup> The HOMO energy level of ST1 ( $-5.24 \text{ eV}$ ) is a bit lower than that of spiro-OMeTAD ( $-5.12 \text{ eV}$ ) and lies above the HOMO level of  $\text{CH}_3\text{NH}_3\text{PbI}_3$  ( $-5.43 \text{ eV}$ ). Its high LUMO energy level, however, can block the electron transport from perovskite layer to Au electrode. The comparable PCE of 15.4% was achieved for PSCs with long-term stability. It has been showed that ST1-based devices have higher stability than the devices based on spiro-OMeTAD, when exposed to air in the dark condition. Zhang and coworkers have designed a series of novel star-shaped TPA-based HTMs with different number of branched arms and conjugated length. Among the HTMs, Z1011 (51) and Z1013 (52) based devices showed efficiencies of 12.4 and 15.4%, respectively.<sup>[172]</sup> After 4 weeks of continuous exposing of the PSCs at room temperature and 80 °C in ambient air of 30% relative humidity in the dark without encapsulation, a slight increase of the PCE has been observed for the devices based on Z1013, while the PCE of spiro-OMeTAD based devices decreased 21.5% of its initial values. The HTM Z34 (53), also designed and synthesized by Zhang et al., has been applied in PSCs without using any dopants or additives and an impressive overall PCE of as high as 16.1% has been reported.<sup>[173]</sup> Whereas, doped spiro-OMeTAD based devices fabricated under the same conditions showed a comparable efficiency of 16.7%. Two novel small molecule HTMs, 6-difluoro-N<sup>1</sup>,N<sup>1</sup>,N<sup>2</sup>,N<sup>2</sup>,N<sup>4</sup>,N<sup>4</sup>,N<sup>5</sup>,N<sup>5</sup>-octakis(4-methoxyphenyl)benzene-1,2,4,5-tetraamine (DFTAB) (54) and 4,4',4'',4'''-(ethene-1,1,2,2-tetrayl)tetrakis(N,N-bis(4-methoxyphenyl)aniline) (TAE) (55), have been introduced by El Labban and coworkers and used in inverted planar PSCs.<sup>[174]</sup> 12.4% efficiency with a  $V_{OC}$  reaching 1.07 V have been reported for perovskite devices based on DFTAB. It has been suggested that DFTAB can be a promising HTM for



**Figure 16.** Molecular structure of polymeric HTMs.

future large-scale applications, due to its low cost and easy synthetic route and no need to additional dopants, which will significantly enhance the long-term stability of the PSCs. An effective dopant-free HTM for PSCs has been developed by Li

et al.<sup>[175]</sup> Using BTPA-TCNE (56) consists of triphenylamine-based Michler's base (as donor) and tricyanovinylene (as acceptor), as HTM, a remarkable PCE of  $\approx 17.0\%$  has been observed for conventional n-i-p PSCs. Based on x-ray crystallography studies,


**Figure 16.** Continued.

there are some different intermolecular interactions in the crystal structure of BTPA-TCNE, formed by three different isomers. Two molecular packing modes, including one centrosymmetric and one non-centrosymmetric, are formed by the interactions between the isomers. Consequently, with all these interactions, a supramolecular structure was created in the solid state and the formed antiparallel molecular packing in the crystal structure canceled out the molecular dipole moments, which led to higher charge transfer.

Two easily synthesized triarylamine based small molecule semiconductors, NTPA (57) and BTPA (58), have been employed as dopant-free HTMs, with high mobilities, in the order of  $10^{-3} \text{ cm}^2 \text{ V}^{-1} \text{ s}^{-1}$ , and strong electron blocking properties, in PSCs with inverted planar structure.<sup>[176]</sup> PSCs with NTPA and BTPA has reached to PCEs of 13.0 and 12.1%, respectively. By

replacing the oxygen atom on HTM with sulfur, Chen et al. have developed two HTMs, TPP-OMeTAD (59) and TPP-SMeTAD (60).<sup>[177]</sup> The presence of sulfur atom in TPP-SMeTAD has provided stronger Pb-S interaction with perovskites, as well as lower HOMO energy level for HTM. Due to their marginal solubility in DMF, the two HTMs diffused back into the crystal grain boundaries during the two-step fabrication of top perovskite layer, which led to a perovskite-HTM heterojunction (Figure 18). The best p-i-n perovskite devices based on TPP-SMeTAD and TPP-OMeTAD HTMs exhibited a PCEs of 16.6 and 14.6%, respectively, with negligible hysteresis.

In 2017, Liu et al. designed new dopant-free, solution processed triphenylamine based HTMs for use in low cost, high performance PSCs.<sup>[178]</sup> A PCE of as high as 15.7% was achieved

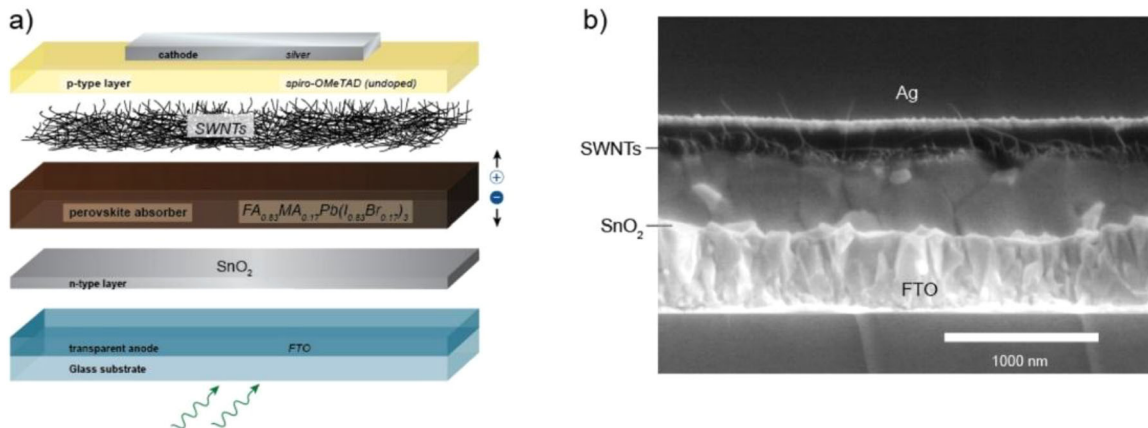


**Figure 17.** a) Device structure of the planar PSC. b) Scanning electron microscope (SEM) image of a device cross section. Reproduced with permission.<sup>[104]</sup> Copyright 2017, American Chemical Society.

for a PSC based on IDTT-TPA (61) as HTM without adding any dopants. Rooted from its extended fused-ring and rigid coplanar structure, which are beneficial for  $\pi$ -electron delocalization, preventing rotational disorder, and increasing  $\pi$ - $\pi$  interactions, IDTT-TPA provided hole mobility of  $6.46 \times 10^{-4} \text{ cm}^2 \text{ V}^{-1} \text{ s}^{-1}$ . In 2018, the same group synthesized two new IDT-based compounds, IDTC<sub>4</sub>-TPA (62) and IDTC<sub>6</sub>-TPA (63) with different aryl side chains to achieve tuned electronic properties, controllable solubility and molecular packing, and successfully employed in  $\text{CH}_3\text{NH}_3\text{PbI}_3$  perovskite solar cells. The IDTC<sub>6</sub> backbone enabled a tight molecular arrangement stacked by  $\pi$ - $\pi$  interactions (3.399 Å), leading to a higher hole mobility than that of the IDTC<sub>4</sub>-base HTM. Consequently, IDTC<sub>6</sub>-TPA based devices showed superior photovoltaic properties compared to those using IDTC<sub>4</sub>-TPA, exhibiting an optimal performance of 15.43%, which was much higher than that of the value obtained using the same state-of-the-art spiro-MeOTAD based device (7.39%) and comparable to spiro-MeOTAD with dopant (17.35%).<sup>[179]</sup> Stable perovskite devices have been developed by Paek et al. using star-shaped D- $\pi$ -A-type HTMs coded as FA-CN (64) and TPA-CN (65).<sup>[180]</sup> The optimized devices with dopant-free FA-CN and FA-TPA have showed impressive PCEs

of 18.9 and 17.5% under standard global AM 1.5 illuminations. Long-term stability of the devices has also been improved by avoiding hygroscopic *p*-type chemical dopants. The maximum power output of PSCs based on FA-CN, collected after 1300 h remained 65% of its initial value. A remarkable efficiency of 17.54% was observed recently for inverted planar PSCs based on novel triarylamine derivatives as additive free HTMs in a study by Park et al.<sup>[181]</sup> They used three HTMs, TPAC0M (66), TPAC2M (67), TPAC3M (68), with different number of methoxy substituents in their structures. Analyzed by X-ray photoelectron spectroscopy, the methoxy units could act as a Lewis base passivating the defect sites at the interface between HTM and perovskite, which led to reducing charge recombination. Pham et al. developed two novel triarylamine based HTMs, TPA-TVT-TPA (69) and TPA-NAP-TPA (70).<sup>[182]</sup> Employing these cost-efficient solution processable small molecule HTMs in inverted PSCs have led to the PCE of 16.32% for TPA-TVT-TPA and 14.63% for TPA-NAP-TPA. In a very recent study, Pham et al. have reported highly efficient and humidity-resistant PSCs, based on new small molecule hole transporting material (HTM) made from a cost-effective precursor anthanthrone (ANT) dye.<sup>[183]</sup> The developed HTM, 4,4'-(6,12-bis(octyloxy)-6,12-

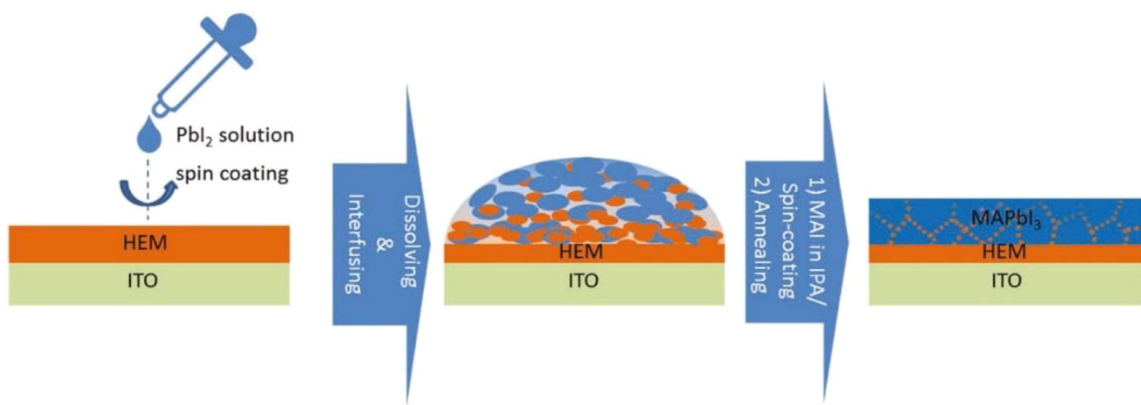


**Figure 18.** A schematic diagram of the deposition method; the orange dashed line represents HEMs allocating along the grain boundary. Reproduced with permission.<sup>[177]</sup> Copyright 2017, Wiley-VCH.

dihydronaphtho[7,8,1,2,3-nopqr]tetraphene-4,10-diylybis(*N,N*-bis(4-methoxyphenyl)aniline) (TPA-ANT-TPA) (71) was employed in mesoscopic PSCs with no dopants and efficiencies as high as 17.5% was achieved. It was demonstrated that using TPA-ANT-TPA as HTM led to an improved charge collection efficiency in devices and increased short-circuit current and photovoltage. Considering these remarkable characteristics of anthranthrone dyes, along with their low cost, it has been suggested that it is possible to use them as a new efficient, stable and low cost scalable HTMs for roll-to-roll printed PSC modules for large area applications. Highly efficient solution-processed flexible and rigid inverted-type planar heterojunction PSCs have been recently designed by Reddy et al. using a new small molecule HTM, (*N*-(4-(9Hcarbazol-9-yl)phenyl)-7-(4-(bis(4-methoxyphenyl)amino)phenyl)-*N*-(7-(4-(bis(4-methoxyphenyl)amino)phenyl)-9,9-diethyl-9H-fluoren-2-yl)9,9-diethyl-9H-fluoren-2-amine, CzPAF-TPA (72).<sup>[184]</sup> A PCE of 15.71% has been observed for dopant-free PSC. A

stabilized PCE of 18.80% is achieved with minor hysteresis for the p-i-n type PSC based on the  $\pi$ -conjugated organic small molecule HTM, 4,4'-cyclohexyliidenebis[N,N-bis(4-methylphenyl)benzenamine] (TAPC) (73).<sup>[185]</sup> Yang et al. have demonstrated that the thickness of TAPC layer did not effectively change the PCE of PSC, but thermal annealing could improve hole conductivity of TAPC through an increase in its crystallinity. In a recent study, two new organic molecules with spiro[fluorene-9,9'-xanthene] (SFX)-based pendant groups, X26 (74) and X36 (75), have been developed as HTMs by Zhang et al.<sup>[186]</sup> The SFX pendant group showed significant influence on the conductivity, energy levels, and thin-film surface morphology. In its structure, fluorene and xanthene moieties connected by a  $sp^3$ -hybridized carbon. This may cause the perpendicular arrangement of the molecule, which resulted in a good 3D intermolecular interaction and electrical conductivity in X26 and X36. An outstanding efficiency of 20.2% has been achieved using X26 as HTM in PSCs. The X26-based devices have also exhibited impressive stability maintaining a high PCE of 18.8% after 5 months of aging in controlled (20%) humidity in the dark.

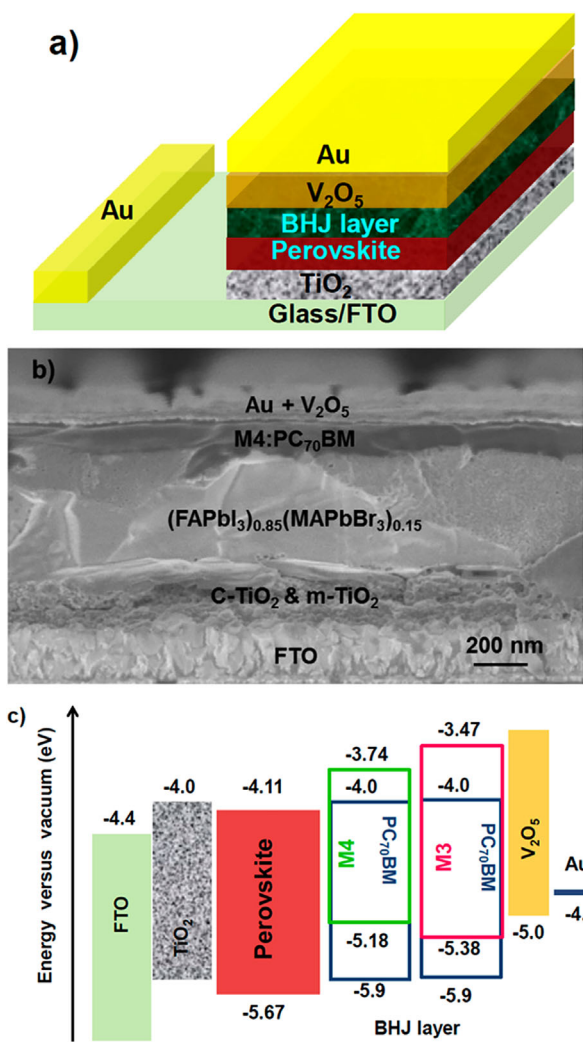


**Figure 19.** a) Schematic structure of integrated devices containing M3 or M4 based BHJ layers. b) SEM image of cross-sectional structure of PSCs containing an M4:PC<sub>70</sub>BM BHJ layer. c) Energy level diagram showing HOMO and LUMO level of various components of the PSC. Reproduced with permission.<sup>[193]</sup> Copyright 2016, American Chemical Society.

### 2.3.2. Thiophene

In 2014, Li et al. reported a novel electron-rich small molecule HTM, 2,5-bis(4,4'-bis(methoxyphenyl)aminophen-4"-yl)-3,4-ethylenedioxythiophene, H101 (76), for PSCs.<sup>[187]</sup> Without using any *p*-type dopants, average PCE of 10.6% achieved under AM 1.5G solar simulation for perovskite devices based on H101. It was also demonstrated that chemical doping of H101 by FK102 could lower the Fermi level of H101 to generate higher voltages in devices, from 0.97 V for an undoped cell to 1.05 V with 15% doping, led to higher PCE of 13.8%. However, the photovoltaic data of the cells placed in an oven at 70 °C for 7 days showed that thermal stability of doped H101 and spiro-OMeTAD are comparable. In a study in 2014, KTM3 (77), a novel 3,3'-thiophene based HTM was developed.<sup>[188]</sup> PSC devices with the efficiency of 7.3% were achieved without adding *p*-type dopants to KTM3. A high hydrophobic oligothiophene derivative named DR3TBTT (78), the donor-acceptor-donor type molecule with benzodithiophene (BDT) as the central donor and rhodanine as the

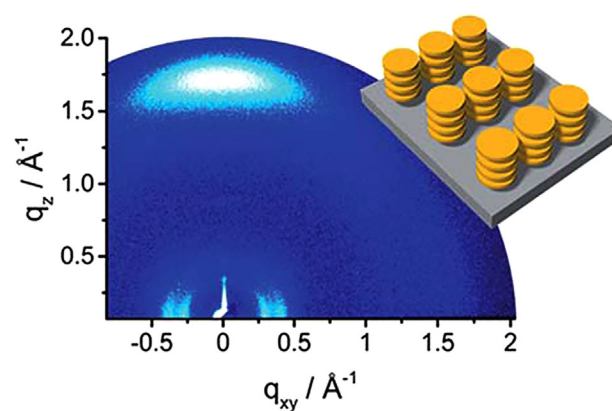


**Figure 20.** GIWAXS pattern of the KR321 film coated from tetrachloroethane on a silica wafer (schematic illustration of the molecular surface arrangement). Reproduced with permission.<sup>[204]</sup> Copyright 2017, the Royal Society of Chemistry.

end group, has been synthesized and employed as HTM in perovskite devices by Zheng et al.<sup>[189]</sup> An efficiency of 8.8% was obtained for  $\text{CH}_3\text{NH}_3\text{PbI}_{3-x}\text{Cl}_x$  based planar solar cells, while a small amount of polydimethylsiloxane (PDMS), but no ion additive was added to HTM. After 13 days storing under relatively low humidity of  $\approx 20\%$ , perovskite devices based on dopant-free DR3TBDTT have showed no decline in their performances. Another 1D linear donor-acceptor conjugated small molecule, DOR3T-TBDT (79), with a very similar structure to DR3TBDTT, has been used as dopant free HTM and a PCE of 14.9% has been reached by a planar perovskite device.<sup>[190]</sup> In their study, Liu et al. have used  $\text{CH}_3\text{NH}_3\text{PbI}_{3-x}\text{Cl}_x$  as light absorber, with valence band of  $\approx 5.4$  eV. Using ultraviolet photoelectron spectroscopy (UPS) and the optical band gap, HOMO and LUMO energy level of DOR3T-TBDT have been determined to be  $-5.1$  eV and  $-3.3$  eV. A high-performance PSC device has been reported by the same group with designing and introducing another derivative molecule with BDT central donor and tunable energy levels.<sup>[191]</sup> Using DERDTS-TBDT (80), as dopant-free HTM has been resulted in an impressive efficiency of 16.2% for a perovskite photovoltaic device with a conventional planar structure. In 2016, Chen and coworkers also introduced a novel small molecule HTMs with benzodithiophene as core unit.<sup>[192]</sup> Due to its high hole mobility and conductivity, BDT-C1 (81) was found as a good candidate for hole selective layer in perovskite devices. The PSC based on BDT-C1 showed an average PCE of 13.4%. Moreover, higher hydrophobicity of BDT-C1 provided a better protection of the perovskite layer from humidity and improved the stability of the devices. Later, the same group introduced a series of acceptor-donor-acceptor conjugated small molecules as additive free HTMs.<sup>[193]</sup> M3 (82) and M4 (83) have been synthesized and employed in PSCs both in their pristine form and in the form of bulk heterojunction with PC<sub>70</sub>BM. The PSCs based on M3 and M4 with the structure FTO/compact TiO<sub>2</sub>/mesoporous TiO<sub>2</sub>/(FAPbI<sub>3</sub>)<sub>0.85</sub>(MAPbBr<sub>3</sub>)<sub>0.15</sub>/HTM/Au have exhibited relatively high efficiencies of 14.8 and 12.3%, respectively. However, incorporation of PC<sub>70</sub>BM with M3 or M4 to form a BHJ bulk heterojunction has facilitated exciton dissociation, which has been led to improved efficiencies of 16.2 and 15.0% for the (FAPbI<sub>3</sub>)<sub>0.85</sub>(MAPbBr<sub>3</sub>)<sub>0.15</sub>/BHJ integrated devices containing M3:PC<sub>70</sub>BM and M4:PC<sub>70</sub>BM, respectively (Figure 19). The highest efficiency of 17.4% has been achieved for PSCs based on ionic molecule M7-TFSI (84) in the absence of any additives. The high efficiency was attributed to a deep HOMO energy level of M7-TFSI, along with its high hole mobility and high conductivity.

Yun et al. have prepared a series of small molecules based on 7,7'-(4,4-bis(2-ethylhexyl)-4H-silolo[3,2-b:4,5-b']dithiophene-2,6-diyl)bis(4-(5'-hexyl-[2,2'-bithiophene]-5-yl)benzo-[c]<sup>[1,2,5]</sup>thiadiazole) with different fluorine substitution patterns. PSCs have been fabricated based on these new HTMs with no additives.<sup>[194]</sup> Maximum PCE of 14.45%, achieved by the device based on 2F (85), has been originated from its better edge-on orientations and higher crystalline properties in the film state and consequently its highest OTFT mobility of  $0.217 \text{ cm}^2 \text{ V}^{-1} \text{ s}^{-1}$  compared to other compounds.

### 2.3.3. Carbazole

In a very recent study, Lu et al. have developed three new carbazole based HTMs with starburst structure, named SGT-405

(3,6) (86), SGT-410(3,6) (87), and SGT-411(3,6) (88).<sup>[195]</sup> Tuning the substitution position from (2,7) to (3,6) of carbazole moiety led to significantly increased  $T_g$  ( $192.7^\circ\text{C}$ ), improved film forming ability, reduced hole reorganization energy, and enhanced hole mobility of the obtained carbazole derivatives compared to its parent molecule SGT-405(2,7) (89) and spiro-OMeTAD. Dopant-free perovskite devices based on SGT-405 (3,6), SGT-410(3,6), and SGT-411(3,6) and with the structure of FTO/compact TiO<sub>2</sub>/meso-porous TiO<sub>2</sub>/ $\text{CH}_3\text{NH}_3\text{PbI}_{3-x}\text{Cl}_x$ /HTM/Au, have exhibited efficiencies of 8.48, 5.41, and 3.23%, respectively. A remarkable conversion efficiency of 18.87% has also obtained by the device based on doped SGT-405(3,6). In addition, due to the good uniform capping layer of SGT-405(3,6) on top of perovskite layer and the prevention of the moisture penetration into the perovskite layer, the stability of fabricated devices has been improved. In another study in 2017, a dopant-free HTM with (2-ethylhexyl)-9H-carbazole as core and N,N-di-p-methylthiophenylamine as end groups, termed CMT (90), was reported by Xu et al.<sup>[196]</sup> The presence of four methylthiol groups at the para-positions of the diphenylamine instead of methoxy groups has lowered the HOMO energy level of CMT. Perovskite devices with conventional planar structure based on pristine CMT have exhibited efficiencies as high as 13.05% with a  $V_{OC}$  of 1.03 V,  $J_{SC}$  of  $21.82 \text{ mA cm}^{-2}$ , and an FF of 58.23%.

### 2.3.4. Tetrathiafulvalene

In 2014, perovskite devices based on tetrathiafulvalene derivatives as the first dopant free molecular HTM were introduced by Liu and coworkers.<sup>[38a]</sup> With no additives for TTF-1 (91) HTM, a PCE of as high as 11.03% was reported. The obtained results for dopant-free devices were comparable with *p*-type doped spiro-OMeTAD based device (11.4%). Without using any hygroscopic dopants, the TTF-1 based devices showed two time more stability in air at a relative humidity of 40%, in comparison with devices with doped spiro-OMeTAD. It was demonstrated that the efficient hole conductivity of TTF-1 was originated from the inherent  $\pi-\pi$  stacking and strong S-S interaction between adjacent and highly rigid conjugated units. However, low solubility or insolubility of TTF-1 in most common organic solvents led to apply expensive and time-consuming vacuum sublimation method to fabricate thin film. In a recent study in 2017, Chen et al. introduced another tetrathiafulvalene derivative anchored with eight carboxyl groups, TTA (92) to use as a dopant-free HTM in PSCs.<sup>[197]</sup> Higher solubility of TTA compared to TTF-1, made it possible to use the solution processed method for thin film making. The inverted planar perovskite devices based on TTA reached to remarkable efficiency of 16.7% and this was 44% higher compared to the reference device without HTM. The higher efficiencies were ascribed to factors including well-aligned energy level and high hole mobility of TTA, as well as improved perovskite morphology.

### 2.3.5. Triazatruxene

In an extended delocalized  $\pi$ -system, three indole units are combined by one benzene ring in triazatruxene. With their

electron rich aromatic structure, triazatruxene derivatives has been widely used to produce electroactive discotic liquid crystalline materials,<sup>[198]</sup> organic-light-emitting diodes (OLEDs),<sup>[199]</sup> and two photon absorption (TPA) materials.<sup>[200]</sup> In 2015, Ramos et al. designed and synthesized two novel triazatruxene core based HTMs, HMDI (93) and HPDI (94) to exploit in PSCs.<sup>[201]</sup> Without using any chemical dopants for HTMs, devices based on HMDI and HPDI exhibited average efficiencies of 8.62 and 9.83%, respectively. While using *p*-type dopants for HPDI slightly increase the PCE of the PSC to 10.82%, doping of HMDI lowered both  $V_{OC}$  and  $J_{SC}$  of the perovskite device. In the same year, Zhang et al. used another triazatruxene derivative HTM with excellent thermal stability, good solubility and high hole mobility in PSCs.<sup>[202]</sup> Doped and pristine TPDI (95) were applied in perovskite devices and PCEs of 15.5 and 13.6% were achieved, respectively. In 2017, a vacuum deposited p-i-n perovskite device employing a triazatruxene based HTM, named TBDI (96) were reported.<sup>[203]</sup> Without any dopants, a PCE of 7.3% has been exhibited in a reverse scan by TBDI based device. However, using a thin buffer layer of MoO<sub>3</sub> together with TBDI, improved the PCE to 14.85% and with negligible degree of hysteresis. It was demonstrated that the thin MoO<sub>3</sub> layer deposited between the ITO contact and TBDI works as a dielectric layer and fine-tune TBDI energy level, building a favorable interface for enhanced hole extraction. Recently, an outstanding efficiency over 19% has been reported by Rakstys et al. for a PSC with mixed-perovskite (FAPbI<sub>3</sub>)<sub>0.85</sub>(MAPbBr<sub>3</sub>)<sub>0.15</sub> and using KR321 (97), with triazatruxene central core and thiophene-based arms, as an additive free star-shaped HTM.<sup>[204]</sup> It has been revealed a particular face-on organization on perovskite film has been formed by KR321, which was a crucial factor to improve the vertical charge carrier transport, and resulted in a high PCE. The supramolecular organization has also been determined by Grazing-Incidence Wide-Angle X-ray Scattering (GIWAXS) (**Figure 20**).

In 2016, Trux-OMeTAD (98), with its C<sub>3h</sub> truxene-core and planar and rigid geometry was designed and introduced by Huang et al. to use as a dopant-free HTM for PSCs with p-i-n architecture.<sup>[205]</sup> The HOMO energy level of trux-OMeTAD (−5.28 eV) is deeper than that of spiro-OMeTAD (−5.10 eV) and the hole mobility of as-cast trux-OMeTAD film is  $2.3 \times 10^{-3} \text{ cm}^2 \text{ V}^{-1} \text{ s}^{-1}$ . Outstanding PCEs up to 18.6% was achieved by perovskite devices employing dopant-free trux-OMeTAD as hole contact layer. It was demonstrated that PSCs with trux-OMeTAD also showed good reproducibility. More than 75% of fabricated devices had PCE higher than 17%. Recently, Grisorio and coworkers have compared the efficiencies of direct and inverted structured PSCs employing two new truxene based HTMs, Trux1 (99) and Trux2 (100).<sup>[206]</sup> It has been suggested that the lower performances (4–5%), observed for the devices with n-i-p architecture, was originated from the reduced hole-transport properties of HTM, which was likely ascribable to the mandatorily thicker HTM layer. However, the photovoltaic performances observed for p-i-n architecture devices have been completely reversed. It has been demonstrated that more favorable perovskite/HTM layer with 2D structure of trux based HTMs in a very thin layer has boosted the performance of Trux1 and Trux2 based devices to 10.2 and 13.4%, respectively.

### 2.3.6. Acenes

In 2015, Kazim et al. reported a linear acene derivative exploited as dopant-free HTM for mesoscopic perovskite devices.<sup>[207]</sup> The solution processable, small molecule semiconductor, TIPS-pentacene (101) gave an efficiency of 11.8% in its pristine form, through solvent engineering and concentration optimization. Two novel  $\pi$ -conjugated oligothiophenes based on S,N-heteropentacene, (102) and (103) have been developed by Qin et al. and used as hole selective layer in perovskite devices.<sup>[208]</sup> With their high photo-absorptivity in the low energy region, these materials can contribute to the light harvesting of the solar spectrum. PCEs of 9.5–10.5% has been yielded by devices employing these HTMs with no chemical *p*-type additives. Two other acceptor–donor–acceptor type low band gap HTMs comprising S,N-heteropentacene central units, (104) and (105) have been designed by Steck et al. for PSCs.<sup>[209]</sup> Without the use of any additive or dopant, PCEs of 10.3–11.4% have been generated by mesoscopic perovskite devices prepared by solution-processing using these HTMs. PCEs as high as 16.9% were reported by Bi et al. for mixed perovskite devices in 2016.<sup>[210]</sup> In their study, a novel HTM with a S,N-heteropentacene  $\pi$ -bridge connecting a triarylamine donor and a dicyanovinyl acceptor group (106), was developed and applied in a solution processable (FAPbI<sub>3</sub>)<sub>0.85</sub>(MAPbBr<sub>3</sub>)<sub>0.15</sub>-based PSC.

### 2.3.7. Organometallic and Coordination Compounds as HTM

Phthalocyanine compounds have high stability and efficient light-harvesting ability throughout a large portion of the solar emission spectrum.<sup>[211]</sup> In 2015, Ke et al. introduced copper phthalocyanine (CuPc) (107) as HTM with no additives and demonstrated an efficient room-temperature fully-vacuum-processed planar PSC.<sup>[212]</sup> CuPc exhibits high hole mobility, and is relatively inexpensive. The HOMO level of CuPc is −5.20 eV and it is thermally and chemically stable. Due to the higher LUMO level of CuPc than that of perovskite, electrons can also be blocked by CuPc hole selective layer. The optimized thickness of 60 nm for CuPc led to the highest PCE of 15.42% with a  $V_{OC}$  of 1.04 V, a  $J_{SC}$  of 18.91 mA cm<sup>−2</sup>, and an FF of 78.11%. The steady-state efficiency of fabricated PSCs however was 14.5%. They also reported a PCE of 7.26% for the best-performing flexible planar PSC. Ramos et al. have introduced a solution processable non-aggregated Zn(II)octa(2,6-diphenylphenoxy) phthalocyanine, named TT80 (108) to apply as HTM for PSCs.<sup>[213]</sup> Using chlorobenzene as the uptake solvent and no additives, an efficiency of 2.6% has been reported. Employing  $\beta$ -TiOPc (109) as HTM in perovskite devices with a thickness of 40 nm and without doping resulted in a PCE of 5.05%.<sup>[214]</sup> In 2016, CoPcNO<sub>2</sub>-OPh (110), a novel asymmetric phthalocyanine based HTM for PSCs was designed and synthesized by Guo et al.<sup>[215]</sup> Based on density functional theory calculation results, HOMO and LUMO energy levels of the HTM are −5.14 and −3.05 eV, respectively, which were influenced and adjusted by introduction of phenoxy and nitro groups. With the optimized concentration of 20 mg mL<sup>−1</sup> HTM in chlorobenzene, an overall efficiency of 8.24% was achieved. In another study, Guo et al. have used ZnPcNO<sub>2</sub>-OPh (111) and CuPcNO<sub>2</sub>-OPh (112) as

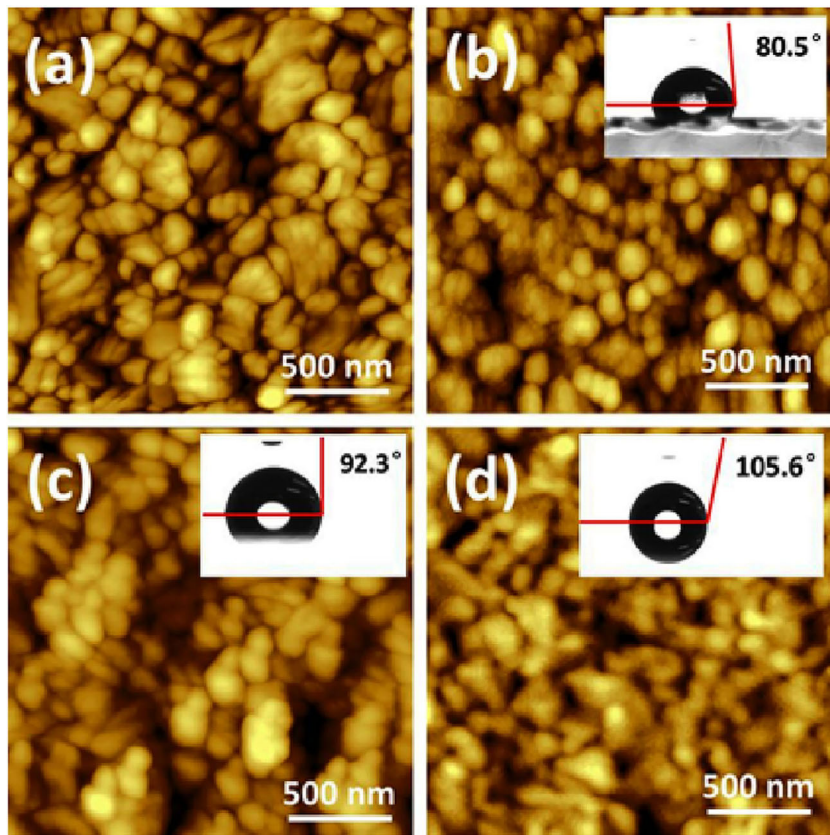


**Figure 21.** Atomic force microscopy images of a) perovskite, b) CuPc, c) CuMePc, and d) CuEtPc deposited on FTO/SnO<sub>2</sub>. (Inset: Droplets of water on (b) CuPc (c) CuMePc, and (d) CuEtPc). Reproduced with permission.<sup>[221]</sup> Copyright 2017, Elsevier.

dopant-free HTMs in (FAPbI<sub>3</sub>)<sub>0.85</sub>-(MAPbBr<sub>3</sub>)<sub>0.15</sub> perovskite devices.<sup>[216]</sup> Their results confirmed that metal core plays a crucial role in photovoltaic performance of fabricated devices. With ZnPcNO<sub>2</sub>-OPh as HTM, the maximum PCE of 14.35% with a high open-circuit voltage of 1.071 V have been reported. While, the efficiency of 12.72% with a  $V_{OC}$  of 1.064 V has been achieved for PSCs based on CuPcNO<sub>2</sub>-OPh HTM. Sfyri et al. have introduced butyl substitutes to CuPc and synthesized soluble substituted CuPc HTMs, n-CuBuPc (113) and *tert*-CuBuPc (114) to exploit in PSCs.<sup>[217]</sup> Solution processed perovskite devices based on n-CuBuPc to efficiencies of 8.5 and 5.6%, respectively. ZnPc(*t*Bu)<sub>4</sub> (115) also has been used as dopant-free HTM in PSCs and efficiencies of 5.16 and 7.98% have been measured under forward and reverse voltage scanning, respectively.<sup>[218]</sup> In two other studies in 2016, Sfyri et al. used vacuum deposited tetra methyl substituted Cu(II) phthalocyanine (CuMePc) (116) and solution processable tetratriphenylamine Zn phthalocyanine (TPA-Pc) (117) HTMs in perovskite devices.<sup>[219]</sup> Maximum efficiency of 5.2% has been achieved for CuMePc based devices. Higher charge mobility has been observed for CuMePc compared to CuPc, which was attributed to stronger  $\pi-\pi$  interaction in CuMePc ( $\approx 3.8 \text{ \AA}$  in CuMePc vs.  $3.4 \text{ \AA}$  in CuPc).<sup>[220]</sup> PCE of 5.6% has also been

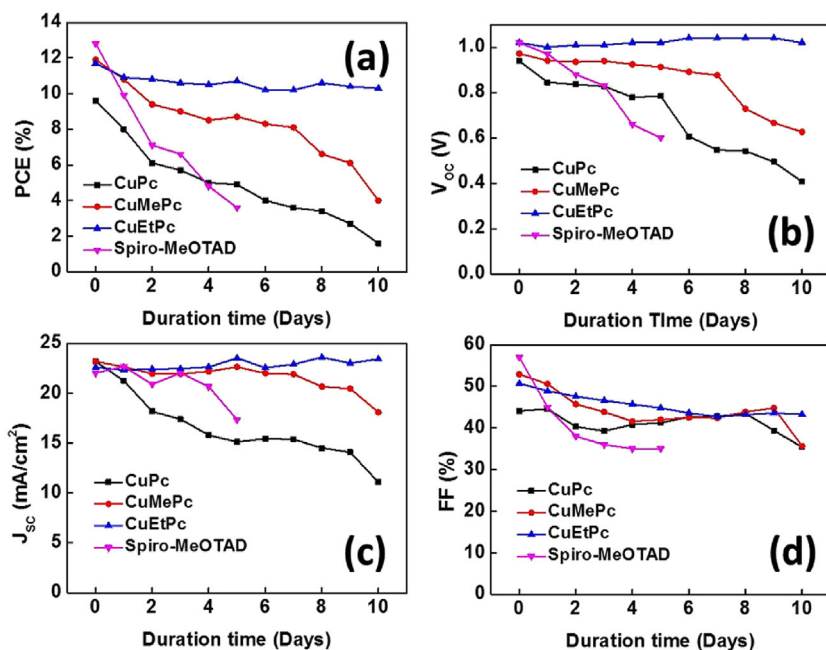


**Figure 22.** a) PCE, b)  $J_{SC}$ , c)  $V_{OC}$ , and d) fill factor values of the best devices as a function of ambient storage time of devices with different phthalocyanine and spiro-MeOTAD hole conductors at a relative humidity of  $\sim 70\%$  without any encapsulations. Reproduced with permission.<sup>[221]</sup> Copyright 2017, Elsevier.

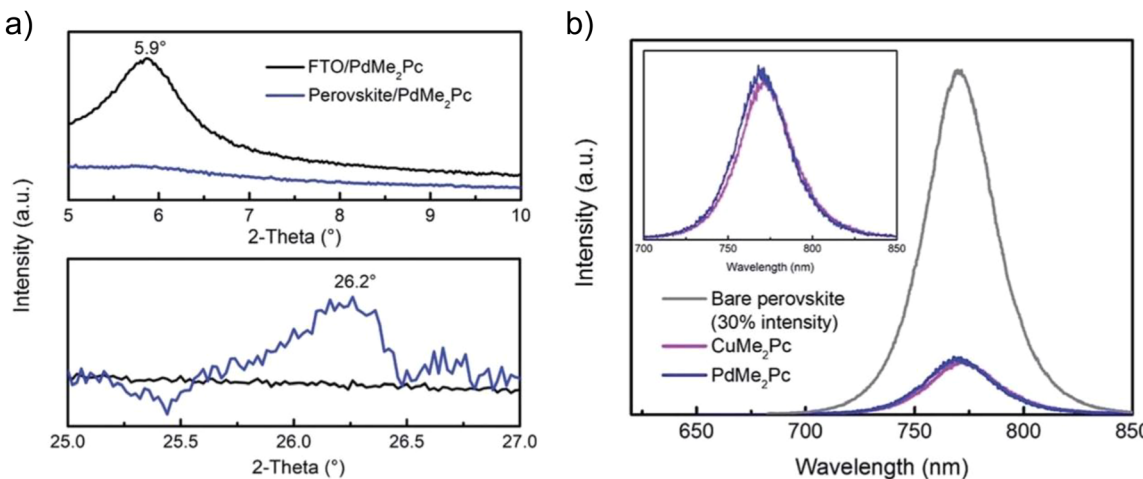


**Figure 23.** a) The GIXRD patterns of PdMe<sub>2</sub>Pc deposited on FTO and perovskite/FTO substrates for 2θ of 5–10° (up) and 2θ of 25–27° (down). b) Steady-state PL spectra of bare perovskite, perovskite/PdMe<sub>2</sub>Pc, and perovskite/CuMe<sub>2</sub>Pc samples. Note that the intensity of the bare perovskite was artificially reduced to 30% of its initial value to facilitate comparison. Reproduced with permission.<sup>[224]</sup> Copyright 2017, the Royal Society of Chemistry.

reported for TPA-Pc based devices. In their work, Wang et al. have incorporated CuPc, CuMePc, and CuEtPc (118) as a dopant-free hole transport layer for planar PSCs.<sup>[221]</sup> Highest efficiency of 11.9% has been measured for the devices based on CuMePc. A slightly lower efficiency of 11.7% has been observed for CuEtPc based PSCs. However, the CuEtPc-based device exhibited the best operational stability and highest  $V_{OC}$ . The introduction of tetra-alkyl groups resulted in a more hydrophobic surface and more condensed thin-film structure (Figure 21). As seen in Figure 22, after a 10-day stability test, the PCEs of PSCs with CuPc, CuMePc and CuEtPc as the HTMs retained 16.6, 33.6, and 88% of their initial value, respectively. In a very recent study, a new HTM of copper (II) phthalocyanine with tetrapropyl-substituted function groups (CuPrPc) (119) is reported by Liu et al. It is found that CuPrPc could form face-on molecular orientation when spin-coated on perovskite, resulting in high hole mobility and hydrophobic surface. These properties are more favorable for hole transport and moisture resistance applications in PSCs. An average PCE of  $17.0 \pm 0.5\%$  and a highest PCE of 17.8% were achieved for PSC devices fabricated

by a simple solution process using CuPrPc as a dopant-free HTM. Furthermore, beneficial from the hydrophobic nature of CuPrPc, the devices with CuPrPc as HTM show improved stability and retain over 94% of their initial efficiency even after storage in humidity about 75% for 800 h without encapsulation, which is much better than the performance of PSCs based on Spiro-OMeTAD HTM.<sup>[222]</sup>

In a recent study, stable PSCs have been fabricated using octamethyl-substituted copper (II) phthalocyanine (CuMe<sub>2</sub>Pc) (120) as an additive free HTM.<sup>[223]</sup> Through vacuum deposition method, a condense thin film with hydrophobic surface and high hole mobility has been obtained, in which a face-on molecular alignment played an important role in achieving high photovoltaic performance for the fabricated devices. CuMe<sub>2</sub>Pc has been easily synthesized in a one-step synthetic route from 4,5-dimethylphthalonitrile. CuMe<sub>2</sub>Pc based perovskite devices have showed efficiencies as high as 15.73%. They have retained over 95% of their initial efficiencies even after storage in the humidity about 50% for 2000 h without encapsulation.

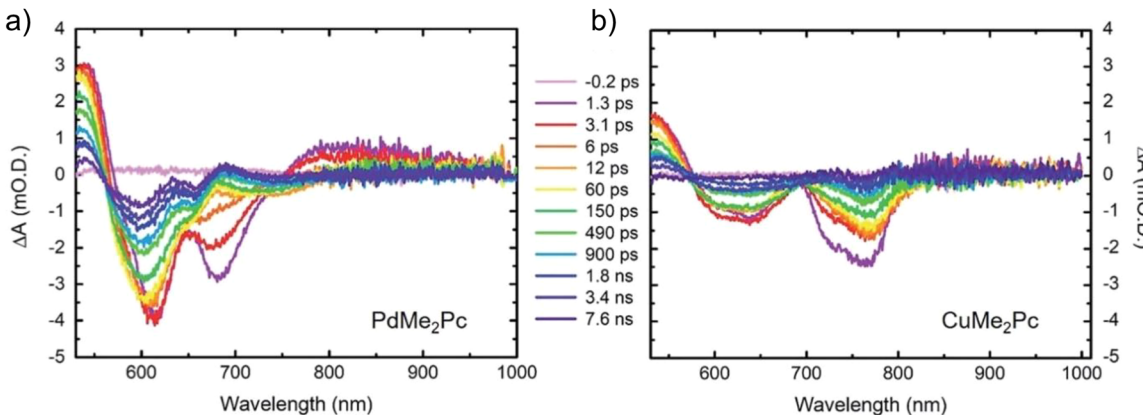


**Figure 24.** TA spectra evolution of a) PdMe<sub>2</sub>Pc and b) CuMe<sub>2</sub>Pc at indicated delay times. Reproduced with permission.<sup>[224]</sup> Copyright 2017, the Royal Society of Chemistry.

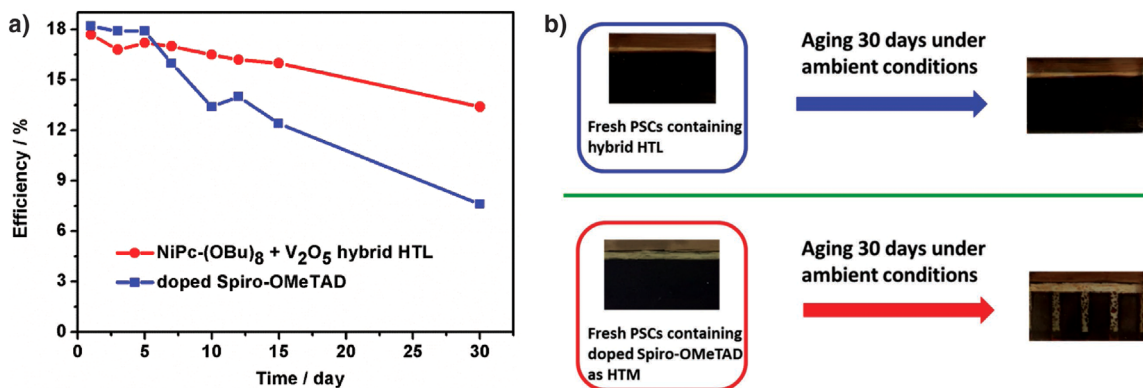


**Figure 25.** a) Shelf stability of not encapsulated PSCs under dark ambient conditions (humidity about 40%–45% and temperature of 20–25°C). b) Photographs of PSCs containing different HTLs before and after aging tests. Reproduced with permission.<sup>[227]</sup> Copyright 2017, Wiley-VCH.

In a study in 2017, Zheng et al. changed the metal center from Cu(II) to Pd(II) and synthesized PdMe<sub>2</sub>Pc (121).<sup>[224]</sup> An improvement was observed for planar PSC devices employing PdMe<sub>2</sub>Pc as HTM, compared to its counterpart with Cu metal center. The cell based on dopant-free PdMe<sub>2</sub>Pc exhibited a  $V_{OC}$  of 1.06 V,  $J_{SC}$  of 21.08 mA cm<sup>-2</sup>, FF of 73%, and PCE of 16.28%, while the CuMe<sub>2</sub>Pc-based device displayed a  $V_{OC}$  of 1.01 V,  $J_{SC}$  of 21.46 mA cm<sup>-2</sup>, FF of 72%, and PCE of 15.58%. Based on the grazing incidence X-ray diffraction (GIXRD) patterns of PdMe<sub>2</sub>Pc deposited on perovskite and FTO (Figure 23a), only on perovskite, PdMe<sub>2</sub>Pc exhibited the face-on orientation, which resulted in stronger  $\pi$ – $\pi$  interactions between the molecules and led to an enhanced hole mobility. Photoluminescence (PL) measurements indicated the slightly more efficient hole extraction of CuMe<sub>2</sub>Pc than to PdMe<sub>2</sub>Pc (Figure 23b). However, determined by transient absorption (TA) spectroscopy, the carrier lifetime ( $\tau_E$ ) of PdMe<sub>2</sub>Pc was found to be approximately 7.7 ns, which is more than twice the value for CuMe<sub>2</sub>Pc (3.4 ns) (Figure 24). Therefore, PdMe<sub>2</sub>Pc exhibited a long carrier diffusion length,  $L_D$  (26 nm), which reduced the charge recombination. The higher LUMO level and longer  $L_D$  of PdMe<sub>2</sub>Pc provided a better hole-blocking efficiency and thus leading to a higher  $V_{OC}$  and FF. The device with PdMe<sub>2</sub>Pc also showed a good long-term stability and retained over 96% of its initial PCEs after 600 h of storage.

Utilizing metal free C<sub>5</sub>PcH<sub>2</sub> (122) as a dopant-free HTM with thermal annealing, the best PSC devices in FTO/compact TiO<sub>2</sub>/mesoporous TiO<sub>2</sub>:CH<sub>3</sub>NH<sub>3</sub>PbI<sub>3</sub>/C<sub>5</sub>PcH<sub>2</sub>/MoO<sub>x</sub>/Au structure have shown the efficiencies up to 12.2%.<sup>[225]</sup> In 2017, Jiang et al. reported the use of a solution-processable copper(II) phthalocyanine derivative coded as CuPc-TIPS (123) as a HTM for PSCs, in combination with a mixed-ion perovskite absorber (FAPbI<sub>3</sub>)<sub>0.85</sub>(MAPbBr<sub>3</sub>)<sub>0.15</sub> and a low-cost vacuum-free carbon counter electrode.<sup>[226]</sup> Optimized PSC based on pristine CuPc-TIPS showed an efficiency of 14.0%, together with long-term stability. Efficient PSCs with good stability under dark ambient conditions have been reported in a research carried out by Cheng et al. using an organic–inorganic integrated hole transport layer composed of the solution-processable nickel phthalocyanine (NiPc-(OBu)<sub>8</sub>) (124) and vanadium (V) oxide (V<sub>2</sub>O<sub>5</sub>).<sup>[227]</sup> The optimized NiPc-(OBu)<sub>8</sub>/V<sub>2</sub>O<sub>5</sub> integrated HTL based PSCs

displayed an impressive average PCE of 17.6%. The devices retained 75% of their initial efficiencies over the time span of 30 days. While, the PSCs based on doped Spiro-OMeTAD dramatically decayed after the same aging period (Figure 25).

Recently, porphyrin based HTMs has also attracted some attentions in researches in the field of perovskite devices. Two novel symmetric ethynylaniline-substituted porphyrin based HTMs Y2 (125) and Y2A2 (126), have been employed in conventional planar PSCs and PCEs of 16.60 and 10.55% have been measured, respectively.<sup>[228]</sup> In 2017, Chen et al. have

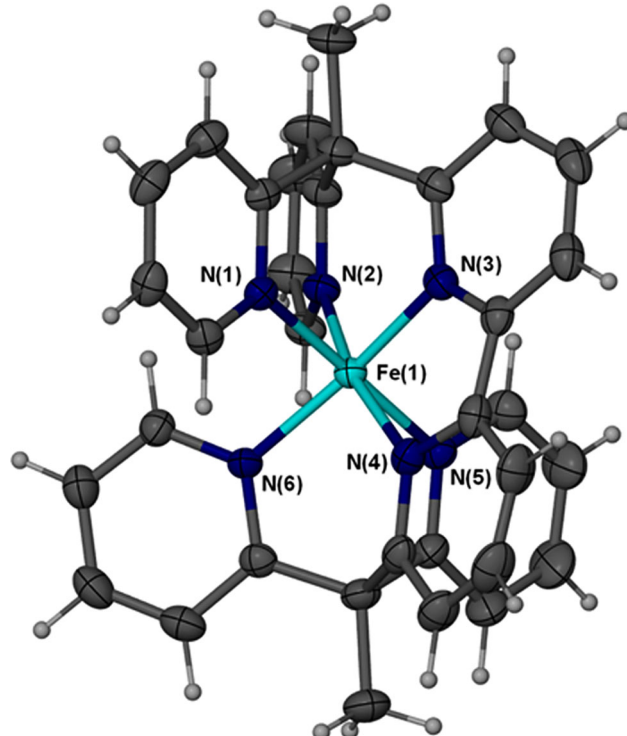


**Figure 26.** Structure of [Fe(bpyPY4)]<sup>3+</sup> inferred by single-crystal X-ray analysis with 50% thermal ellipsoids. Reproduced with permission.<sup>[231]</sup> Copyright 2017, American Chemical Society.

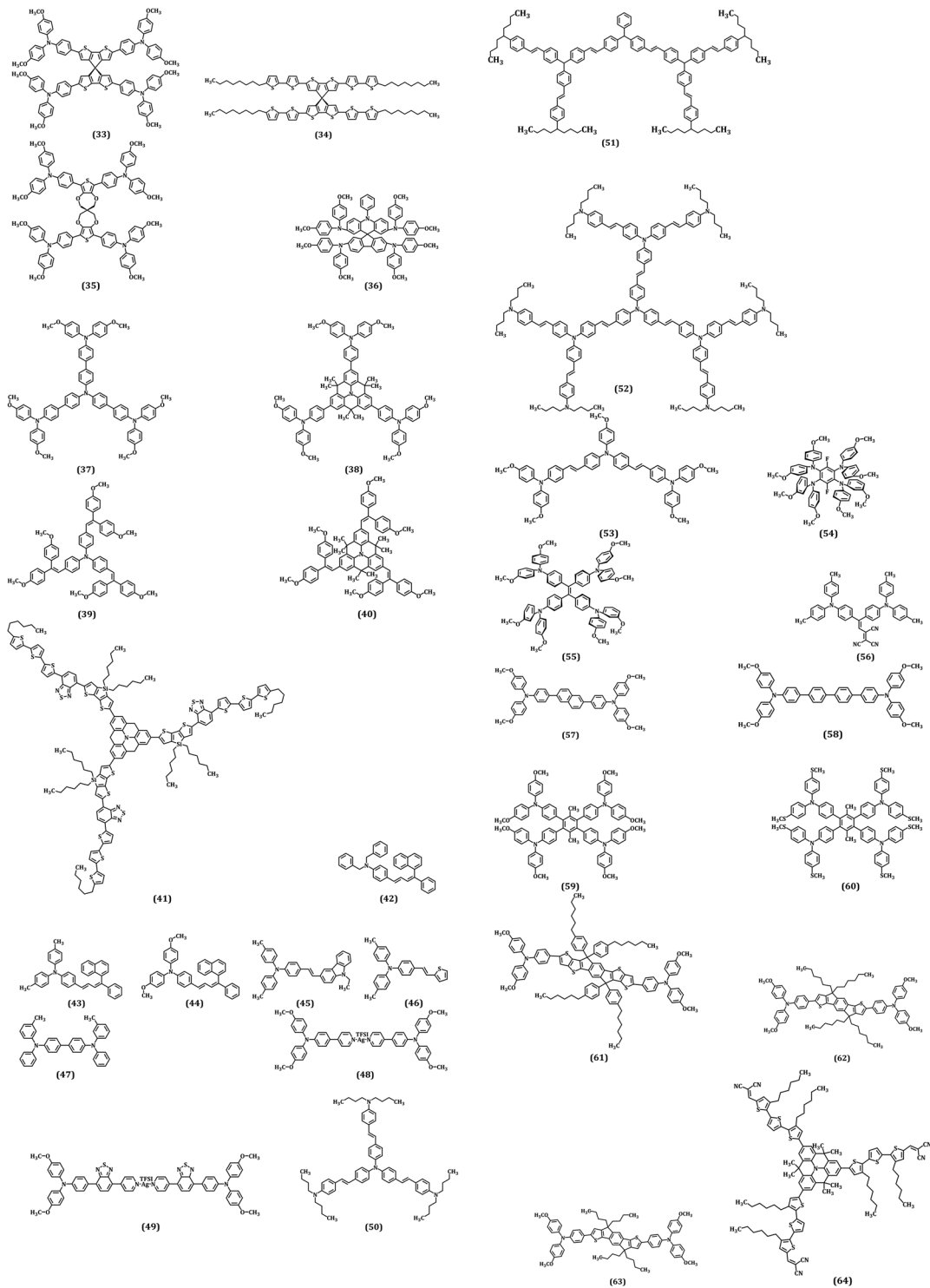
**Table 3.** Photovoltaic properties of some selected perovskite devices with small molecule HTMs.

$V_{OC}$ [V]	$J_{SC}$ [mA cm $^{-2}$ ]	FF [%]	PCE [%]	ETL	Perovskite	HTM	Band edges (HOMO)	Hole mobility [cm $^2$ V $^{-1}$ s $^{-1}$ ]	Device architecture	References
1.04	18.91	78.1	15.32	C <sub>60</sub>	MAPbI <sub>3</sub>	CuPc	-5.20	10 $^{-2}$	n-i-p planar	[212]
1.085	20.7	70	15.6	TiO <sub>2</sub>	(FAPbI <sub>3</sub> ) <sub>0.85</sub> (MAPbBr <sub>3</sub> ) <sub>0.15</sub>	M3	-5.38		n-i-p Mesoporous	[193a]
0.99	22.82	73	16.60	TiO <sub>2</sub>	MAPbI <sub>3</sub>	Y2	-5.25	2.04 × 10 $^{-4}$	n-i-p Mesoporous	[228]
1.02	23.2	79	18.6	PCBM	MAPbI <sub>3</sub>	Trux-OMeTAD	-5.3		p-i-n planar	[205]
1.04	20.84	78	16.94	SnO <sub>2</sub> /PCBM	MAPbI <sub>3</sub>	BTPA-TCNE	-5.35	3.14 × 10 $^{-5}$	n-i-p	[175]
1.05	21.2	73	16.2	TiO <sub>2</sub>	MAPbI <sub>3</sub>	DERDTS-TBDT	-5.2	1.0 × 10 $^{-4}$	n-i-p	[191]
1.053	21.27	69	16.1	TiO <sub>2</sub>	MAPbI <sub>3</sub>	Z34	-5.14	7.46 × 10 $^{-4}$	n-i-p Mesoporous	[173]
1.059	21.07	66	15.4	TiO <sub>2</sub>	MAPbI <sub>3</sub>	ST1	-5.24	2 × 10 $^{-4}$	n-i-p Mesoporous	[171]
1.07	20.15	77	16.6	PCBM	MAPbI <sub>3</sub>	TPP-SMeTAD	-5.18	10 $^{-4}$ –10 $^{-5}$	p-i-n	[177]
1.04	20.4	78	16.7	PCBM	MAPbI <sub>3</sub>	TTA	-5.26	9.68 × 10 $^{-4}$	p-i-n	[197]
1.03	21.55	68	15.7	PCBM	MAPbI <sub>3</sub>	IDTT-TPA	-5.0	6.46 × 10 $^{-4}$	n-i-p planar	[178]
1.13	21.71	77	18.9	TiO <sub>2</sub>	(FAPbI <sub>3</sub> ) <sub>0.85</sub> (MAPbBr <sub>3</sub> ) <sub>0.15</sub>	FA-CN	-5.30	1.2 × 10 $^{-4}$	n-i-p Mesoporous	[180]
1.09	20.85	77	17.5	TiO <sub>2</sub>	(FAPbI <sub>3</sub> ) <sub>0.85</sub> (MAPbBr <sub>3</sub> ) <sub>0.15</sub>	TPA-CN	-5.38	1.1 × 10 $^{-4}$	n-i-p Mesoporous	[180]
0.99	22.11	75	17.54	PCBM	MAPbI <sub>3</sub>	TPAC3M	-4.96	1.1 × 10 $^{-5}$	p-i-n planar	[181]
1.07	21.49	71	16.32	PCBM	MAPbI <sub>3</sub>	TPA-TVT-TPA	-5.37	5.1 × 10 $^{-5}$	p-i-n planar	[182]
1.13	21.70	78	19.03	TiO <sub>2</sub>	(FAPbI <sub>3</sub> ) <sub>0.85</sub> (MAPbBr <sub>3</sub> ) <sub>0.15</sub>	KR321	-5.24	2.6 × 10 $^{-4}$	n-i-p Mesoporous	[204]
1.05	20.00	75	15.71	PCBM	MAPbI <sub>3</sub>	CzPAF-TPA	-5.07	3.13 × 10 $^{-4}$	n-i-p	[184]
1.04	22.32	81	18.80	PCBM	MAPbI <sub>3</sub>	TAPC	-5.5	2.58 × 10 $^{-2}$	p-i-n planar	[185]

developed CuP (127) and ZnP (128), two arylamine-substituted porphyrin based HTMs for perovskite devices.<sup>[229]</sup> Efficient and stable PSCs have been fabricated with PCEs as high as 15.36 and 17.78% for CuP and ZnP based devices, respectively. The observed high photovoltaic performances were attributed to the suitable energy levels, efficient exciton dissociation, and charge transfer in HTM/perovskite films. Li et al. have used chlorophyll-based materials as HTMs for perovskite devices and without the use of typical additives, they have measured efficiencies of 11.44 and 8.06% for the devices based on Chl-1 (129) and Chl-2 (130), respectively.<sup>[230]</sup> The HTM aggregate films have been obtained through a simple spin coating process, resulted in an ultra-smooth film surface with high hole mobility, which has provided an appropriate energy levels and efficient hole injection efficiencies. In a very recent study in 2017, Kashif and coworkers demonstrated the capability of transition metal complexes to act as dopant-free, solution-processable HTMs in PSCs.<sup>[231]</sup> As a new category of small molecule HTMs, in which the conductivity is provided by a redox transformation of a transition metal, planar FAPbBr<sub>3</sub> PSCs were fabricated using [Fe(bpyPY4)](OTf)<sub>2+x</sub> (Figure 26) as HTM and a maximum PCE of 2.2% was reported for PSC based on [Fe(bpyPY4)](OTf)<sub>2.5</sub>.

### 2.3.8. Other Small Molecule HTMs

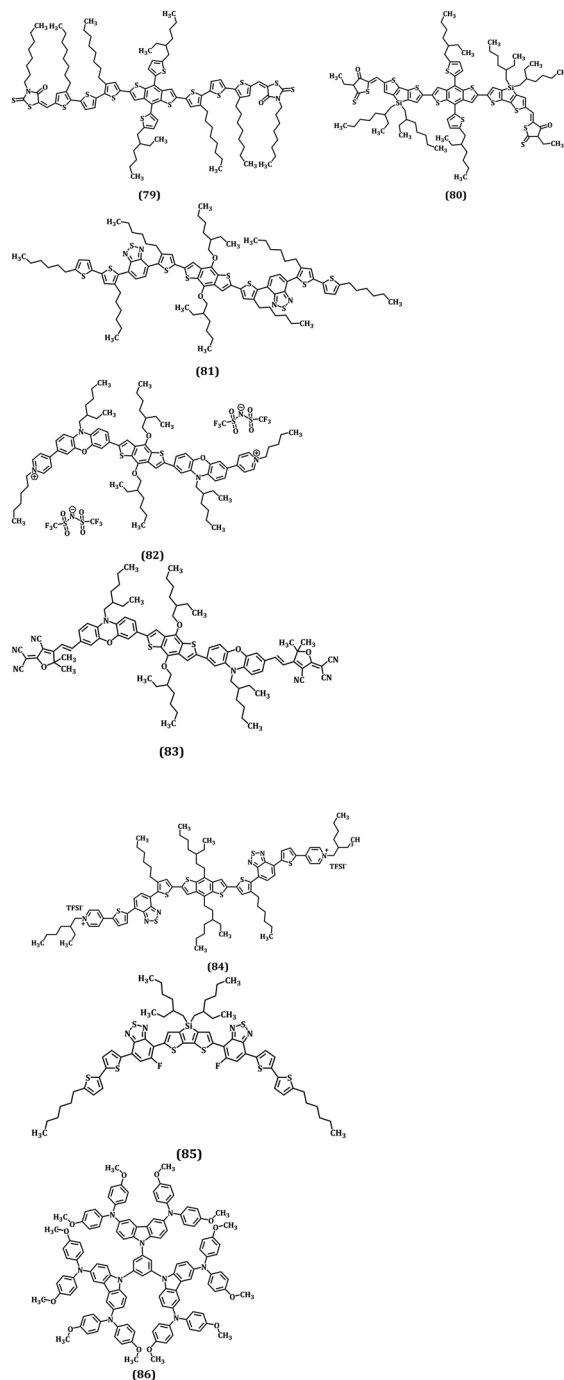
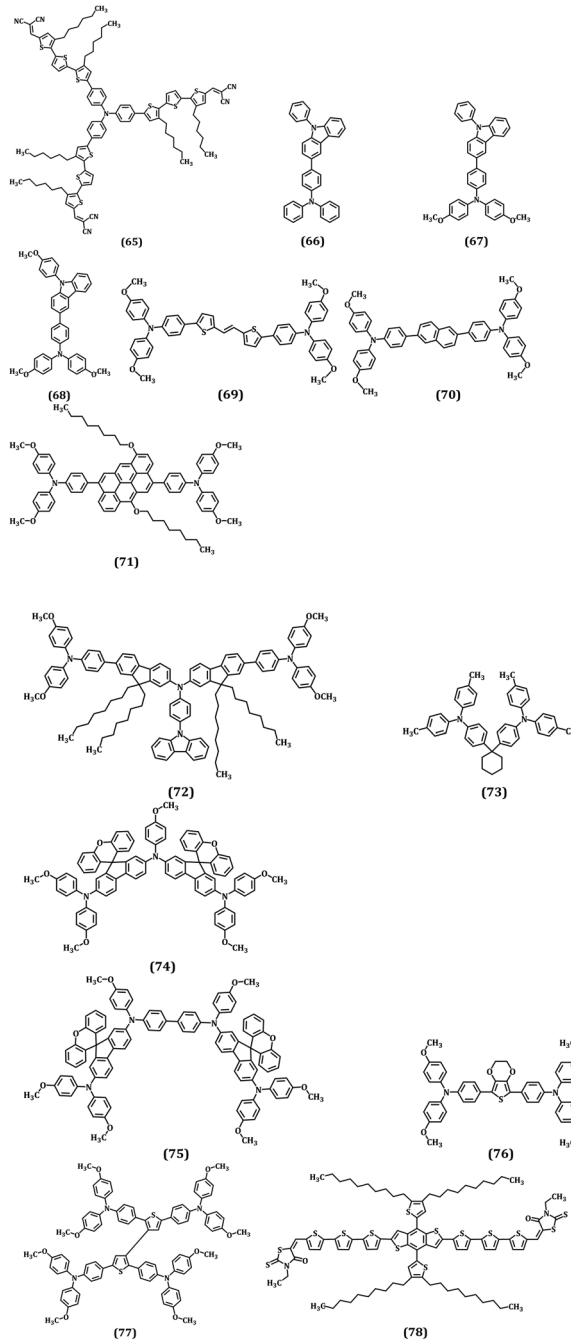
In 2015, Cabau et al. developed a tetraarylethene based HTM, named TAE-1 (131) as HTM for PSCs.<sup>[232]</sup> The solar cell based on this HTM exhibited a PCE of as high as 11.0% with no additional dopants. Recently, Zhu and coworkers have synthesized TTBCPE (132) with tetraphenylethene as core and t-butyl-carbazole as terminal units and employed it as doped and undoped HTM for PSCs.<sup>[233]</sup> While the doped spiro-OMeTAD showed an efficiency of 14.46%, a comparable PCE of 12.65% has been recorded by the more stable devices based on undoped TTBCPE under the same conditions. Electron rich small molecule HTM, S101 (133), containing silafluorene as the core with arylamine side groups, has been synthesized through a short efficient route by Krishna et al. and incorporated into a PSC as dopant-free HTM.<sup>[234]</sup> An overall PCE of ≈11% has been measured. SDF-OMeTAD has been recently designed and synthesized via a two-step reaction by Li et al.<sup>[235]</sup> The SDF-OMeTAD (134) was exploited in lead halide planar perovskite solar cells using low-temperature solution-processed SnO<sub>2</sub> as the electron transporting layer, delivering a PCE of 13.01% with a  $V_{OC}$  of 1.10 V under 100 mW cm $^{-2}$  AM 1.5G solar illumination.



**Figure 27.** Molecular structure of small molecule based HTMs.

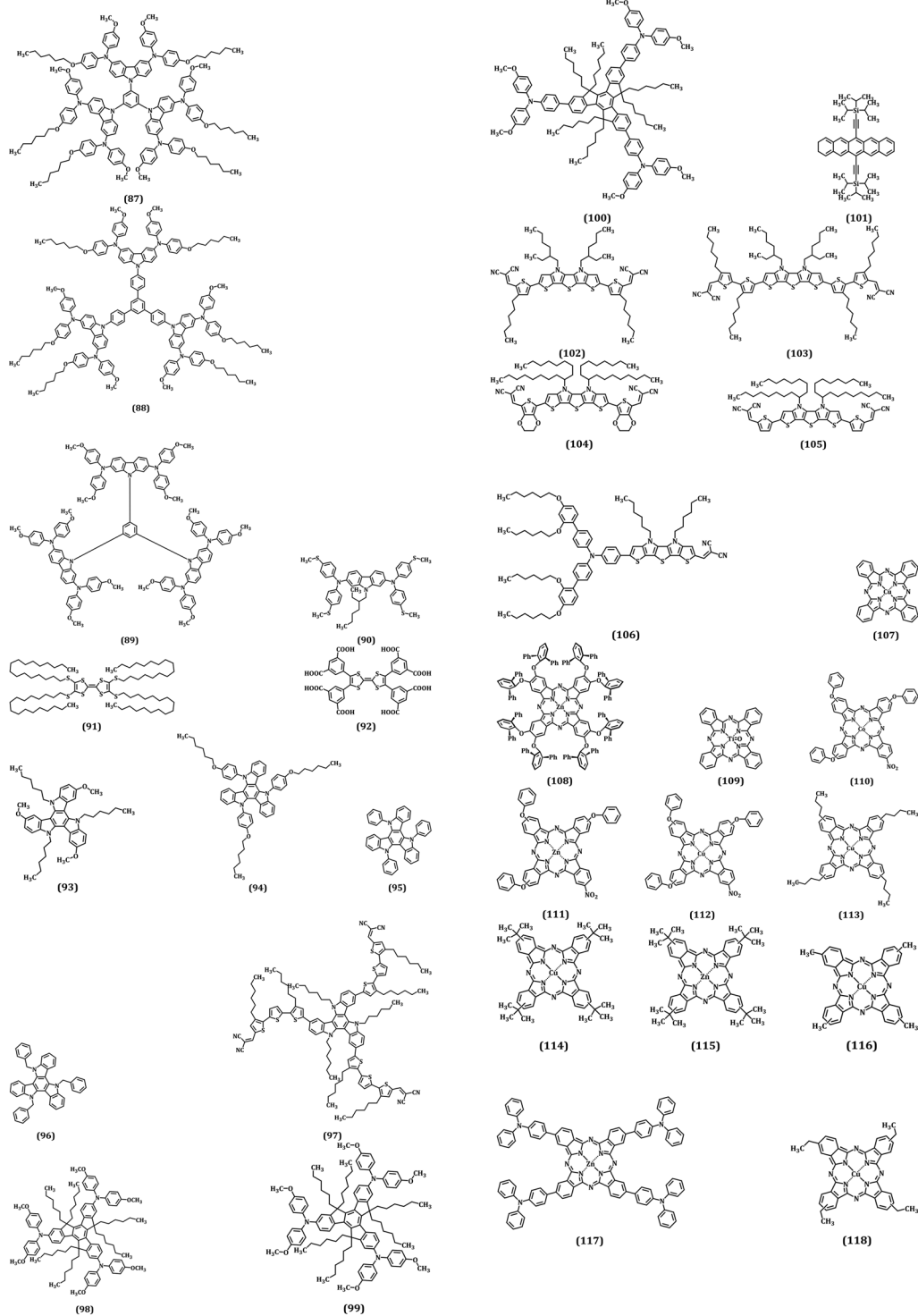
In 2016, two novel phenonaphthazine derivatives, BPZTPA (135) and MeO-BPZTPA (136), were synthesized and employed in the fabrication of PSCs.<sup>[23,6]</sup> The prepared HTMs exhibited excellent thermal stability, hole mobility ( $\approx 10^{-4} \text{ cm}^2 \text{ V}^{-1} \text{ s}^{-1}$ ) and suitable HOMO energy levels ( $-5.34 \text{ eV}$  for BPZTPA and  $-5.29 \text{ eV}$  for

MeO-BPZTPA). Fabricated mesoscopic  $\text{TiO}_2/\text{CH}_3\text{NH}_3\text{PbI}_3/\text{HTM}/\text{Au}$  perovskite devices based on dopant-free BPZTPA and MeO-BPZTPA showed efficiencies of 8.2 and 10.36%, respectively. Using phenoxazine as core unit, Cheng et al. have designed a small molecule HTM, POZ6 (137), which has


**Figure 27.** Continued.

dicyanovinyl units as electron-withdrawing terminal groups.<sup>[237]</sup> Regarding well-matched energy level between POZ6 and perovskite and good solubility of the HTM in organic solvents, as well as its high hole mobility and conductivity in its pristine form, POZ6 has been used as dopant-free HTM in PSCs, which has led to a PCE of 10.3%. However, using dopants has improved the efficiency up to 12.3%. Maximum efficiency of 12.22% has been achieved for perovskite devices using a dopant-free HTM

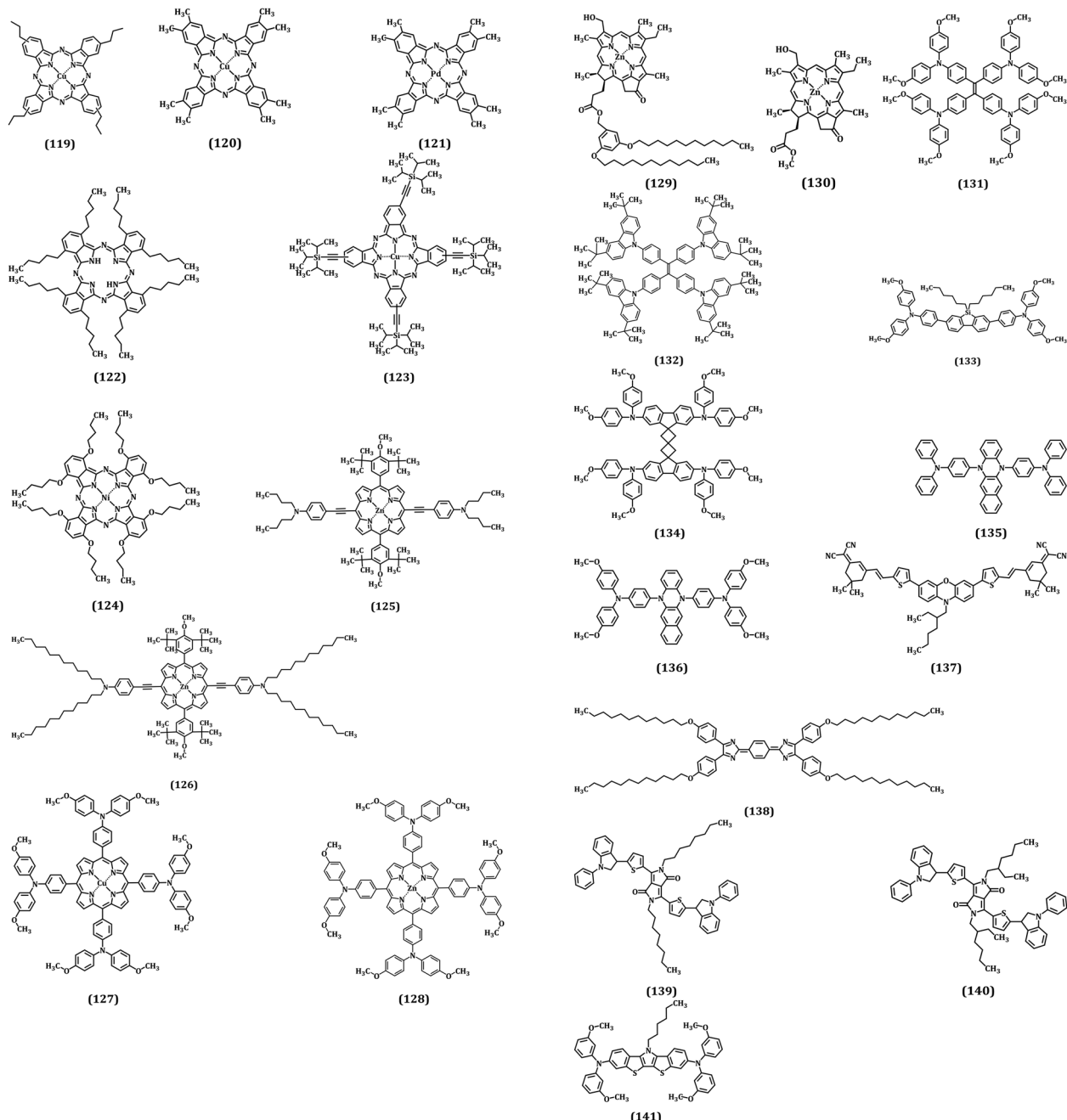
with rigid quinoid core, DIQ-C12 (**138**).<sup>[238]</sup> Fabricated in same conditions, devices using doped spiro-OMeTAD exhibited a comparable PCE of 12.6%. Jeon et al. introduced Novel conjugated materials, DPIO (**139**) and DPIE (**140**), for applying as HTM in PSCs, in 2016.<sup>[239]</sup> These materials have same molecular configuration, consist of an electron donating N-phenylindole and an electron accepting diketopyrrolopyrrole derivative, but different side chains. It has been suggested that



**Figure 27.** Continued.

linear side chain in DPIO, alongside with its planar backbone geometry could be the reason of its strong aggregation behavior, which provided a higher efficiency over 10% for the devices compared to DPIE based PSCs. In 2018, Azmi et al. developed high-performance dopant-free HTM, mDPA-DBTP (141), for low-temperature processed PSCs which showed sufficient hole-

transport properties with appropriate energy levels. PSC device based on the dopant-free mDPA-DBTP achieved a PCE of 18.09% ( $V_{OC} = 1.12$  V,  $J_{SC} = 21.13$  mA cm<sup>-2</sup>, FF = 0.76) with negligible hysteresis. This result is even superior to that of doped spiro-OMeTAD device (PCE = 17.82%) stemming from the improved charge extraction properties. The higher


**Figure 27.** Continued.

hydrophobicity and lack of additional dopants in mDPA-DBTP effectively improved the air storage stability of L-PSCs. The dopant-free mDPA-DBTP device retained 81% of its original PCE after 33 days of storage, during which the doped spiro-OMeTAD devices lost their PCE completely.<sup>[240]</sup> Although HTMs exhibited a higher PCE than doped spiro-OMeTAD is very scarce, but there are a promising number of reported small molecule HTMs showed comparable efficiencies. The photovoltaic properties of some selected perovskite devices using small molecule HTMs are summarized in Table 3. Molecular structure

of all discussed small molecule based HTMs are shown in Figure 27.

### 3. Conclusion

Over the past few years, significant progress has been made in perovskite solar cells with both mesoscopic and planar architecture and a dramatic improve has been observed in their PCEs. Due to the high temperature (ca. 500 °C) process of the

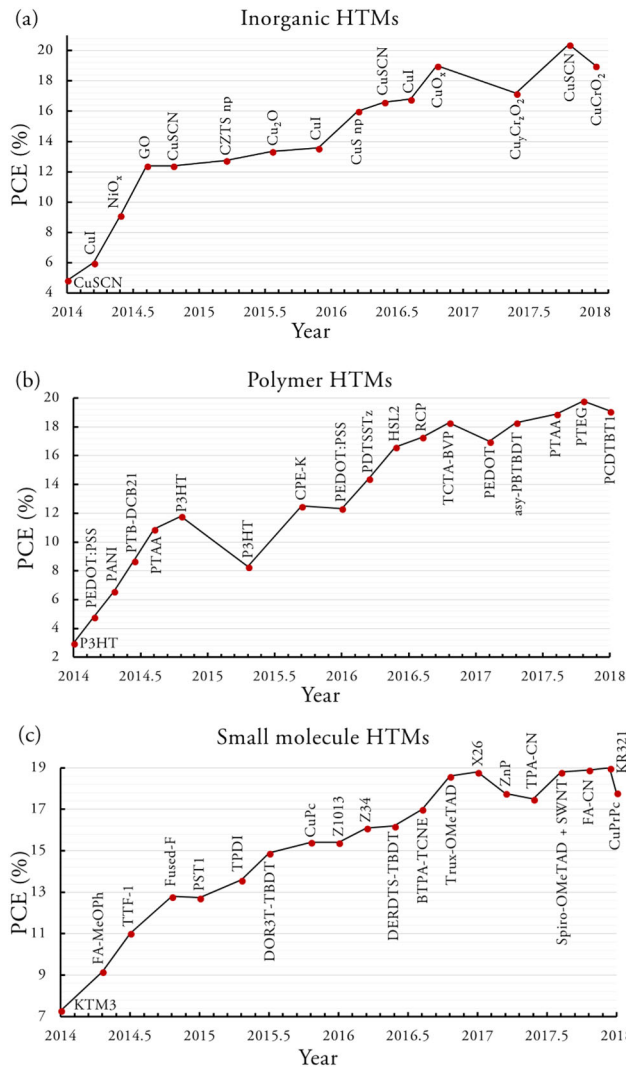


**Figure 28.** The PCE growth in PSCs using dopant free a) inorganic, b) polymer and c) small molecule HTMs.

mesoporous layer, a great attention has been paid to planar PSCs and PCEs above 20% have been reported for both n-i-p and p-i-n device structures. PSCs consist of different components, including light absorbing layer, hole and electron selective layers, conductive electrodes and in some cases, buffer layers and various interlayers. To further improve the performance of PSCs, all the components are crucial to be optimized. However, HTM plays a key role in the efficiency and stability of PSCs.

Here, we reviewed recent studies in design and development of categories of dopant-free HTMs used in PSCs, including their performance and developed fabrication methods, with the focus on the stability enhancement of PSCs. Three main categories including inorganic, polymeric, and small molecule HTMs were covered in this review. According to molecular structure, each category was further classified into subcategories. Tables and figures were also provided in this study to shed light on the development of dopant-free HTMs in classified directions. An HTM should fulfil some main features including having low lying HOMO level located above the perovskite HOMO level and close to it, wide optical band gap ( $E_g$ ), resulting in LUMO with

high enough energy level that blocks electron transfer at the interface of perovskite/HTM, high hole conductivity to reduce the series resistance of the PSC, good solubility in common organic solvents and being thermally and chemically stable. Reviewing the literature revealed that doped spiro-OMeTAD is still the most popular and successful choice as HTM in PSCs, mostly with n-i-p structure. While, its low conductivity, cumbersome synthetic process and high production cost are considered as the main obstacles to move towards the commercial application of spiro-OMeTAD based PSCs. Widely use of p-type dopants, like LiTFSI, tBP, and cobalt complexes are observed for the HTMs, which cannot provide sufficient conductivity and a suitable HOMO level. However, air stability of PSCs is influenced by the hygroscopicity of Li-TFSI and light induced photolysis of t-BP. Attempts have been made through last years to introduce alternative HTMs meeting the desired requirements with the goal of achieving high performance PSCs. **Figure 28** represents the PCE growth in three different categories of HTMs during last few years. Inorganic HTMs brought the good air stability for PSCs due to their high

**Table 4.** Stability parameters and testing methods of some selective stable PSCs with dopant-free HTMs of three main categories in comparison with two high performance stable PSCs with doped spiro-OMeTAD as HTM.

HTM	Category	Doped or dopant-free	PCE	Stability	Testing method	Main stress	Encapsulation	Ref.
CuO <sub>x</sub>	Inorganic	Dopant-free	17.43%	650 h – the PCE maintain 90% of its initial efficiency	An ambient environment at 20 °C and with 20–30% humidity.	Oxygen	Not encapsulated	[82]
CuGaO <sub>2</sub>	Inorganic	Dopant-free	18.51%	30 days	Ambient environment at 25 °C and with 30–55% humidity	Oxygen	Not encapsulated	[88]
CuSCN	Inorganic	Dopant-free	20.4%	1000 h – retain >95% of their initial efficiency	At 60 Celsius.	Temperature	Not encapsulated	[56]
PVK	Polymer	Dopant-free	15.8	1000 h – the PCE maintain 82.5% of its initial efficiency	At ambient conditions (with the room temperature at ca. 25 °C, and the relative humidity ca. 50%) and stored in a laboratory sample drawer when they were not tested.	Moisture	Encapsulated with epoxy glue and glass slices upon UV light curing for 10 s	[155]
asy-PBTBDT	Polymer	Dopant-free	18.3	30-day – the PCE maintain 91% of its initial efficiency	Stored under 50–75% RH conditions	Moisture	Not encapsulated	[139]
RCP	Polymer	Dopant-free	17.3	1400 h – the PCE maintain 100% of its initial efficiency	At humidity of 25%	Oxygen	Not encapsulated	[142]
TTBCPE	Small molecule	Dopant-free	12.65%	30 days – a slight increase of the PCE	Exposed to the room environment at 30% relative humidity	Oxygen	Not encapsulated	[233]
CuMe <sub>2</sub> Pc	Small molecule	Dopant-free	15.73%	2000 h – kept 95% of PCE	At the temperature of 25 °C and relative humidity of 50%	Moisture	Not encapsulated	[223]
CzPAF-TPA	Small molecule	Dopant-free	15.71%	30 days – the PCE maintain 82% of its initial efficiency	At room temperature, exposure to air	Oxygen	Not encapsulated	[184]
Spiro-OMeTAD	Small molecule	Doped	13.07%	350 h – PCE decreases of only 5%	Shining a 100 mW cm <sup>-2</sup> light on the devices held at open circuit conditions	Light	Encapsulated with epoxy resin	[241]
Spiro-OMeTAD	Small molecule	Doped	18%	70 days – retaining about 70% of the initial PCE	A stepwise increase in humidity conditions (from 40% to 50–70%)	Moisture	Not encapsulated	[242]

hydrophobicity and intrinsic high stability and provided high hole mobility with using no additives, but their deposition methods are still needed to be optimized. Most of solvents for deposition of inorganic HTMs can also dissolve perovskite layer and it is usually hard to deposit uniform and homogenous films of inorganic HTMs with fully coverage on perovskite layer. Therefore, only a few of them, such as CuI, CuSCN, NiO<sub>x</sub>, CuO<sub>x</sub> have been vastly employed in PSCs. So far, the highest PCE of 20.4% has been reported for dopant-free CuSCN based PSCs (Figure 28a). Polymer HTMs, such as triarylamine-based, thiophene-based, and donor acceptor conjugated polymers showed moderate hole conductivity and high hydrophobicity and provided low cost materials and the ability of tuning the ionization potential. High-performance PSCs with polymer HTMs have been reported in literature. The efficiency growth in PSCs from 3% in 2014 to 19.8% in 2017 has been achieved by employing polymer HTMs with no additives (Figure 28b). Various classes of small molecules with variety of chemical structures have been designed, synthesized, and employed in PSCs to enhance the device photovoltaic performances. Due to their good solubility in organic solvent and film forming, well-

defined structure, distinct molecular weight, and their ability of being tailored to meet the requirements of perovskite, small molecules can be promising candidates to high efficiency perovskite devices. However, their drawbacks such as multi-step synthesis, high cost and low yield and low to moderate hole conductivity, which in most cases led to using hygroscopic dopants remains to be overcome. The highest PCE of 19.0% has been reported recently for perovskite devices using KR321 as a dopant-free small molecule HTM (Figure 28c). It has been found that the possibility of forming face-on molecular orientation on perovskite film surface by KR321 can be considered as a crucial factor for facilitating the vertical charge transfer and as a result, high efficiency for PSCs. It has also been the case for some phthalocyanine based HTMs such as CuMe<sub>2</sub>Pc and PdMe<sub>2</sub>Pc.

Stability of PSCs are considerably improved with using dopant-free HTMs. Doped HTMs are typically providing high efficiencies for PSCs, but compared to their pristine counterparts, they are more prone to degradation over time. PCEs of some of most stable dopant-free PSCs in three main categories of HTMs, along with the stability test processes and their results are listed in **Table 4**. Stability of PSCs can be affected by different

stresses, such as light, temperature, moisture, and oxygen, which were also highlighted in Table 4. It is very impressive that PSC based on dopant-free CuMe<sub>2</sub>Pc with high PCE of 15.73% keeps 95% of its efficiency even after 2000 h. This remarkable long-term stability can also be observed in PSCs using other dopant-free organic, inorganic, or polymer HTMs. Although the highest reported PCEs have been achieved for PSCs with doped HTMs, but air stable undoped perovskite devices with simpler fabrication procedure and lower production cost have attracted a great deal of attention in recent years, as achieved outstanding efficiencies over 20%.

## Acknowledgements

E.R. and X.L. contributed equally to this work. This work was supported by Special Funds for the Development of Strategic Emerging Industries in Shenzhen (JCYJ20170412154240645).

## Keywords

dopant-free, hole transporting materials, perovskite solar cells, renewable energy, stability of perovskite solar cells

Received: July 17, 2018

Revised: August 15, 2018

Published online:

- [1] a) M. A. Green, K. Emery, Y. Hishikawa, W. Warta, E. D. Dunlop, *Prog. Photovoltaics* **2012**, *20*, 606; b) M. A. Green, *Semicond. Sci. Technol.* **1993**, *8*, 1.
- [2] M. A. Green, K. Emery, Y. Hishikawa, W. Warta, E. D. Dunlop, *Prog. Photovoltaics* **2012**, *20*, 12.
- [3] a) J. Britt, C. Ferekides, *Appl. Phys. Lett.* **1993**, *62*, 2851; b) I. Repins, M. A. Contreras, B. Egaas, C. Dehart, J. Scharf, C. L. Perkins, B. To, R. Noufi, *Prog. Photovoltaics* **2008**, *16*, 235.
- [4] A. P. Alivisatos, *Science* **1996**, *271*, 933.
- [5] C. Eberspacher, J. Ermer, C. Fredric, C. Jensen, R. Gay, D. Pier, D. Willett, F. Karg, *Recent Advances in Single-Junction and Tandem Thin Film Modules Based On CuInSe2*. Springer, Netherlands, Dordrecht **1991**.
- [6] B. C. Oregan, M. Gratzel, *Nature* **1991**, *353*, 737.
- [7] R. F. Service, *Science* **2014**, *344*, 458.
- [8] K. Yoshikawa, H. Kawasaki, W. Yoshida, T. Irie, K. Konishi, K. Nakano, T. Uto, D. Adachi, M. Kanematsu, H. Uzu, K. Yamamoto, *Nat. Energy* **2017**, *2*, 17032.
- [9] A. Kojima, K. Teshima, Y. Shirai, T. Miyasaka, *J. Am. Chem. Soc.* **2009**, *131*, 6050.
- [10] J. Im, C. Lee, J. Lee, S. Park, N. Park, *Nanoscale* **2011**, *3*, 4088.
- [11] H. Kim, C. Lee, J. Im, K. Lee, T. Moehl, A. Marchioro, S. Moon, R. Humphrybaker, J. Yum, J. Moser, *Sci. Rep.* **2012**, *2*, 591.
- [12] a) H. Zhou, Q. Chen, G. Li, S. Luo, T. Song, H. Duan, Z. Hong, J. You, Y. Liu, Y. Yang, *Science* **2014**, *345*, 542; b) F. J. H. S. Noh, N. J. Jeon, Y. C. Kim, S. Ryu, J. Seo, S. I. Seok, *Science* **2015**, *348*, 1234; c) National Renewable Energy Labs (NREL) Efficiency Chart, NREL. <https://www.nrel.gov/pv/assets/images/efficiency-chart.png>.
- [13] a) D. Bi, S. Moon, L. Haggman, G. Boschloo, L. Yang, E. M. J. Johansson, M. K. Nazeeruddin, M. Gratzel, A. Hagfeldt, *RSC Adv.* **2013**, *3*, 18762; b) G. E. Eperon, V. M. Burlakov, P. Docampo, A. Goriely, H. J. Snaith, *Adv. Funct. Mater.* **2014**, *24*, 151.
- [14] a) J. Im, I. Jang, N. Pellet, M. Gratzel, N. Park, *Nat. Nanotechnol.* **2014**, *9*, 927; b) L. Qiu, L. K. Ono, Y. Qi, *Mater. Today Energy* **2018**, *7*, 169.
- [15] a) J. Lee, D. Seol, A. Cho, N. Park, *Adv. Mater.* **2014**, *26*, 4991; b) G. E. Eperon, S. D. Stranks, C. Menelaou, M. B. Johnston, L. M. Herz, H. J. Snaith, *Energy, Environ. Sci.*, **2014**, *7*, 982.
- [16] a) A. Yella, L. Heiniger, P. Gao, M. K. Nazeeruddin, M. Gratzel, *Nano Lett.* **2014**, *14*, 2591; b) X. Gao, J. Li, J. Baker, Y. Hou, D. Guan, J. Chen, C. Yuan, *Chem. Commun.* **2014**, *50*, 6368.
- [17] G. A. Casas, M. A. Cappelletti, A. P. Cédola, B. M. Soucase, E. L. Peltzer y Blancá, *Superlattices Microstruct* **2017**, *107*, 136.
- [18] a) A. Kojima, K. Teshima, Y. Shirai, T. Miyasaka, *210th ECS Meeting, Cancun, Mexico, Oct. 29–Nov. 3, 2006*; b) A. Kojima, K. Teshima, Y. Shirai, T. Miyasaka, *214th F ECS S Meeting, Honolulu, Hawaii Oct. F 12–17, 2008*.
- [19] T. J. Savenije, C. S. Poncea, Jr., L. Kunneman, M. Abdellah, K. Zheng, Y. Tian, Q. Zhu, S. E. Canton, I. G. Scheblykin, T. Pullerits, *J. Phys. Chem. Lett.* **2014**, *5*, 2189.
- [20] Q. Dong, Y. Fang, Y. Shao, P. Mulligan, J. Qiu, L. Cao, J. Huang, *Science* **2015**, *347*, 967.
- [21] a) Q. Chen, H. Zhou, Z. Hong, S. Luo, H.-S. Duan, H.-H. Wang, Y. Liu, G. Li, Y. Yang, *J. Am. Chem. Soc.* **2013**, *136*, 622; b) D. Liu, T. L. Kelly, *Nat. Photonics* **2014**, *8*, 133.
- [22] a) L. Etgar, P. Gao, Z. Xue, Q. Peng, A. K. Chandiran, B. Liu, M. K. Nazeeruddin, M. Grätzel, *J. Am. Chem. Soc.* **2012**, *134*, 17396; b) J. M. Ball, M. M. Lee, A. Hey, H. J. Snaith, *Energy Environ. Sci.* **2013**, *6*, 1739.
- [23] M.-H. Li, P.-S. Shen, K.-C. Wang, T.-F. Guo, P. Chen, *J. Mater. Chem. A* **2015**, *3*, 9011.
- [24] M. M. Lee, J. Teuscher, T. Miyasaka, T. N. Murakami, H. J. Snaith, *Science* **2012**, *338*, 643.
- [25] J. A. Christians, R. C. Fung, P. V. Kamat, *J. Am. Chem. Soc.* **2013**, *136*, 758.
- [26] S. Chen, L. Lei, S. Yang, Y. Liu, Z.-S. Wang, *ACS Appl. Mater. Interfaces* **2015**, *7*, 25770.
- [27] M. Era, T. Hattori, T. Taira, T. Tsutsui, *Chem. Mater.* **1997**, *9*, 8.
- [28] a) W. S. Yang, B. Park, E. H. Jung, N. J. Jeon, Y. C. Kim, D. U. Lee, S. S. Shin, J. Seo, E. K. Kim, J. H. Noh, *Science* **2017**, *356*, 1376; b) J. Lee, H. Kang, G. Kim, H. Back, J. Kim, S. Hong, B. Park, E. Lee, K. Lee, *Adv. Mater.* **2017**, *29*, 1606363; c) Z. Yang, S. Zhang, L. Li, W. Chen, *J. Materomics* **2017**, *3*, 231.
- [29] a) J. H. Heo, M. H. Lee, H. J. Han, B. R. Patil, J. S. Yu, S. H. Im, *J. Mater. Chem.* **2016**, *4*, 1572; b) Y. Li, L. Meng, Y. Yang, G. Xu, Z. Hong, Q. Chen, J. You, G. Li, Y. Yang, Y. Li, *Nat. Commun.* **2016**, *7*, 10214.
- [30] F. Matteocci, L. Cina, F. D. Giacomo, S. Razza, A. L. Palma, A. Guidobaldi, A. Depifanio, S. Licoccia, T. M. Brown, A. Reale, *Prog. Photovoltaics* **2016**, *24*, 436.
- [31] A. Marchioro, J. Teuscher, D. Friedrich, M. Kunst, R. Van De Krol, T. Moehl, M. Grätzel, J.-E. Moser, *Nat. Photonics* **2014**, *8*, 250.
- [32] E. Edri, S. Kirmayer, A. Henning, S. Mukhopadhyay, K. Gartsman, Y. Rosenwaks, G. Hodes, D. Cahen, *Nano Lett.* **2014**, *14*, 1000.
- [33] S. Aharon, S. Gamliel, B. El Cohen, L. Etgar, *Phys. Chem. Chem. Phys.* **2014**, *16*, 10512.
- [34] a) A. Guerrero, G. Garcia-Belmonte, I. Mora-Sero, J. Bisquert, Y. S. Kang, T. J. Jacobsson, J.-P. Correa-Baena, A. Hagfeldt, *J. Phys. Chem. C* **2016**, *120*, 8023; b) E. J. Juarez-Perez, M. Wußler, F. Fabregat-Santiago, K. Lukas-Wollny, E. Mankel, T. Mayer, W. Jaegermann, I. Mora-Sero, *J. Phys. Chem. Lett.* **2014**, *5*, 680.
- [35] a) W. A. Laban, L. Etgar, *Energy Environ. Sci.* **2013**, *6*, 3249; b) J. Shi, J. Dong, S. Lv, Y. Xu, L. Zhu, J. Xiao, X. Xu, H. Wu, D. Li, Y. Luo, *Appl. Phys. Lett.* **2014**, *104*, 063901; c) Y. Li, S. Ye, W. Sun, W. Yan, Y. Li, Z. Bian, Z. Liu, S. Wang, C. Huang, *J. Mater. Chem. A* **2015**, *3*, 18389; d) W. Ke, G. Fang, J. Wan, H. Tao, Q. Liu, L. Xiong, P. Qin, J. Wang, H. Lei, G. Yang, *Nat. Commun.* **2015**, *6*, 6700.

- [36] a) B. Xu, D. Bi, Y. Hua, P. Liu, M. Cheng, M. Grätzel, L. Kloo, A. Hagfeldt, L. Sun, *Energy Environ. Sci.* **2016**, *9*, 873. b) S. S. Reddy, K. Gunasekar, J. H. Heo, S. H. Im, C. S. Kim, D. H. Kim, J. H. Moon, J. Y. Lee, M. Song, S. H. Jin, *Adv. Mater.* **2016**, *28*, 686; c) P. Gratia, A. Magomedov, T. Malinauskas, M. Daskeviciene, A. Abate, S. Ahmad, M. Grätzel, V. Getautis, M. K. Nazeeruddin, *Angew. Chem. Int. Ed.* **2015**, *54*, 11409.
- [37] F. Fabregat-Santiago, J. Bisquert, L. Cevey, P. Chen, M. Wang, S. M. Zakeeruddin, M. Grätzel, *J. Am. Chem. Soc.* **2009**, *131*, 558.
- [38] a) J. Liu, Y. Wu, C. Qin, X. Yang, T. Yasuda, A. Islam, K. Zhang, W. Peng, W. Chen, L. Han, *Energy Environ. Sci.* **2014**, *7*, 2963; b) W. Yan, Y. Li, W. Sun, H. Peng, S. Ye, Z. Liu, Z. Bian, C. Huang, *RSC Adv.* **2014**, *4*, 33039.
- [39] , A. Kahn, S. R. Forrest, *J. Appl. Phys.* **2001**, *89*, 4986.
- [40] W. Chen, Y. Wu, J. Fan, A. B. Djuricic, F. Liu, H. W. Tam, A. Ng, C. Surya, W. K. Chan, D. Wang, *Adv. Energy Mater.* **2018**, *8*, 1703519.
- [41] S. Inudo, M. Miyake, T. Hirato, *Phys. Status Solidi A* **2013**, *210*, 2395.
- [42] J. A. Christians, R. C. Fung, P. V. Kamat, *J. Am. Chem. Soc.* **2014**, *136*, 758.
- [43] S. Gharibzadeh, B. A. Nejand, A. Moshaii, N. Mohammadian, A. H. Alizadeh, R. Mohammadpour, V. Ahmadi, A. Alizadeh, *ChemSusChem* **2016**, *9*, 1929.
- [44] W.-Y. Chen, L.-L. Deng, S.-M. Dai, X. Wang, C.-B. Tian, X.-X. Zhan, S.-Y. Xie, R.-B. Huang, L.-S. Zheng, *J. Mater. Chem. A* **2015**, *3*, 19353.
- [45] W. Sun, S. Ye, H. Rao, Y. Li, Z. Liu, L. Xiao, Z. Chen, Z. Bian, C. Huang, *Nanoscale* **2016**, *8*, 15954.
- [46] N. Wijeyasinghe, T. D. Anthopoulos, *Semicond. Sci. Technol.* **2015**, *30*, 104002.
- [47] P. Pattanasattayavong, N. Yaacobi-Gross, K. Zhao, G. O. N. Ndjawa, J. Li, F. Yan, B. C. O'Regan, A. Amassian, T. D. Anthopoulos, *Adv. Mater.* **2013**, *25*, 1504.
- [48] J. A. Christians, P. V. Kamat, *ACS nano* **2013**, *7*, 7967.
- [49] N. Yaacobi-Gross, N. D. Treat, P. Pattanasattayavong, H. Faber, A. K. Perumal, N. Stingelin, D. D. Bradley, P. N. Stavrinou, M. Heeney, T. D. Anthopoulos, *Adv. Energy Mater.* **2015**, *5*, 1401529.
- [50] E. Premalal, G. Kumara, R. Rajapakse, M. Shimomura, K. Murakami, A. Konno, *Chem. Commun.* **2010**, *46*, 3360.
- [51] Y. Guo, W. Sato, K. Shoyama, H. Halim, Y. Itabashi, R. Shang, E. Nakamura, *J. Am. Chem. Soc.* **2017**, *139*, 9598.
- [52] S. Ito, S. Tanaka, H. Vahlman, H. Nishino, K. Manabe, P. Lund, *Chemphyschem* **2014**, *15*, 1194.
- [53] S. Chavhan, O. Miguel, H.-J. Grande, V. Gonzalez-Pedro, R. S. Sánchez, E. M. Barea, I. Mora-Seró, R. Tena-Zaera, *J. Mater. Chem. A* **2014**, *2*, 12754.
- [54] P. Qin, S. Tanaka, S. Ito, N. Tetreault, K. Manabe, H. Nishino, M. K. Nazeeruddin, M. Gratzel, *Nat. Commun.* **2014**, *5*, 3834.
- [55] V. E. Madhavan, I. Zimmermann, C. Roldán-Carmona, G. Grancini, M. Buffiere, A. Belaidi, M. K. Nazeeruddin, *ACS Energ. Lett.* **2016**, *1*, 1112.
- [56] N. Arora, M. I. Dar, A. Hinderhofer, N. Pellet, F. Schreiber, S. M. Zakeeruddin, M. Grätzel, *Science* **2017**, *358*, 768.
- [57] K. Zhao, R. Munir, B. Yan, Y. Yang, T. Kim, A. Amassian, *J. Mater. Chem. A* **2015**, *3*, 20554.
- [58] N. Wijeyasinghe, A. Regoutz, F. Eisner, T. Du, L. Tsetseris, Y. H. Lin, H. Faber, P. Pattanasattayavong, J. Li, F. Yan, M. A. McLachlan, D. J. Payne, M. Heeney, T. D. Anthopoulos, *Adv. Funct. Mater.* **2017**, *27*, 1701818.
- [59] P. Pattanasattayavong, G. O. N. Ndjawa, K. Zhao, K. W. Chou, N. Yaacobigross, B. C. Oregan, A. Amassian, T. D. Anthopoulos, *Chem. Commun.* **2013**, *49*, 4154.
- [60] M. T. Borgstrom, E. Blart, G. Boschloo, E. Mukhtar, A. Hagfeldt, L. Hammarstrom, F. Odobel, *J. Phys. Chem. B* **2005**, *109*, 22928.
- [61] M. D. Irwin, D. B. Buchholz, A. W. Hains, R. P. Chang, T. J. Marks, *Proc. Natl. Acad. Sci. USA* **2008**, *105*, 2783.
- [62] a) E. A. Gibson, A. L. Smeigh, L. Le Pleux, J. Fortage, G. Boschloo, E. Blart, Y. Pellegrin, F. Odobel, A. Hagfeldt, L. Hammarström, *Angew. Chem.* **2009**, *121*, 4466; b) A. Nattestad, A. J. Mozer, M. K. Fischer, Y.-B. Cheng, A. Mishra, P. Bäuerle, U. Bach, *Nat. Mater.* **2010**, *9*, 31; c) H.-Q. Wang, N. Li, N. S. Guldal, C. J. Brabec, *Org. Electron.* **2012**, *13*, 3014; d) J. R. Manders, S. W. Tsang, M. J. Hartel, T. H. Lai, S. Chen, C. M. Amb, J. R. Reynolds, F. So, *Adv. Funct. Mater.* **2013**, *23*, 2993.
- [63] P. Docampo, J. M. Ball, M. Darwich, G. E. Eperon, H. J. Snaith, *Nat. Commun.* **2013**, *4*, 2761.
- [64] H. Wang, X. Zeng, Z. Huang, W. Zhang, X. Qiao, B. Hu, X. Zou, M. Wang, Y. B. Cheng, W. Chen, *ACS Appl. Mater. Interfaces* **2014**, *6*, 12609.
- [65] Z. Zhu, Y. Bai, T. Zhang, Z. Liu, X. Long, Z. Wei, Z. Wang, L. Zhang, J. Wang, F. Yan, S. Yang, *Angewandte Chemie* **2014**, *53*, 12571.
- [66] K. C. Wang, J. Y. Jeng, P. S. Shen, Y. C. Chang, E. W. Diau, C. H. Tsai, T. Y. Chao, H. C. Hsu, P. Y. Lin, P. Chen, T. F. Guo, T. C. Wen, *Sci. Rep.* **2014**, *4*, 4756.
- [67] X. Yin, P. Chen, M. Que, Y. Xing, W. Que, C. Niu, J. Shao, *ACS Nano* **2016**, *10*, 3630.
- [68] M. B. Islam, M. Yanagida, Y. Shirai, Y. Nabetani, K. Miyano, *ACS Omega* **2017**, *2*, 2291.
- [69] X. Yin, Z. Yao, Q. Luo, X. Dai, Y. Zhou, Y. Zhang, Y. Zhou, S. Luo, J. Li, N. Wang, H. Lin, *ACS Appl. Mater. Interfaces* **2017**, *9*, 2439.
- [70] J. Cao, H. Yu, S. Zhou, M. Qin, T.-K. Lau, X. Lu, N. Zhao, C.-P. Wong, *J. Mater. Chem. A* **2017**, *5*, 11071.
- [71] K.-C. Wang, P.-S. Shen, M.-H. Li, S. Chen, M.-W. Lin, P. Chen, T.-F. Guo, *ACS Appl. Mater. Interfaces* **2014**, *6*, 11851.
- [72] W. Chen, Y. Wu, Y. Yue, J. Liu, W. Zhang, X. Yang, H. Chen, E. Bi, I. Ashraful, M. Grätzel, *Science* **2015**, *350*, 944.
- [73] J. H. Kim, P. W. Liang, S. T. Williams, N. Cho, C. C. Chueh, M. S. Glaz, D. S. Ginger, A. K. Y. Jen, *Adv. Mater.* **2015**, *27*, 695.
- [74] C. Zhang, W. Li, C. Liu, J. Fan, Y. Mai, *Sol. RRL* **2017**, *1*, 1700141.
- [75] Y. Wang, Z. Xia, J. Liang, X. Wang, Y. Liu, C. Liu, S. Zhang, H. Zhou, *Semicond. Sci. Technol.* **2015**, *30*, 054004.
- [76] M. I. Hossain, F. H. Alharbi, N. Tabet, *Sol. Energy* **2015**, *120*, 370.
- [77] C. Zuo, L. Ding, *Small* **2015**, *11*, 5528.
- [78] S. Chatterjee, A. J. Pal, *J. Phys. Chem. C* **2016**, *120*, 1428.
- [79] B. A. Nejand, V. Ahmadi, S. Gharibzadeh, H. R. Shahverdi, *ChemSusChem* **2016**, *9*, 302.
- [80] W. Sun, Y. Li, S. Ye, H. Rao, W. Yan, H. Peng, Y. Li, Z. Liu, S. Wang, Z. Chen, L. Xiao, Z. Bian, C. Huang, *Nanoscale* **2016**, *8*, 10806.
- [81] H. Rao, S. Ye, W. Sun, W. Yan, Y. Li, H. Peng, Z. Liu, Z. Bian, Y. Li, C. Huang, *Nano Energy* **2016**, *27*, 51.
- [82] Z.-K. Yu, W.-F. Fu, W.-Q. Liu, Z.-Q. Zhang, Y.-J. Liu, J.-L. Yan, T. Ye, W.-T. Yang, H.-Y. Li, H.-Z. Chen, *Chin. Chem. Lett.* **2017**, *28*, 13.
- [83] Q. L. Wu, C. Xue, Y. Li, P. C. Zhou, W. F. Liu, J. Zhu, S. Y. Dai, C. F. Zhu, S. F. Yang, *ACS Appl. Mater. Interfaces* **2015**, *7*, 28466.
- [84] B. Koo, H. Jung, M. Park, J.-Y. Kim, H. J. Son, J. Cho, M. J. Ko, *Adv. Funct. Mater.* **2016**, *26*, 5400.
- [85] H. Rao, W. Sun, S. Ye, W. Yan, Y. Li, H. Peng, Z. Liu, Z. Bian, C. Huang, *ACS Appl. Mater. Interfaces* **2016**, *8*, 7800.
- [86] H. Choi, J. H. Heo, S. Ha, B. W. Kwon, S. P. Yoon, J. Han, W.-S. Kim, S. H. Im, J. Kim, *Chem. Eng. J.* **2017**, *310*, 179.
- [87] X. Jin, X. Lei, C. Wu, G. Jiang, H. Zeng, T. Chen, C. Zhu, *J. Mater. Chem. A* **2017**, *5*, 19884.
- [88] H. Zhang, H. Wang, W. Chen, A. K. Jen, *Adv. Mater.* **2017**, *29*, 1604984.
- [89] a) X. Nie, S.-H. Wei, S. Zhang, *Phys. Rev. Lett.* **2002**, *88*, 066405; b) R. Gillen, J. Robertson, *Phys. Rev. B* **2011**, *84*, 035125; c) M. Yu, T. I. Draskovic, Y. Wu, *Inorg. Chem.* **2014**, *53*, 5845.
- [90] D. H. Jara, S. J. Yoon, K. G. Stamplecoskie, P. V. Kamat, *Chem. Mater.* **2014**, *26*, 7221.
- [91] W. W. Yu, L. Qu, W. Guo, X. Peng, *Chem. Mater.* **2003**, *15*, 2854.

- [92] W. A. Tisdale, K. J. Williams, B. A. Timp, D. J. Norris, E. S. Aydil, X.-Y. Zhu, *Science* **2010**, *328*, 1543.
- [93] O. E. Semionin, J. M. Luther, S. Choi, H.-Y. Chen, J. Gao, A. J. Nozik, M. C. Beard, *Science* **2011**, *334*, 1530.
- [94] Z. Pan, I. n. Mora-Seró, Q. Shen, H. Zhang, Y. Li, K. Zhao, J. Wang, X. Zhong, J. Bisquert, *J. Am. Chem. Soc.* **2014**, *136*, 9203.
- [95] L. Hu, W. Wang, H. Liu, J. Peng, H. Cao, G. Shao, Z. Xia, W. Ma, J. Tang, *J. Mater. Chem. A* **2015**, *3*, 515.
- [96] M. Lv, J. Zhu, Y. Huang, Y. Li, Z. P. Shao, Y. F. Xu, S. Y. Dai, *ACS Appl. Mater. Interfaces* **2015**, *7*, 17482.
- [97] M. Yuan, X. Zhang, J. Kong, W. Zhou, Z. Zhou, Q. Tian, Y. Meng, S. Wu, D. Kou, *Electrochim. Acta* **2016**, *215*, 374.
- [98] Z. Wu, S. Bai, J. Xiang, Z. Yuan, Y. Yang, W. Cui, X. Gao, Z. Liu, Y. Jin, B. Sun, *Nanoscale* **2014**, *6*, 10505.
- [99] W. Li, H. Dong, X. Guo, N. Li, J. Li, G. Niu, L. Wang, *J. Mater. Chem. A* **2014**, *2*, 20105.
- [100] A. Agresti, S. Pescetelli, B. Taheri, A. E. Del Rio Castillo, L. Cinà, F. Bonaccorso, A. Di Carlo, *ChemSusChem* **2016**, *9*, 2609.
- [101] Q.-D. Yang, J. Li, Y. Cheng, H.-W. Li, Z. Guan, B. Yu, S.-W. Tsang, *J. Mater. Chem. A* **2017**, *5*, 9852.
- [102] A. Mei, X. Li, L. Liu, Z. Ku, T. Liu, Y. Rong, M. Xu, M. Hu, J. Chen, Y. Yang, *Science* **2014**, *345*, 295.
- [103] Z. Li, P. P. Boix, G. Xing, K. Fu, S. A. Kulkarni, S. K. Batabyal, W. Xu, A. Cao, T. C. Sum, N. Mathew, L. H. Wong, *Nanoscale* **2016**, *8*, 6352.
- [104] S. N. Habisreutinger, B. Wenger, H. J. Snaith, R. J. Nicholas, *ACS Energ. Lett.* **2017**, *2*, 622.
- [105] L.-C. Chen, Z.-L. Tseng, C.-C. Chen, S. H. Chang, C.-H. Ho, *Appl. Phys. Express* **2016**, *9*, 122301.
- [106] E. M. Sanehira, B. J. Tremolet de Villers, P. Schulz, M. O. Reese, S. Ferrere, K. Zhu, L. Y. Lin, J. J. Berry, J. M. Luther, *ACS Energ. Lett.* **2016**, *1*, 38.
- [107] P. Huang, Z. Wang, Y. Liu, K. Zhang, L. Yuan, Y. Zhou, B. Song, Y. Li, *ACS Appl. Mater. Interfaces* **2017**, *9*, 25323.
- [108] P.-L. Qin, Q. He, C. Chen, X.-L. Zheng, G. Yang, H. Tao, L.-B. Xiong, L. Xiong, G. Li, G.-J. Fang, *Sol. RRL* **2017**, *1*, 1700058.
- [109] H. Zhang, H. Wang, H. Zhu, C.-C. Chueh, W. Chen, S. Yang, A. K. Y. Jen, *Adv. Energy Mater.* **2018**, *8*, 1702762.
- [110] X. Yao, W. Xu, X. Huang, J. Qi, Q. Yin, X. Jiang, F. Huang, X. Gong, Y. Cao, *Org. Electron.* **2017**, *47*, 85.
- [111] J. H. Heo, S. H. Im, J. H. Noh, T. N. Mandal, C.-S. Lim, J. A. Chang, Y. H. Lee, H.-j. Kim, A. Sarkar, M. K. Nazeeruddin, *Nat. Photonics* **2013**, *7*, 486.
- [112] D. Bi, G. Boschloo, A. Hagfeldt, *Nano* **2014**, *09*, 1440001.
- [113] N. J. Jeon, J. H. Noh, Y. C. Kim, W. S. Yang, S. Ryu, S. I. Seok, *Nat. Mater.* **2014**, *13*, 897.
- [114] K. Neumann, M. Thelakkat, *RSC Adv.* **2014**, *4*, 43550.
- [115] T. Matsui, I. Petrikyte, T. Malinauskas, K. Domanski, M. Daskeviciene, M. Steponaitis, P. Gratia, W. Tress, J. P. Correa-Baena, A. Abate, A. Hagfeldt, M. Gratzel, M. K. Nazeeruddin, V. Getautis, M. Saliba, *ChemSusChem* **2016**, *9*, 2567.
- [116] C.-C. Chang, J.-H. Tao, C.-E. Tsai, Y.-J. Cheng, C.-S. Hsu, *ACS Appl. Mater. Interfaces* **2018**, *10*, 21466.
- [117] M. Stolterfoht, C. M. Wolff, Y. Amir, A. Paulke, L. Perdigón-Toro, P. Caprioglio, D. Neher, *Energy Environ. Sci.* **2017**, *10*, 1530.
- [118] S. Agarwal, M. Seetharaman, N. K. Kumawat, A. S. Subbiah, S. K. Sarkar, D. Kabra, M. A. Namboothiry, P. R. Nair, *J. Phys. Chem. Lett.* **2014**, *5*, 4115.
- [119] B. Conings, L. Baeten, C. De Dobbelaere, J. D'Haen, J. Manca, H. G. Boyen, *Adv. Mater.* **2014**, *26*.
- [120] D. Liu, M. K. Gangishetty, T. L. Kelly, *J. Mater. Chem. A* **2014**, *2*, 19873.
- [121] D. Liu, J. Yang, T. L. Kelly, *J. Am. Chem. Soc.* **2014**, *136*, 17116.
- [122] W. Y. Chen, X. C. Bao, Q. Q. Zhu, D. Q. Zhu, M. Qiu, M. L. Sun, R. Q. Yang, *J. Mater. Chem. C* **2015**, *3*, 10070.
- [123] a) S. Lv, S. Pang, Y. Zhou, N. P. Padture, H. Hu, L. Wang, X. Zhou, H. Zhu, L. Zhang, C. Huang, G. Cui, *Phys. Chem. Chem. Phys.* **2014**, *16*, 19206; b) S. Pang, H. Hu, J. Zhang, S. Lv, Y. Yu, F. Wei, T. Qin, H. Xu, Z. Liu, G. Cui, *Chem. Mater.* **2014**, *26*, 1485.
- [124] M. Cai, V. T. Tiong, T. Hreib, J. Bell, H. Wang, *J. Mater. Chem. A* **2015**, *3*, 2784.
- [125] J. Ye, X. Li, J. Zhao, X. Mei, Q. Li, *RSC Adv.* **2016**, *6*, 36356.
- [126] S. Colodrero, *AIMS Mater. Sci.* **2017**, *4*, 956.
- [127] Y. Xiao, G. Han, J. Wu, J.-Y. Lin, *J. Power Sources* **2016**, *306*, 171.
- [128] I. Gelmetti, L. Cabau, N. F. Montcada, E. Palomares, *ACS Appl. Mater. Interfaces* **2017**, *9*, 21599.
- [129] X. Jiang, Z. Yu, Y. Zhang, J. Lai, J. Li, G. G. Gurzadyan, X. Yang, L. Sun, *Sci. Rep.* **2017**, *7*, 42564.
- [130] S. Ameen, M. S. Akhtar, Y. S. Kim, O.-B. Yang, H.-S. Shin, *J. Phys. Chem. C* **2010**, *114*, 4760.
- [131] S. Ameen, M. S. Akhtar, S. Ansari, O.-B. Yang, H.-S. Shin, *Superlattices Microstruct.* **2009**, *46*, 872.
- [132] H.-K. Seo, S. Ameen, M. S. Akhtar, H. S. Shin, *Talanta* **2013**, *104*, 219.
- [133] Y. Xiao, G. Han, Y. Chang, H. Zhou, M. Li, Y. Li, *J. Power Sources* **2014**, *267*, 1.
- [134] K. Lee, K. H. Cho, J. Ryu, J. Yun, H. Yu, J. Lee, W. Na, J. Jang, *Electrochim. Acta* **2017**, *224*, 600.
- [135] J. W. Lee, S. Park, M. J. Ko, H. J. Son, N. G. Park, *Chemphyschem* **2014**, *15*, 2595.
- [136] J. M. Marin-Beloqui, J. P. Hernandez, E. Palomares, *Chem. Commun.* **2014**, *50*, 14566.
- [137] P. Nagarjuna, K. Narayanaswamy, T. Swetha, G. H. Rao, S. P. Singh, G. D. Sharma, *Electrochim. Acta* **2015**, *151*, 21.
- [138] H.-C. Liao, T. L. D. Tam, P. Guo, Y. Wu, E. F. Manley, W. Huang, N. Zhou, C. M. M. Soe, B. Wang, M. R. Wasielewski, L. X. Chen, M. G. Kanatzidis, A. Facchetti, R. P. H. Chang, T. J. Marks, *Adv. Energy Mater.* **2016**, *6*, 1600502.
- [139] J. Lee, M. Malekshahi Byranvand, G. Kang, S. Y. Son, S. Song, G. W. Kim, T. Park, *J. Am. Chem. Soc.* **2017**, *139*, 12175.
- [140] G.-W. Kim, J. Lee, G. Kang, T. Kim, T. Park, *Adv. Energy Mater.* **2017**, *1701935*.
- [141] M. Kyeong, J. Lee, K. Lee, S. Hong, *ACS Appl. Mater. Interfaces* **2018**, *10*, 23254.
- [142] G.-W. Kim, G. Kang, J. Kim, G.-Y. Lee, H. I. Kim, L. Pyeon, J. Lee, T. Park, *Energy Environ. Sci.* **2016**, *9*, 2326.
- [143] K. Kranthiraja, K. Gunasekar, H. Kim, A. N. Cho, N. G. Park, S. Kim, B. J. Kim, R. Nishikubo, A. Saeki, M. Song, *Adv. Mater.* **2017**, *29*, 1700183.
- [144] F. Cai, J. Cai, L. Yang, W. Li, R. S. Gurney, H. Yi, A. Iraqi, D. Liu, T. Wang, *Nano Energy* **2018**, *45*, 28.
- [145] Z. Wang, Q. Dong, Y. Xia, H. Yu, K. Zhang, X. Liu, X. Guo, Y. Zhou, M. Zhang, B. Song, *Org. Electron.* **2016**, *33*, 142.
- [146] J. C. Bijleveld, A. P. Zoombelt, S. G. Mathijssen, M. M. Wien, M. Turbiez, D. M. de Leeuw, R. A. Janssen, *J. Am. Chem. Soc.* **2009**, *131*, 16616.
- [147] A. Dubey, N. Adhikari, S. Venkatesan, S. Gu, D. Khatiwada, Q. Wang, L. Mohammad, M. Kumar, Q. Qiao, *Sol. Energy Mater. Sol. Cells* **2016**, *145*, 193.
- [148] H. W. Chen, T. Y. Huang, T. H. Chang, Y. Sanehira, C. W. Kung, C. W. Chu, M. Ikegami, T. Miyasaka, K. C. Ho, *Sci. Rep.* **2016**, *6*, 34319.
- [149] X. Xu, C. Ma, Y. Cheng, Y.-M. Xie, X. Yi, B. Gautam, S. Chen, H.-W. Li, C.-S. Lee, F. So, S.-W. Tsang, *J. Power Sources* **2017**, *360*, 157.
- [150] Y. Cheng, X. Xu, Y. Xie, H.-W. Li, J. Qing, C. Ma, C.-S. Lee, F. So, S.-W. Tsang, *Sol. RRL* **2017**, *1*, 1700097.

- [151] a) P.-L. T. Boudreault, S. Beaupré, M. Leclerc, *Polym. Chem.* **2010**, *1*, 127; b) J. Li, A. C. Grimsdale, *Chem. Soc. Rev.* **2010**, *39*, 2399.
- [152] a) F. Durnur, *Org. Electron.* **2015**, *25*, 345; b) N. Blouin, A. Michaud, S. Wakim, P. L. T. Boudreault, M. Leclerc, B. Vercelli, S. Zecchin, G. Zotti, *Macromol. Chem. Phys.* **2006**, *207*, 166; c) R. B. Aich, N. Blouin, A. Bouchard, M. Leclerc, *Chem. Mater.* **2009**, *21*, 751; d) Z. Ma, L. Chen, J. Ding, L. Wang, X. Jing, F. Wang, *Adv. Mater.* **2011**, *23*, 3726.
- [153] W. Li, M. Otsuka, T. Kato, Y. Wang, T. Mori, T. Michinobu, *Beilstein J. Org. Chem.* **2016**, *12*, 1401.
- [154] P.-Y. Su, L.-B. Huang, J.-M. Liu, Y.-F. Chen, L.-M. Xiao, D.-B. Kuang, M. Mayor, C.-Y. Su, *J. Mater. Chem. A* **2017**, *5*, 1913.
- [155] L. Yang, Y. Yan, F. Cai, J. Li, T. Wang, *Sol. Energy Mater. Sol. Cells* **2017**, *163*, 210.
- [156] H. Choi, C. K. Mai, H. B. Kim, J. Jeong, S. Song, G. C. Bazan, J. Y. Kim, A. J. Heeger, *Nat. Commun.* **2015**, *6*, 7348.
- [157] Z. a. Li, Z. Zhu, C.-C. Chueh, J. Luo, A. K. Y. Jen, *Adv. Energy Mater.* **2016**, *6*, 1601165.
- [158] Q. Xue, G. Chen, M. Liu, J. Xiao, Z. Chen, Z. Hu, X.-F. Jiang, B. Zhang, F. Huang, W. Yang, H.-L. Yip, Y. Cao, *Adv. Energy Mater.* **2016**, *6*, 1502021.
- [159] Y. Xu, T. Bu, M. Li, T. Qin, C. Yin, N. Wang, R. Li, J. Zhong, H. Li, Y. Peng, J. Wang, L. Xie, W. Huang, *ChemSusChem* **2017**, *10*, 2578.
- [160] M. Franckevicius, A. Mishra, F. Kreuzer, J. S. Luo, S. M. Zakeeruddin, M. Grätzel, *Mater. Horiz.* **2015**, *2*, 613.
- [161] S. Ma, H. Zhang, N. Zhao, Y. Cheng, M. Wang, Y. Shen, G. Tu, *J. Mater. Chem. A* **2015**, *3*, 12139.
- [162] P. Ganeshan, K. Fu, P. Gao, I. Raabe, K. Schenk, R. Scopelliti, J. Luo, L. H. Wong, M. Grätzel, M. K. Nazeeruddin, *Energy Environ. Sci.* **2015**, *8*, 1986.
- [163] Y.-K. Wang, Z.-C. Yuan, G.-Z. Shi, Y.-X. Li, Q. Li, F. Hui, B.-Q. Sun, Z.-Q. Jiang, L.-S. Liao, *Adv. Funct. Mater.* **2016**, *26*, 1375.
- [164] H. Choi, S. Paek, N. Lim, Y. H. Lee, M. K. Nazeeruddin, J. Ko, *Chemistry* **2014**, *20*, 10894.
- [165] H. Choi, S. Park, S. Paek, P. Ekanayake, M. K. Nazeeruddin, J. Ko, *J. Mater. Chem. A* **2014**, *2*, 19136.
- [166] P. Qin, S. Paek, M. I. Dar, N. Pellet, J. Ko, M. Grätzel, M. K. Nazeeruddin, *J. Am. Chem. Soc.* **2014**, *136*, 8516.
- [167] J. Xiao, L. Han, L. Zhu, S. Lv, J. Shi, H. Wei, Y. Xu, J. Dong, X. Xu, Y. Xiao, D. Li, S. Wang, Y. Luo, X. Li, Q. Meng, *RSC Adv.* **2014**, *4*, 32918.
- [168] a) S. Lv, Y. Song, J. Xiao, L. Zhu, J. Shi, H. Wei, Y. Xu, J. Dong, X. Xu, S. Wang, Y. Xiao, Y. Luo, D. Li, X. Li, Q. Meng, *Electrochim. Acta* **2015**, *182*, 733; b) S. Lv, L. Han, J. Xiao, L. Zhu, J. Shi, H. Wei, Y. Xu, J. Dong, X. Xu, D. Li, S. Wang, Y. Luo, X. Li, Q. Meng, X. Li, *Chem. Commun.* **2014**, *50*, 6931.
- [169] Y. Ma, Y. H. Chung, L. Zheng, D. Zhang, X. Yu, L. Xiao, Z. Chen, S. Wang, B. Qu, Q. Gong, D. Zou, *ACS Appl. Mater. Interfaces* **2015**, *7*, 6406.
- [170] Y. Hua, B. Xu, P. Liu, H. Chen, H. Tian, M. Cheng, L. Kloo, L. Sun, *Chem. Sci.* **2016**, *7*, 2633.
- [171] X. Zhao, F. Zhang, C. Yi, D. Bi, X. Bi, P. Wei, J. Luo, X. Liu, S. Wang, X. Li, S. M. Zakeeruddin, M. Grätzel, *J. Mater. Chem. A* **2016**, *4*, 16330.
- [172] a) F. Zhang, X. Zhao, C. Yi, D. Bi, X. Bi, P. Wei, X. Liu, S. Wang, X. Li, S. M. Zakeeruddin, *Dyes Pigm.* **2017**, *136*, 273. b) Z. Fei, Y. Chenyi, W. Peng, B. Xiangdong, L. Jingshan, J. Gwénolé, W. Shirong, L. Xianggao, X. Yin, Z. S. Mohammed, G. Michael, *Adv. Energy Mater.* **2016**, *6*, 1600401.
- [173] F. Zhang, X. Liu, C. Yi, D. Bi, J. Luo, S. Wang, X. Li, Y. Xiao, S. M. Zakeeruddin, M. Grätzel, *ChemSusChem* **2016**, *9*, 2578.
- [174] A. E. Labban, H. Chen, M. Kirkus, J. Barbe, S. Del Gobbo, M. Neophytou, I. McCulloch, J. Eid, *Adv. Energy Mater.* **2016**, *6*, 1502101.
- [175] Z. Li, Z. Zhu, C. C. Chueh, S. B. Jo, J. Luo, S. H. Jang, A. K. Jen, *J. Am. Chem. Soc.* **2016**, *138*, 11833.
- [176] M. Neophytou, J. Griffiths, J. Fraser, M. Kirkus, H. Chen, C. B. Nielsen, I. McCulloch, *J. Mater. Chem. C* **2017**, *5*, 4940.
- [177] H. Chen, W. Fu, C. Huang, Z. Zhang, S. Li, F. Ding, M. Shi, C.-Z. Li, A. K. Y. Jen, H. Chen, *Adv. Energy Mater.* **2017**, *7*, 1700012.
- [178] X. Liu, X. Zheng, Y. Wang, Z. Chen, F. Yao, Q. Zhang, G. Fang, Z. K. Chen, W. Huang, Z. X. Xu, *ChemSusChem* **2017**, *10*, 2833.
- [179] X. Liu, E. Rezaee, H. Shan, J. Xu, Y. Zhang, Y. Feng, J. Dai, Z.-K. Chen, W. Huang, Z.-X. Xu, *J. Mater. Chem. C* **2018**, *6*, 4706.
- [180] S. Paek, P. Qin, Y. Lee, K. T. Cho, P. Gao, G. Grancini, E. Oveisi, P. Gratia, K. Rakstys, S. A. Al-Muhtaseb, C. Ludwig, J. Ko, M. K. Nazeeruddin, *Adv. Mater.* **2017**, *29*, 1606555.
- [181] S. J. Park, S. Jeon, I. K. Lee, J. Zhang, H. Jeong, J.-Y. Park, J. Bang, T. K. Ahn, H.-W. Shin, B.-G. Kim, H. J. Park, *J. Mater. Chem. A* **2017**, *5*, 13220.
- [182] H. D. Pham, H. Hu, K. Feron, S. Manzhos, H. Wang, Y. M. Lam, P. Sonar, *Sol. RRL* **2017**, *1*, 1700105.
- [183] H. D. Pham, T. T. Do, J. Kim, C. Charbonneau, S. Manzhos, K. Feron, W. C. Tsoi, J. R. Durrant, S. M. Jain, P. Sonar, *Adv. Energy Mater.* **2018**, *8*, 1703007.
- [184] S. S. Reddy, S. Shin, U. K. Aryal, R. Nishikubo, A. Saeki, M. Song, S.-H. Jin, *Nano Energy* **2017**, *41*, 10.
- [185] L. Yang, F. Cai, Y. Yan, J. Li, D. Liu, A. J. Pearson, T. Wang, *Adv. Funct. Mater.* **2017**, *27*, 1702613.
- [186] J. Zhang, B. Xu, L. Yang, C. Ruan, L. Wang, P. Liu, W. Zhang, N. Vlachopoulos, L. Kloo, G. Boschloo, *Adv. Energy Mater.* **2017**, *8*, 1701209.
- [187] H. Li, K. Fu, A. Hagfeldt, M. Grätzel, S. G. Mhaisalkar, A. C. Grimsdale, *Angewandte Chemie* **2014**, *53*, 4085.
- [188] T. Krishnamoorthy, F. Kunwu, P. P. Boix, H. Li, T. M. Koh, W. L. Leong, S. Powar, A. Grimsdale, M. Grätzel, N. Mathews, S. G. Mhaisalkar, *J. Mater. Chem. A* **2014**, *2*, 6305.
- [189] L. Zheng, Y. H. Chung, Y. Ma, L. Zhang, L. Xiao, Z. Chen, S. Wang, B. Qu, Q. Gong, *Chem. Commun.* **2014**, *50*, 11196.
- [190] Y. S. Liu, Q. Chen, H. S. Duan, H. P. Zhou, Y. Yang, H. J. Chen, S. Luo, T. B. Song, L. T. Dou, Z. R. Hong, Y. Yang, *J. Mater. Chem. A* **2015**, *3*, 11940.
- [191] Y. Liu, Z. Hong, Q. Chen, H. Chen, W. H. Chang, Y. M. Yang, T. B. Song, Y. Yang, *Adv. Mater.* **2016**, *28*, 440.
- [192] C. Chen, M. Cheng, P. Liu, J. Gao, L. Kloo, L. Sun, *Nano Energy* **2016**, *23*, 40.
- [193] a) M. Cheng, C. Chen, K. Aitola, F. Zhang, Y. Hua, G. Boschloo, L. Kloo, L. Sun, *Chem. Mater.* **2016**, *28*, 8631. b) M. Cheng, K. Aitola, C. Chen, F. Zhang, P. Liu, K. Sveinbjörnsson, Y. Hua, L. Kloo, G. Boschloo, L. Sun, *Nano Energy* **2016**, *30*, 387.
- [194] J. H. Yun, S. Park, J. H. Heo, H. S. Lee, S. Yoon, J. Kang, S. H. Im, H. Kim, W. Lee, B. Kim, M. J. Ko, D. S. Chung, H. J. Son, *Chem. Sci.* **2016**, *7*, 6649.
- [195] H. K. Kim, C. Lu, I. Choi, J. Kim, *J. Mater. Chem. A* **2017**, *5*, 20263.
- [196] L. Xu, P. Huang, J. Zhang, X. Jia, Z. Ma, Y. Sun, Y. Zhou, N. Yuan, J. Ding, *J. Phys. Chem. C* **2017**, *121*, 21821.
- [197] Q. Chen, X. Li, T. Jiu, S. Ma, J. Li, X. Xiao, W. Zhang, *Dyes Pigm.* **2017**, *147*, 113.
- [198] a) B. Gomez-Lor, B. Alonso, A. Omenat, J. L. Serrano, *Chem. Commun.* **2006**, *5012*, 435. b) B. Zhao, B. Liu, R. Q. Png, K. Zhang, K. A. Lim, J. Luo, J. Shao, P. K. H. Ho, C. Chi, J. Wu, *Chem. Mater.* **2010**, *22*, 435.
- [199] W. Y. Lai, Q. Y. He, R. Zhu, Q. Q. Chen, W. Huang, *Adv. Funct. Mater.* **2008**, *18*, 265.
- [200] J. Shao, Z. Guan, Y. Yan, C. Jiao, Q.-H. Xu, C. Chi, *J. Org. Chem.* **2011**, *76*, 780.
- [201] F. J. Ramos, K. Rakstys, S. Kazim, M. Grätzel, M. K. Nazeeruddin, S. Ahmad, *RSC Adv.* **2015**, *5*, 53426.

- [202] F. Zhang, X. Yang, M. Cheng, J. Li, W. Wang, H. Wang, L. Sun, *J. Mater. Chem. A* **2015**, *3*, 24272.
- [203] L. Calió, C. Momblona, L. Gil-Escríg, S. Kazim, M. Sessolo, Á. Sastre-Santos, H. J. Bolink, S. Ahmad, *Sol. Energy Mater. Sol. Cells* **2017**, *163*, 237.
- [204] K. Rakstys, S. Paek, P. Gao, P. Gratia, T. Marszalek, G. Grancini, K. T. Cho, K. Genevicius, V. Jankauskas, W. Pisula, M. K. Nazeeruddin, *J. Mater. Chem. A* **2017**, *5*, 7811.
- [205] C. Huang, W. Fu, C. Z. Li, Z. Zhang, W. Qiu, M. Shi, P. Heremans, A. K. Jen, H. Chen, *J. Am. Chem. Soc.* **2016**, *138*, 2528.
- [206] R. Grisorio, R. Iacobellis, A. Listorti, L. De Marco, M. P. Cipolla, M. Manca, A. Rizzo, A. Abate, G. Gigli, G. P. Suranna, *ACS Appl. Mater. Interfaces* **2017**, *9*, 24778.
- [207] S. Kazim, F. J. Ramos, P. Gao, M. K. Nazeeruddin, M. Grätzel, S. Ahmad, *Energy Environ. Sci.* **2015**, *8*, 1816.
- [208] P. Qin, H. Kast, M. K. Nazeeruddin, S. M. Zakeeruddin, A. Mishra, P. Bauerle, M. Grätzel, *Energy Environ. Sci.* **2014**, *7*, 2981.
- [209] C. Steck, M. Franckevicius, S. M. Zakeeruddin, A. Mishra, P. Bauerle, M. Gratzel, *J. Mater. Chem. A* **2015**, *3*, 17738.
- [210] D. Bi, A. Mishra, P. Gao, M. Franckevicius, C. Steck, S. M. Zakeeruddin, M. K. Nazeeruddin, P. Bauerle, M. Gratzel, A. Hagfeldt, *ChemSusChem* **2016**, *9*, 433.
- [211] a) G. D. La Torre, C. G. Claessens, T. Torres, *Chem. Commun.* **2007**, *0*, 2000; b) J. Mack, N. Kobayashi, *Chem. Rev.* **2011**, *111*, 281.
- [212] W. Ke, D. Zhao, C. R. Grice, A. J. Cimaroli, G. Fang, Y. Yan, *J. Mater. Chem. A* **2015**, *3*, 23888.
- [213] F. Javier Ramos, M. Ince, M. Urbani, A. Abate, M. Gratzel, S. Ahmad, T. Torres, M. K. Nazeeruddin, *Dalton Trans.* **2015**, *44*, 10847.
- [214] M. Sun, S. Wang, Y. Xiao, Z. Song, X. Li, *J. Energy Chem.* **2015**, *24*, 756.
- [215] J.-J. Guo, X.-F. Meng, J. Niu, Y. Yin, M.-M. Han, X.-H. Ma, G.-S. Song, F. Zhang, *Synth. Met.* **2016**, *220*, 462.
- [216] J.-J. Guo, Z.-C. Bai, X.-F. Meng, M.-M. Sun, J.-H. Song, Z.-S. Shen, N. Ma, Z.-L. Chen, F. Zhang, *Sol. Energy* **2017**, *155*, 121.
- [217] G. Sfyri, Q. Chen, Y.-W. Lin, Y.-L. Wang, E. Nouri, Z.-X. Xu, P. Lianos, *Electrochim. Acta* **2016**, *212*, 929.
- [218] S. Wu, Y. Zheng, Q. Liu, R. Li, T. Peng, *RSC Adv.* **2016**, *6*, 107723.
- [219] a) G. Sfyri, C. V. Kumar, Y.-L. Wang, Z.-X. Xu, C. A. Krontiras, P. Lianos, *Appl. Surf. Sci.* **2016**, *360*, 767; b) G. Sfyri, N. Vamshikrishna, C. V. Kumar, L. Giribabu, P. Lianos, *Sol. Energy* **2016**, *140*, 60.
- [220] Z. X. Xu, V. A. L. Roy, *Chin. Phys. B* **2013**, *22*, 4.
- [221] Y. Wang, X. Liu, H. Shan, Q. Chen, T. Liu, X. Sun, D. Ma, Z. Zhang, J. Xu, Z.-X. Xu, *Dyes Pigm.* **2017**, *139*, 619.
- [222] X. Liu, Y. Wang, E. Rezaee, Q. Chen, Y. Feng, X. Sun, L. Dong, Q. Hu, C. Li, Z.-X. Xu, *Sol. RRL* **2018**, *2*, 1800050.
- [223] G. Yang, Y.-L. Wang, J.-J. Xu, H.-W. Lei, C. Chen, H.-Q. Shan, X.-Y. Liu, Z.-X. Xu, G.-J. Fang, *Nano Energy* **2017**, *31*, 322.
- [224] X. Zheng, Y. Wang, J. Hu, G. Yang, Z. Guo, J. Xia, Z. Xu, G. Fang, *J. Mater. Chem. A* **2017**, *5*, 24416.
- [225] Q.-D. Dao, A. Fujii, R. Tsuji, Y. Takeoka, M. Ozaki, *Org. Electron.* **2017**, *43*, 156.
- [226] X. Jiang, Z. Yu, H.-B. Li, Y. Zhao, J. Qu, J. Lai, W. Ma, D. Wang, X. Yang, L. Sun, *J. Mater. Chem. A* **2017**, *5*, 17862.
- [227] M. Cheng, Y. Li, M. Safdari, C. Chen, P. Liu, L. Kloo, L. Sun, *Adv. Energy Mater.* **2017**, *7*, 1602556.
- [228] H.-H. Chou, Y.-H. Chiang, M.-H. Li, P.-S. Shen, H.-J. Wei, C.-L. Mai, P. Chen, C.-Y. Yeh, *ACS Energ. Lett.* **2016**, *1*, 956.
- [229] S. Chen, P. Liu, Y. Hua, Y. Li, L. Kloo, X. Wang, B. Ong, W. K. Wong, X. Zhu, *ACS Appl. Mater. Interfaces* **2017**, *9*, 13231.
- [230] M. Li, Y. Li, S. I. Sasaki, J. Song, C. Wang, H. Tamiaki, W. Tian, G. Chen, T. Miyasaka, X. F. Wang, *ChemSusChem* **2016**, *9*, 2862.
- [231] M. K. Kashif, I. Benesperi, R. A. Milhuisen, S. Meyer, J. Hellerstedt, D. Zee, N. W. Duffy, B. Halstead, M. S. Fuhrer, J. Cashion, Y.-B. Cheng, L. Spiccia, A. N. Simonov, U. Bach, *ACS Energ. Lett.* **2017**, *2*, 1855.
- [232] L. Cabau, I. Garcia-Benito, A. Molina-Ontoria, N. F. Montcada, N. Martin, A. Vidal-Ferran, E. Palomares, *Chem. Commun.* **2015**, *51*, 13980.
- [233] H. Zhu, F. Zhang, X. Liu, M. Sun, J. Han, J. You, S. Wang, Y. Xiao, X. Li, *Energy Technol.* **2017**, *5*, 1257.
- [234] A. Krishna, D. Sabba, J. Yin, A. Bruno, L. J. Antila, C. Soci, S. Mhaisalkar, A. C. Grimsdale, *J. Mater. Chem. A* **2016**, *4*, 8750.
- [235] Z. Li, J. Chen, H. Li, Q. Zhang, Z. Chen, X. Zheng, G. Fang, Y. Hao, *RSC Adv.* **2017**, *7*, 41903.
- [236] V. O. Eze, T. Mori, *J. Photopolym. Sci. Technol.* **2016**, *29*, 581.
- [237] M. Cheng, C. Chen, B. Xu, Y. Hua, F. Zhang, L. Kloo, L. Sun, *J. Energy Chem.* **2015**, *24*, 698.
- [238] J. S. Ni, H. C. Hsieh, C. A. Chen, Y. S. Wen, W. T. Wu, Y. C. Shih, K. F. Lin, L. Wang, J. T. Lin, *ChemSusChem* **2016**, *9*, 3139.
- [239] S. Jeon, U. K. Thakur, D. Lee, Y. Wenping, D. Kim, S. Lee, T. K. Ahn, H. J. Park, B.-G. Kim, *Org. Electron.* **2016**, *37*, 134.
- [240] R. Azmi, S. Y. Nam, S. Sinaga, Z. A. Akbar, C.-L. Lee, S. C. Yoon, I. H. Jung, S.-Y. Jang, *Nano Energy* **2018**, *44*, 191.
- [241] S. Guarnera, A. Abate, W. Zhang, J. M. Foster, G. Richardson, A. Petrozza, H. J. Snaith, *J. Phys. Chem. Lett.* **2015**, *6*, 432.
- [242] D. Koushik, W. J. H. Verhees, Y. Kuang, S. Veenstra, D. Zhang, M. A. Verheijen, M. Creatore, R. E. I. Schropp, *Energy Environ. Sci.* **2017**, *10*, 91.